TG–956
MARCH 1968
Copy No.

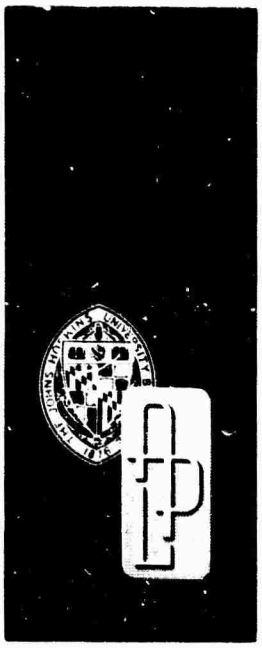

Technical Memorandum

ARRAY ANTENNAS

by T. C. CHESTON and J. FRANK

THE JOHNS HOPKINS UNIVERSITY • APPLIED PHYSICS LABORATORY

TG–956
MARCH 1968

Technical Memorandum

ARRAY ANTENNAS

by T. C. CHESTON and J. FRANK

SPONSORED BY ARPA UNDER AO-805

THE JOHNS HOPKINS UNIVERSITY • APPLIED PHYSICS LABORATORY
8621 Georgia Avenue, Silver Spring, Maryland 20910

Operating under Contract NOw 62-0604-c with the Department of the Navy

THE JOHNS HOPKINS UNIVERSITY
APPLIED PHYSICS LABORATORY
SILVER SPRING MARYLAND

ABSTRACT

Array antennas in their various forms are discussed and analyzed with special reference to electronic scanning. The effects of mutual coupling of the radiating elements are considered and methods of matching are given. Quantization errors, particularly those found in phased arrays, are calculated and bandwidth limitations are derived. Specific array antenna systems are described.

TABLE OF CONTENTS

TABLE OF CONTENTS (cont'd)

TABLE OF CONTENTS (cont'd)

TABLE OF CONTENTS (cont'd)

LIST OF ILLUSTRATIONS

LIST OF ILLUSTRATIONS (cont'd)

LIST OF ILLUSTRATIONS (cont'd)

LIST OF ILLUSTRATIONS (cont'd)

LIST OF ILLUSTRATIONS (cont'd)

BLANK PAGE

THE JOHNS HOPKINS UNIVERSITY
APPLIED PHYSICS LABORATORY
SILVER SPRING MARYLAND

I. INTRODUCTION

Array Radars

Multifunction Radar

Early radar systems used antenna arrays formed by the combination of individual radiators. The origin of such antennas dates back to the turn of the century (Refs. 1 and 2). The antenna characteristics are determined by the geometric position of the radiators and the amplitude and phase of their excitation. As radars progressed to shorter wavelengths, arrays were displaced by simpler antennas such as parabolic reflectors. For modern radar applications the advent of electronically controlled phase shifters and switches has once more directed attention to array antennas. The aperture excitation may now be modulated by controlling the individual elements to give beams that are scanned electronically (Refs. 3 through 6). This report will be devoted to arrays of this type.

The capability of rapidly and accurately switching beams permits the radar to perform multiple functions either simultaneously or interlaced in time. An electronically steered array radar may track a great multiplicity of targets, illuminate a number of targets with RF energy and guide missiles towards them, perform complete hemispherical search with automatic target selection and hand over to track; it may even act as a communication system, directing high-gain beams toward distant receivers and transmitters. Complete flexibility is possible; search and track rates may be adjusted to best meet particular situations, all within the limitations set by the total use of time. The antenna beamwidth may be changed to more rapidly search some areas with less gain. Frequency agility is

possible with the frequency of transmission changing at will from pulse to pulse or, with coding, within a pulse. Very high powers may be generated from a multiplicity of generators distributed across the aperture. The difficulty in obtaining a best fit of parameters for a given situation increases rapidly with the available flexible possibilities, and the actual use of the tempting potentials is finally limited by the problems of controlling and coordinating the many variables with effective automatic management and programming.

Array Antennas

The array antenna has an aperture that is assembled from a great many similar radiating elements, such as slots or dipoles, each element being individually controlled in phase and amplitude. High efficiencies can be achieved with radiation patterns and beam-pointing directions that are accurately predictable.

The general planar array characteristics are readily obtained from a few simple equations, given here but discussed later in greater detail. With the elements spaced by $\lambda/2$ (λ = wavelength) to avoid the generation of multiple beams, called grating lobes, the number of radiating elements, N, for a pencil beam is related to the beamwidth by:

$$N \approx \frac{10,000}{(\theta_B)^2} ,$$

$$\text{or } \theta_B \approx \frac{100}{\sqrt{N}} ,$$

where θ_B is the 3 db beamwidth in degrees. The corresponding gain when the beam points broadside to the aperture is:

$$G_o \approx \pi N .$$

When scanning to an angle θ_o, the gain of a planar array is reduced to that of the projected aperture:

$$G(\theta) \approx \pi N \cos\theta_o \quad .$$

Similarly, the scanned beamwidth is increased from the broadside beamwidth (except in the vicinity of end-fire, $\theta_o = 90°$) to:

$$\theta_B \text{ (scanned)} \approx \frac{\theta_B \text{ (broadside)}}{\cos\theta_o} \quad .$$

The total number of beams M (with broadside beamwidth) that fits into a sphere is approximately equal to the gain and is thus simply related to N by:

$$M \approx \pi N \quad .$$

In a planar array where the beamwidth changes with scan angle, the number of beams that can actually be generated and fitted into a sphere is:

$$M' \approx \frac{\pi}{2} N \quad .$$

An array where the elements are fed in parallel (see Fig. 38 in Section VII) and which is scanned by phase shift, modulo 2π, has limited bandwidth since for wideband operation constant path lengths rather than constant phases are required. The limit is given by:

Bandwidth (%) $\approx$ Beamwidth (degrees).

This is equivalent to bandwidth limitations given by:

Pulse length $\approx$ 2 x aperture size.

With these criteria the scanned radiation pattern at 60° is steered by $\pm \frac{1}{4}$ of the local, scanned, beamwidth as the frequency is changed over the band. At 60° scan the beam steers with frequency through an angle $\delta\theta$ so that at the extreme frequency:

$$\delta\theta \text{ (degrees)} \approx \text{Bandwidth (\%)}.$$

For wider bandwidths, time-delay networks have to be introduced to supplement the phase shifters.

3-D Search

For volumetric (3-D) search the array antenna is required to scan a beam in elevation and azimuth. If a radar has an array antenna system with an electronically scanned beam, it may operate with a high sensitivity leading to a high false alarm rate since the indicated targets may easily be interrogated again and checked. With many arrays there is the additional capability of widening the beam for searching the more elevated positions where less range is required and less gain is therefore permissible. This results in a net saving of search time.

Track – Monopulse

Array radars may readily be designed to give monopulse tracking. The radiating elements of the array are combined in three different ways to give the sum pattern and the azimuth and elevation difference patterns. Contradictory requirements in optimum amplitude distribution for sum and difference patterns exist (Ref. 7), but, as with other antenna systems, they may be independently satisfied. The sum and difference patterns are scanned simultaneously. The array may also be programmed to track with a sequential lobing system or conical scan.

The difference pattern null in a phased array system gives good beam-pointing accuracy. Compared to calculated values, absolute beam-pointing accuracies to within less than 1/50 of a (scanned) beam-width have been measured with scans up to 60°. The accuracy is limited by the accuracy of the phase and amplitude control. Since there is no time delay, as the frequency is changed the direction of the null of the scanned beam is also changed and the beam moves toward broadside as the frequency is increased. The amplitude of the difference pattern output then increases linearly with a change in frequency. With a scan angle of 60° this change is from a zero at the design frequency to a value of about -9 db relative to the sum pattern at the edges of the band, where the band is defined by Bandwidth (%) = Beamwidth (degrees).

Multiple Beams

Independent control of both amplitude and phase at the aperture is necessary for the generation of multiple simultaneous beams. This can

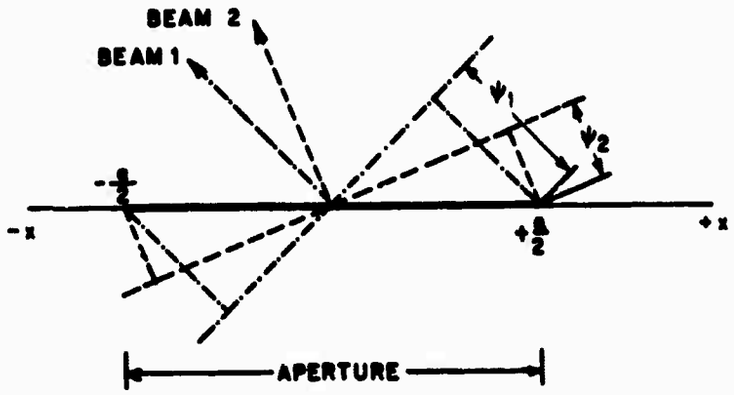

Fig. 1 Aperture Distribution With Two Beams

be seen from Fig. 1 where two independent beams are generated. Both beams have the same amplitude distribution F(x), but differently inclined linear phase fronts. The total aperture excitation with both beams is:

$$F(x,\psi) = F(x)\, e^{j\,2\psi_1 \frac{x}{a}} + F(x)\, e^{j\,2\psi_2 \frac{x}{a}}$$

$$= 2F(x)\left[\cos(\psi_1 - \psi_2)\frac{x}{a}\right] e^{j\,(\psi_1 + \psi_2)\frac{x}{a}},$$

i.e., the aperture amplitude distribution required for two separate beams varies cosinusoidally and the phase distribution is linear and has the average inclination.

In many array systems only the phase at the aperture can be varied. With such systems independent simultaneous beams cannot be generated other than with reduced gain as by splitting the aperture into separate parts.

Shaped Beams

The radiation pattern of an array may be shaped by modifying the aperture distribution. The use of phase only, without amplitude, still leads to good pattern approximations. In particular some broadening of the beam may be obtained by applying a spherical phase law to the aperture or approximating it with a gable (triangular) distribution. Beams of this type are of particular interest since they are easily generated and are efficient. They may be used for transmission in a system where the receiving antenna has a cluster of simultaneous beams or, as previously discussed, they may be used in a search system to reduce the number of angular cells in regions of shorter range.

Monitoring

Electronically scanned arrays are composed of very many parts and include electronic circuitry to drive the phase shifters or the switches that steer the beam. The overall reliability of such arrays can be great, and the failure of a significant number of components can have a negligible effect. Graceful degradation has been claimed for arrays since the failure of 10% of the components leads to a loss in gain of only 1 db. Nevertheless, the functioning of the antenna is complex, and there is need for providing test or monitoring circuitry. The decision to point a beam in a certain direction is made somewhere in the control of the radar and

is normally defined by two direction cosines. A test or monitoring circuit should establish the correct functioning of all components from that point on, including all beam pointing computations, electronic drivers, and phase shifters or switches and all their interconnections. Frequent indications should be available that the antenna system is functioning or capable of functioning. It should be possible further to examine all circuits in detail, perhaps less frequently, and to pinpoint malfunctions. These tests need not necessarily include RF measurements. The correct functioning of most phase shifters, for example, may be determined from their drive currents.

Deployment of Apertures

With planar arrays scanning is limited by the loss in gain and the increase in beamwidth corresponding to the reduction of the projected aperture size. Practical extreme values of scanning are, therefore, in the region of 60° to 70°. A minimum of three planar array apertures is then necessary for hemispherical coverage. For shipborne use, a minimum of four apertures appears desirable, since with pitch and roll, more than hemispherical coverage is necessary. The antennas may be positioned as shown in Fig. 2, permitting a view that is unimpeded by

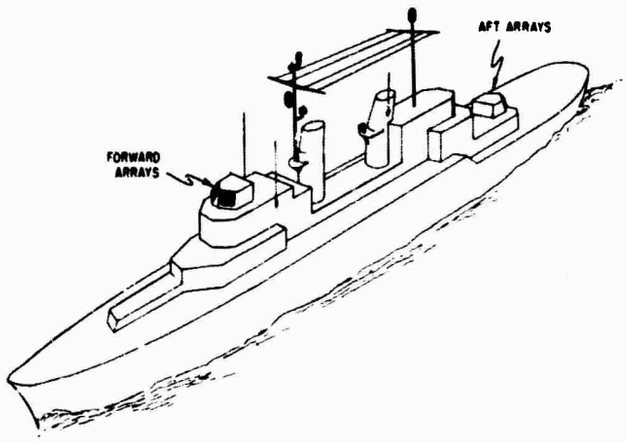

Fig. 2 Shipborne Array Antennas

the central superstructure. The apertures would normally be tilted back from the vertical to balance the scan angles. A smaller and fifth planar aperture may be used advantageously to look upward to cover the space directly overhead containing targets at shorter ranges.

The restriction on scan angle does not necessarily apply to non-planar arrays. In particular, for example, a spherical array can generate beams equally well in all directions.

With a given number of radiators, the shape of a planar array affects the beamwidth and sidelobe structure but not the gain. With a rectangular aperture the sidelobes are highest in the principal planes and lowest in the diagonal planes, whereas with a round aperture the sidelobes fall somewhere between the two extremes of the rectangular aperture.

RF Generation

The RF power for transmitting may be generated by one large amplifier or generator. Alternately, a multiplicity of RF generators may be used (up to one per radiating element), all driven phase coherently and distributed across the aperture. For the first method it can be argued that the advantage lies in having only one single generator where one can afford to go to considerable trouble to properly maintain it, to monitor and check its operation, and to ensure proper functioning with adequate safeguards and standby equipment. The second method could claim as advantages the absence of very high RF power concentrated in some vital components, the capability of generating higher total power into the array and again, gradual degradation.

In many radar applications there are two or more separate array apertures. Under these circumstances it becomes possible to associate

separate RF generators with each of the arrays with a common power supply. The programming may then be arranged such that the arrays fire in sequence.

Radiating Elements

The most commonly used radiators for phased arrays are dipoles, slots, open-ended waveguides (or small horns), and spirals. The primary requirement is that the element be small enough to fit in the array geometry, thereby limiting the element to an area of a little more than $\lambda^2/4$. In addition many radiators are required, and the radiating element should be inexpensive, reliable, and repeatable from unit to unit.

Since the impedance and pattern of a radiator in an array are determined predominantly by the array environment (Section IV), the radiating element may be chosen to best suit the feed system and the physical requirements of the antenna. For example, if the radiator is fed from a stripline phase shifter, a stripline dipole would be a logical choice for the radiator. If a waveguide phase shifter were used, an open ended waveguide or a slot might be convenient. At the lower frequencies, where coaxial components are prevalent, dipoles have been favored for the radiating element. A ground plane is usually placed about $\frac{\lambda}{4}$ behind an array of parallel dipoles so that the antenna forms a beam in only one hemisphere. At the higher frequencies open-ended waveguides and slots are frequently used.

For the case of limited scanning (say less than 10°), it is possible to use directive radiators having effective aperture areas of several square wavelengths. With a separation between elements of several wavelengths – and because directive radiators are used – the mutual coupling effects will be small, and the pattern and impedance of an element in the array will be essentially those of the isolated element.

For circular polarization a cavity backed spiral may be used. Since a single bounce reflection from a target reverses the sense of circularity, separate transmit and receive spiral arrays (with opposite sense radiators) are required.

If polarization diversity is required or if an array is required to transmit one sense of polarization and receive the opposite sense, either crossed dipoles or circular waveguides may be used. With suitable feed systems, both are capable of providing vertical and horizontal polarization independently and may be combined to provide any desired polarization.

Polarization

From the point of view of the antenna designer; the plane of polarization of a planar array is arbitrary. Circular polarization is possible, though difficulties may be encountered in matching for large scan angles. On scanning, a component of the undesired orthogonal polarization will be generated (Ref. 8) and some provision should be made to terminate it (Ref. 9). With a conventional circularly polarized antenna, such as a parabolic dish with a circularly polarized feed, good circularity may be obtained over part of the main beam, with rapid deterioration over the rest of the pattern. With a planar array the relevant beamwidth is the element beamwidth rather than the array beamwidth. The element beamwidth is broad, and good circularity may be expected over wide angles.

Circularly polarized systems may be used to obtain a measure of suppression of rain echoes (Ref. 10). Under ideal conditions this suppression amounts to $20 \log \frac{e^2 + 1}{e^2 - 1}$ db, where e is the voltage ellipticity ratio. An early model of the Raytheon reflect-array (Section VIII) gave an ellipticity ratio of less than 1.5 db with scans up to 30°, corresponding to a theoretical rain rejection of at least 15 db.

Phased Arrays with Very Wide Bandwidth

A radar system that has the capability of changing frequency over very wide bands can, with advantage, adapt its transmission to take into account the frequency dependent propagation characteristics, target response, environmental conditions, and variations in beamwidth.

Phased arrays have the potential of operating over very wide bandwidths. Some ferrite phase shifters will operate over two octaves (Ref. 11), and digital diode phase shifters that switch line lengths (Section X) may function over even wider bands. The high end of the frequency band is limited by the physical size of the elements since these elements must be spaced close enough in the array to avoid the generation of grating lobes.

The impedance of the radiating element at the aperture (with the closely spaced elements) is approximately independent of frequency, but the element must be matched over the wide band. This is difficult to achieve without exciting harmful surface waves when scanning. Nevertheless, matching with octave bandwidth for scanning to ± 60° appears possible.

Scanning of Arrays

Phase Scanning

The beam of an antenna points to a direction that is normal to the phase front. In phased arrays this phase front is adjusted to steer the beam by individual control of the phase of excitation of each radiating element. This is indicated in Fig. 3a. The phase shifters are electronically actuated to permit rapid scanning and are adjusted in phase

to a value between 0 and 2π. With an interelement spacing s, the incremental phase shift ψ between adjacent elements for a scan angle θ_o is $\psi = \frac{2\pi}{\lambda} s \sin\theta_o$. If the phase ψ is constant with frequency, then the scan angle θ_c is frequency dependent such that $\frac{\sin\theta_o}{\lambda}$ is constant.

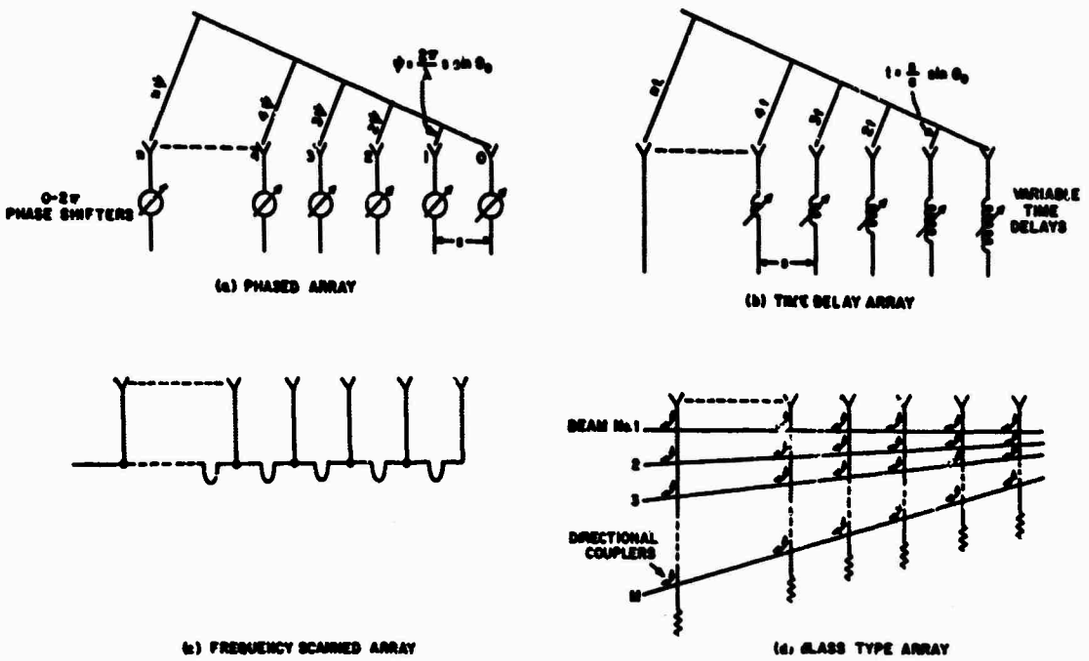

(a) PHASED ARRAY

(b) TIME DELAY ARRAY

(c) FREQUENCY SCANNED ARRAY

(d) GLASS TYPE ARRAY

Fig. 3 Generation of Scanned Beams

Time Delay Scanning

Phase scanning was seen to be frequency sensitive. Time delay scanning is independent of frequency. Delay lines are used instead of phase shifters, as shown in Fig. 3b, providing an incremental delay from element to element of $t = \frac{s}{c} \sin\theta_o$. Individual time delay circuits (Section VI) are normally too complex to be added to each radiating element. A reasonable compromise may be reached by adding one time delay network to a group of elements that have phase shifters.

Frequency Scanning

Frequency rather than phase may be used as the active parameter to exploit the frequency sensitive characteristics of phase scanning. Figure 3c shows the arrangement. At one particular frequency all radiators are in phase. As the frequency is changed, the phase across the aperture tilts linearly, and the beam is scanned.

IF Scanning

When receiving, the output from each radiating element may be heterodyned (mixed) to an IF frequency. All the various methods of scanning are then possible, including the beam switching system described below, and can be carried out at IF where amplification is readily available and lumped constant circuits may be used. Equivalent techniques of mixing may be used for transmitting.

Beam Switching

With lenses or reflectors, a multiplicity of independent beams may be formed by feeds at the focal surface. Each beam has substantially the gain and beamwidth of the whole antenna. Allen (Ref. 12) has shown that there are efficient equivalent transmission networks that use directional couplers and have the same collimating property. A typical form after Blass (Ref. 13) is shown in Fig. 3d. The beams may be selected through a switching matrix requiring (M-1) SPDT switches to select one out of M beams. The beams are stationary in space and overlap at about the 4 db points. This is in contrast to the previously discussed methods of scanning, where the beam could be steered accurately to any position. The beams all lie in one plane. Much more complexity is required for a system giving simultaneous beams in both planes. A more detailed discussion is given in Section IX.

BLANK PAGE

II. ARRAY THEORY

Array with Two Elements

Figure 4 shows two isotropic radiators which are spaced by a distance s and excited with equal amplitude and phase. With unity input power, the vector sum of their contributions, added at a great distance as a function of θ, is the radiation pattern:

$$E_a(\theta) = \frac{1}{\sqrt{2}} \left(e^{j \frac{2\pi}{\lambda} \frac{s}{2} \sin\theta} + e^{-j \frac{2\pi}{\lambda} \frac{s}{2} \sin\theta} \right)$$

where θ is measured from the broadside direction. Normalizing, to give unity amplitude when $\theta = 0$ and simplifying, gives:

$$E_a(\theta) = \cos\left(\pi \frac{s}{\lambda} \sin\theta\right) . \qquad (1)$$

The absolute value of $E_a(\theta)$ is plotted as a function of $\pi \frac{s}{\lambda} \sin\theta$. If the plot had been in terms of the angle θ, then the lobes would have been found to increase in width as $|\theta|$ increased. The main lobe occurs when $\sin\theta = 0$. The other lobes have the same amplitude as the main lobe and are frequently referred to as grating lobes. They occur at angles given by $\sin\theta = \pm \frac{m}{s/\lambda}$, where m is an integer. For the half space given by $-90° < \theta < +90°$, there are 2 m' grating lobes, where m' is the largest integer smaller than s/λ. If $s < \lambda$, grating lobe maxima will not occur and the value at $\pm$ 90 degrees is $\cos(\pi \frac{s}{\lambda})$. This value is for isotropic radiators and will be reduced if the radiator has directivity.

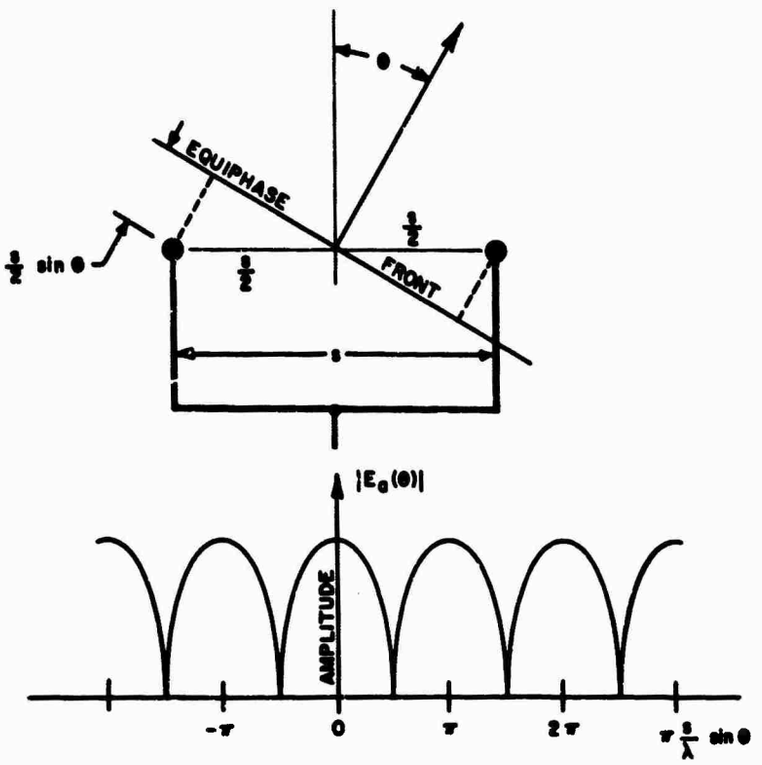

Fig. 4 Radiation Pattern of Two Isotropic Radiators

Linear Array (Ref. 14)

With a linear array of N isotropic radiators, excited with equal amplitudes and phase and separated by distances s, as shown in Fig. 5,

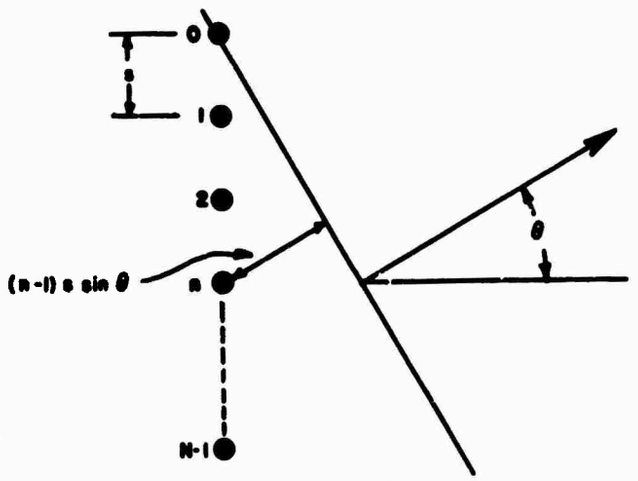

Fig. 5 Linear Array with N Radiators Uniformly Spaced by a Distance s

the condition for the occurrence of grating lobes is unchanged from the simpler case just considered. They will occur for the same values of $\pi \frac{s}{\lambda} \sin\theta$, but the width of the lobes is reduced and they are separated by minor lobes. Summing the vector contributions from all elements, using element No. 0 as phase reference, gives:

$$E_a(\theta) = \frac{1}{\sqrt{N}} \sum_{n=0}^{n=N-1} e^{j\frac{2\pi}{\lambda} n s \sin\theta}$$

The factor $\frac{1}{\sqrt{N}}$ shows that each element is energized with $\frac{1}{N}$ of the (unity) input power. Adjusting the phase relative to the center of the aperture and normalizing the gain to unity at broadside, $\theta = 0$, gives:

$$E_a(\theta) = e^{-j\frac{2\pi}{\lambda}\frac{N-1}{2} s \sin\theta} \frac{1}{N} \sum_{n=0}^{n=N-1} e^{j\frac{2\pi}{\lambda} n s \sin\theta}$$

$$= \frac{\sin(N\pi \frac{s}{\lambda} \sin\theta)}{N \sin(\pi \frac{s}{\lambda} \sin\theta)} \qquad (2)$$

$E_a(\theta)$ gives the radiation pattern with isotropic radiators and is known as the <u>array factor</u>. It is shown in Fig. 6 for N = 10. The pattern is repetitive, and adjacent grating lobes at angles θ_1 and θ_2 are separated by $\pi \frac{s}{\lambda} (\sin\theta_1 - \sin\theta_2) = \pi$.

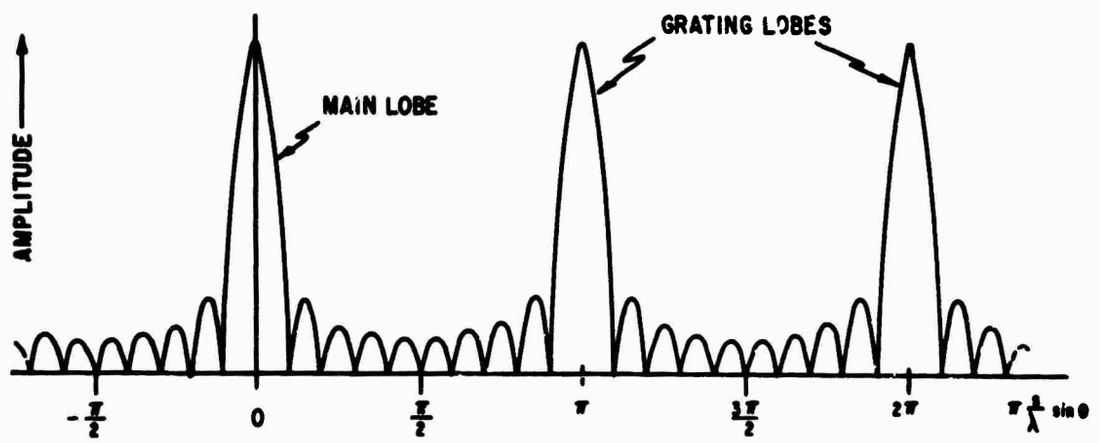

Fig. 6 Array Factor with N = 10 Elements

When the radiating elements are not isotropic but have a radiation pattern $E_e(\theta)$, as measured within the array, known as element factor or element pattern, then the complete radiation pattern $E(\theta)$ is the produce of array factor and element pattern

$$E(\theta) = E_e(\theta) \times E_a(\theta)$$

$$= E_e(\theta) \frac{\sin(N \pi \frac{s}{\lambda} \sin\theta)}{N \sin(\pi \frac{s}{\lambda} \sin\theta)} . \qquad (3)$$

Sometimes the meaning of array factor and element factor is reserved for gain or power patterns

$$P(\theta) = P_e(\theta) \times P_a(\theta) ,$$

where $P(\theta) = |E(\theta)|^2$; $P_a(\theta) = |E_a(\theta)|^2$ and $P_e(\theta) = |E_e(\theta)|^2$.

An approximation to the pattern of Eq. 2 is in the form sin(x)/x:

$$E(\theta) = \frac{\sin(\pi \frac{a}{\lambda} \sin\theta)}{\pi \frac{a}{\lambda} \sin\theta} , \qquad (4)$$

where the effective aperture is $a = Ns$, which extends by $\frac{s}{2}$ beyond the centers of the end elements. In contrast to the array factor, this pattern has only one maximum and is non-repetitive. It is the well known Fourier transform of a continuous constant amplitude distribution and is a reasonable approximation for small values of θ when the aperture is greater than several wavelengths.

The half-power beamwidth is obtained from Eq. 4

$$\theta_B = \frac{0.886}{a/\lambda} \text{ radians} = \frac{50.8}{a/\lambda} \text{ degrees} . \qquad (5)$$

The first sidelobe is 13.2 db down from the main lobe.

For larger values of θ the pattern of a continuous aperture is modified from Eq. 4 by the obliquity factor (Refs. 15 and 16) $\frac{1}{2}(1 + \cos\theta)$, which arises from the definition of a Huygens' source. This gives:

$$E(\theta) = \frac{1}{2}(1 + \cos\theta)\frac{\sin(\pi \frac{a}{\lambda}\sin\theta)}{\pi \frac{a}{\lambda}\sin\theta} \tag{6}$$

For closely spaced elements the obliquity factor is very similar to the element pattern of a well designed radiating element, $\sqrt{\cos\theta}$ (for values up to some 60° or 70°).

Scanned Linear Arrays

The pattern of the array may be steered through an angle θ_o by applying linearly progressive phase increments from element to element, so that the phase between adjacent elements differs by $2\pi\frac{s}{\lambda}\sin\theta_o$. Equation 2 is then modified, giving a normalized array factor:

$$E_a(\theta) = \frac{\sin N\pi\frac{s}{\lambda}(\sin\theta - \sin\theta_o)}{N\sin\pi\frac{s}{\lambda}(\sin\theta - \sin\theta_o)}\ , \tag{7}$$

and the pattern is

$$E(\theta) = E_e(\theta)\frac{\sin N\pi\frac{s}{\lambda}(\sin\theta - \sin\theta_o)}{N\sin\pi\frac{s}{\lambda}(\sin\theta - \sin\theta_o)}\ . \tag{8}$$

Equation 8 describes the fundamental response of a scanned array system. The array factor will have only one single major lobe, and grating lobe maxima will not occur at values of $-90° < \theta < +90°$ as long as

$$\pi \frac{s}{\lambda} (\sin\theta - \sin\theta_o) < \pm \pi ,$$

or

$$\frac{s}{\lambda} < \frac{1}{1 + |\sin\theta_o|} , \qquad (9)$$

which is always true if $\frac{s}{\lambda} < \frac{1}{2}$. When the scanning is limited, then the value of $\frac{s}{\lambda}$ may be increased for example to $\frac{s}{\lambda} < 0.53$ for scanning to a maximum of $\pm 60°$ or to $\frac{s}{\lambda} < 0.59$ for scanning to a maximum of $\pm 45°$.

For a larger values of $\frac{s}{\lambda}$, grating lobes occur at angles θ_1, given by:

$$\sin\theta_1 = \sin\theta_o \pm \frac{n}{s/\lambda} , \qquad (10)$$

where n is an integer.

Equation 8 may again be approximated by the Fourier transform of the illumination across the continuous aperture

$$E(\theta) = \frac{1}{2} (1 + \cos\theta) \frac{\sin \pi \frac{a}{\lambda} (\sin\theta - \sin\theta_o)}{\pi \frac{a}{\lambda} (\sin\theta - \sin\theta_o)} . \qquad (11)$$

If, for small values of s, the element pattern $E_e(\theta)$ is taken to be equal to the obliquity factor, $\frac{1}{2} (1 + \cos\theta)$, then Eq. 11 is too great by the factor $\frac{\sin \pi \frac{s}{\lambda} (\sin\theta - \sin\theta_o)}{\pi \frac{s}{\lambda} (\sin\theta - \sin\theta_o)}$. The error decreases as s/λ gets smaller.

The Fourier transform solutions for continuous apertures (Refs. 7 and 17) may be used to approximate patterns for practical amplitude and phase distributions as long as the element to element spacing is small enough to suppress grating lobes.(Ref. 18). Monopulse difference patterns may be approximated in the same way from the Fourier transforms of the corresponding continuous odd aperture distributions. For example, with a constant amplitude distribution, the difference pattern array factor calculated by the exact vector addition of all radiating elements is

$$E_a(\theta) = \frac{1 - \cos N\pi \frac{s}{\lambda}(\sin\theta - \sin\theta_0)}{N \sin \pi \frac{s}{\lambda}(\sin\theta - \sin\theta_0)}$$, while the Fourier transform gives

the same expression with the sine in the denominator replaced by its argument, giving (in the denominator) $\pi a/\lambda (\sin\theta - \sin\theta_0)$, where $a = Ns$.

For small scan angles θ_0 and small values of θ, the expression $(\sin\theta - \sin\theta_0)$ may be approximated by $(\theta - \theta_0)$. For larger values of θ_0, the expression $(\sin\theta - \sin\theta_0)$ may be expanded to give the response in the general direction of the (narrow) scanned beam in terms of the small angle $(\theta - \theta_0)$:

$$\sin\theta - \sin\theta_0 \approx (\theta - \theta_0)\cos\theta_0 \ . \qquad (12)$$

This gives, with Eq. 11:

$$E(\theta) \approx \frac{1}{2}(1 + \cos\theta) \frac{\sin \frac{\pi a \cos\theta_0}{\lambda}(\theta - \theta_0)}{\frac{\pi a \cos\theta_0}{\lambda}(\theta - \theta_0)} \ . \qquad (13)$$

Equation 13 measures the angle $(\theta - \theta_0)$ from the scanned direction. It shows that the effect of scanning is to reduce the aperture to the size

of its projection normal to the direction of scan. Correspondingly, the beam width is increased to

$$\theta_{B(\text{scanned})} \approx \frac{\theta_{B(\text{broadside})}}{\cos\theta_0} = \frac{0.886}{\frac{a}{\lambda}\cos\theta_0} \text{ radians} = \frac{50.8}{\frac{a}{\lambda}\cos\theta_0} \text{ degrees.} \qquad (14)$$

When the beam is scanned from broadside by an angle $\theta_0 < 60°$ and the aperture $a/\lambda > 5$, then Eq. 14 gives a beamwidth that is too narrow, the error being less than 7%.

When the beam is scanned to very large scan angles, towards end-fire, then more exact calculations become necessary (Ref. 19). Equation 9 still applies and gives, for end-fire with isotropic radiators,

$$\theta_{B(\text{end-fire})} = 2\sqrt{\frac{0.886}{a/\lambda}} \text{ radians} . \qquad (15)$$

A line source, for example, will give an end-fire pencil beam with that beamwidth and corresponding gain. These cases are not normally of interest for array radars and will not be pursued here.

Z-Transforms

The similarity between the array factor of a linear array and the Z-transform of a sampled data system was first recognized by Cheng and Ma (Ref. 20). They considered the discrete element excitations in an array as samples of a continuous function and showed how known Z-transforms could be used for the analysis of an array factor. This discussion follows their treatment.

In a linear array (Fig. 5) the array factor has been shown to be:

$$E_a(\theta) = \frac{1}{\sqrt{N}} \sum_{n=0}^{N-1} e^{jn\frac{2\pi s}{\lambda}\sin\theta} .$$

If the array has an amplitude taper, with A_n being the amplitude at the n^{th} element, and if the array is scanned to an angle θ_o, then the array factor may be written as:

$$E_a(\theta) = \sum_{n=0}^{N-1} A_n e^{jn\frac{2\pi s}{\lambda}(\sin\theta - \sin\theta_o)} , \qquad (16)$$

letting $e^{j\frac{2\pi s}{\lambda}(\sin\theta - \sin\theta_o)} = z^{-1}$,

gives $$E(z) = \sum_{n=0}^{N-1} A_n z^{-n} . \qquad (17)$$

If all of the A_n's are equal (i.e., uniform illumination) the expression may be easily summed giving:

$$E(z) = \frac{1 - z^{-N}}{1 - z^{-1}} .$$

For most amplitude distributions E(z) is not easily summed. However, in many cases the large number of Z-transforms developed for sampled data control systems may be used to sum E(z) and provide closed expressions for the array factor. Jury (Ref. 21) has provided a comprehensive discussion of Z-transforms and an extensive table.

The Z-transform is a special case of the Laplace transform. If a continuous function f(x) is sampled by an impulse at periodic intervals, the resulting train of impulses is given by:

$$f^*(x) = \sum_{n=0}^{\infty} f(x)\,\delta\,(x - ns)\,,$$

where $\delta\,(x - ns)$ = impulse at $x = ns$.

The Laplace transform of $f^*(x)$ is known as the Z-transform $F(z)$.

$$F(z) = \mathcal{L}\,\{f^*(x)\} = \mathcal{L}\,\{\sum_{n=0}^{\infty} f(x)\,\delta(x - ns)\}$$

$$= \int_0^{\infty} \sum_{n=0}^{\infty} f(x)\,\delta(x - ns)\,e^{-x\sigma}\,dx$$

$$= \sum_{n=0}^{\infty} f(ns)\,e^{-ns\sigma}$$

Letting $z = e^{s\sigma}$

$$F(z) = \sum_{n=0}^{\infty} f(ns)\,z^{-n} \qquad (18)$$

It may be seen that the expression for the array factor (Eq. 17) and the expression for the Z-transform (Eq. 18) differ only in that the array factor $E(z)$ is a finite sum and the Z-transform $F(z)$ is an infinite sum. The array factor may be expressed as the difference between two related Z-transforms.

$$E(z) = \sum_{n=0}^{N-1} A_n z^{-n} = \sum_{n=0}^{\infty} f(ns)\,z^{-n} - \sum_{n=N}^{\infty} f(ns)\,z^{-n}$$

$$= F(z) - G(z)\,. \qquad (19)$$

The amplitude at any element, A_n, is taken to be amplitude of the sampled function at ns. That is:

$$A_n = f(ns)\,.$$

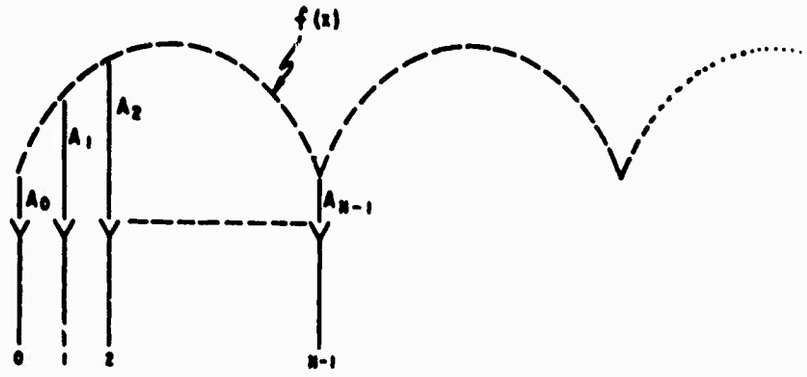

Fig. 7 Linear Array with Extended Envelope of Array Excitation

A relation can be found between the two infinite sums F(z) and G(z), if f(x) is a periodic function. As shown in Fig. 7 an appropriate choice for f(x) is the periodic extension of the envelope of the aperture illumination. For a periodic function:

$$f(x - Ns) = \pm f(x) . \tag{20}$$

Cheng and Ma have shown that G(z) can be expressed in terms of F(x) by:

$$G(z) = \pm z^{-(N - 1)} [F(z) - f(0)] . \tag{21}$$

where f(0) is the amplitude at the first (n = 0) element. The plus and minus signs refer to the periodicity established in Eq. 20. By substituting the expression obtained for G(z) in Eq. 21 into Eq. 19:

$$E(z) = [1 \mp z^{-(N - 1)}] F(z) \pm f(0) z^{-(N - 1)} . \tag{22}$$

In Eq. 22 the array factor E(z) is expressed in a closed form as a function of F(z), the Z-transform of the extended aperture illumination. If F(z) is known, E(z) can be determined regardless of the number of elements used. For antenna analysis the excitation is used to find F(z), and the array factor E(z) can then be determined. Cheng and Ma (Ref. 20) have

discussed techniques for analyzing the beamwidths, nulls, and sidelobes directly in terms of z without using:

$$z = e^{-j\frac{2\pi}{\lambda}(\sin\theta - \sin\theta_0)},$$

to return to angular coordinates.

For array pattern synthesis a Z-transform E(z) which approximates the desired array factor is chosen, and Eq. 22 is solved for F(z). The first N coefficients of F(z), f(0); f(s); f(2s);...f([N - 1]s) are the desired element excitations and the envelope f(x) is the transform of F(z). The restriction of periodicity (Eq. 20) has been removed by Christiansen (Ref. 22) and by Cheng (Ref. 23). Christiansen has also described a procedure for using a known Z-transform as a generating function for new array factors and their excitations.

Element Factor and Gain of Planar Arrays

The gain of a uniformly illuminated and lossless aperture of Area A, with a broadside beam, is given by:

$$G_0 = 4\pi\frac{A}{\lambda^2} \tag{23}$$

If the aperture is considered as a matched receiver, then the amount of energy collected from a scanned beam is proportional to its projected area. The gain on scanning may, therefore, be described by:

$$G(\theta) = 4\pi\frac{A\cos\theta}{\lambda^2}\,. \tag{24}$$

The variation of gain with the cosine of the scan angle agrees with the

equivalent variation in beamwidth of Eq. 14. The gain may be expressed in terms of the actual beamwidth, giving, from Eqs. 14 and 24:

$$G = \frac{32,000}{\theta_B \phi_B} , \tag{25}$$

where θ_B and ϕ_B are the beamwidths (in degrees) in the two principal planes. This equation may be used for most practical cases without regard to the actual aperture distribution that produced the beam.

If the aperture is made up of N equal, discrete, radiating elements and is matched to accept power like the continuous aperture, then the contribution to the overall gain of all elements is the same and

$$G = N G_e , \tag{26}$$

where G_e is the gain per element. It follows from Eq. 24 that the element gain pattern is:

$$G_e = 4\pi \frac{A}{N\lambda^2} \cos\theta , \tag{27}$$

and the normalized radiation pattern of the element, or <u>element pattern</u>, is

$$E_e(\theta) = \sqrt{\cos\theta} . \tag{28}$$

The element pattern will be considered in greater detail in Section IV. It had already been noted that under ideal conditions it is very similar to the obliquity factor $\frac{1}{2}(1 + \cos\theta)$ and only differs markedly near end-fire.

For a given element spacing s, the total number of radiators, N, in the area A is $N = \frac{A}{s^2}$, and Eq. 27 gives

$$G_e = 4\pi \left(\frac{s}{\lambda}\right)^2 \cos\theta .$$

When the element spacing is $s = \frac{\lambda}{2}$, then

$$G_e = \pi \cos\theta \,, \tag{29}$$

and the peak antenna gain in the direction of scan, θ_0 is

$$G(\theta) = N \pi \cos\theta_0 \,. \tag{30}$$

The effects of the element pattern are most marked with wider beams. Figure 8 shows the array and element factors and the resulting pattern for a 10-element array scanned to 60°. The pattern maximum is noted to occur at less than 60° because the gain of the element pattern increases towards broadside. The pattern value at 60° is cos 60° = 0.5 in power or 0.707 in amplitude, relative to the maximum at broadside,

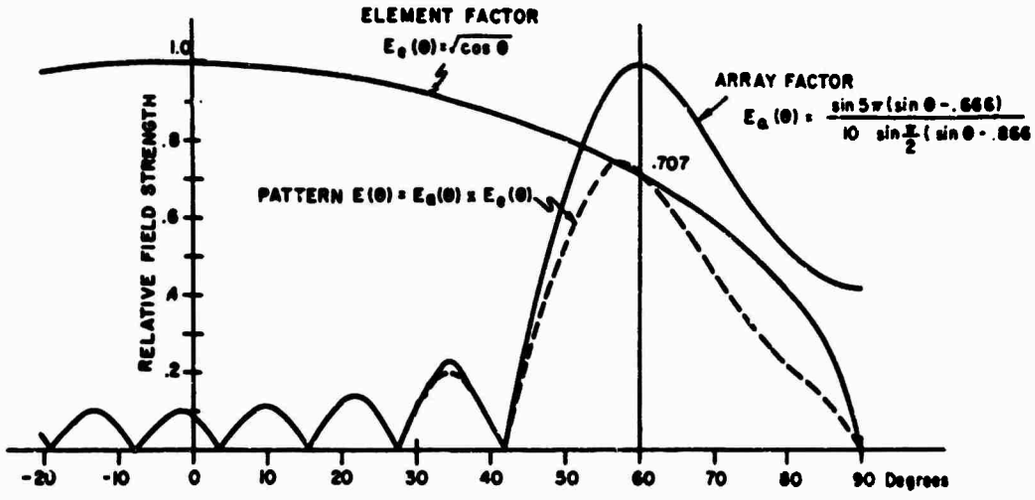

Fig. 8 Ten-Element Linear Array Scanned to 60°; Element Spacing $s = \lambda/2$

as expected. The sidelobes in the general region of broadside are not reduced since in that region the element pattern is approximately unity. Relative to the beam maximum, therefore, the sidelobes near broadside are increased in amplitude by approximately $\frac{1}{\sqrt{\cos\theta}} = \sqrt{2}$.

III. PLANAR ARRAYS AND BEAM STEERING

Planar Arrays

A planar array is capable of steering the beam in two dimensions. In a spherical coordinate system the two coordinates θ and ϕ define points on the surface of a unit hemisphere. As shown in Fig. 9, θ is the angle of scan measured from broadside and ϕ is the plane of scan measured (arbitrarily) from the x axis. Von Aulock (Ref. 24) has presented a simplified method for visualizing the patterns and the effect of scanning. He considers the projection of the points on a hemisphere onto a plane (Fig. 10); the axes of the plane are the direction cosines $\cos\alpha_x$, $\cos\alpha_y$. For any direction on the hemisphere the direction cosines are

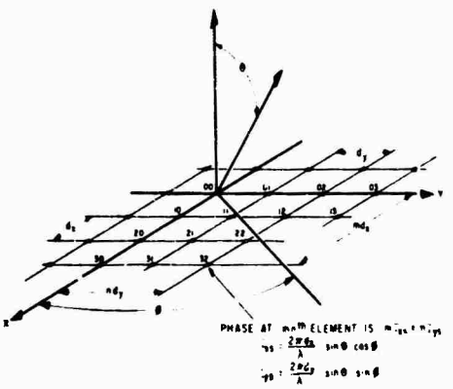

Fig. 9 Planar Array Element Geometry and Phasing

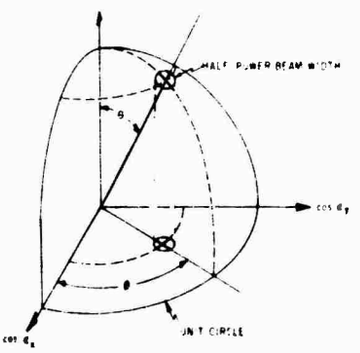

Fig. 10 Projection of Points on a Hemisphere onto the Plane of the Array

$$\cos\alpha_x = \sin\theta\cos\phi ,$$

$$\cos\alpha_y = \sin\theta\sin\phi .$$

The direction of scan is indicated by the direction cosines $\cos\alpha_{xs}$, $\cos\alpha_{ys}$. Here, the plane of scan is defined by the angle ϕ measured counterclockwise from the $\cos\alpha_x$ axis and is given by:

$$\phi = \tan^{-1} \frac{\cos\alpha_{ys}}{\cos\alpha_{xs}} .$$

The angle of scan θ is determined by the distan e of the point ($\cos\alpha_{xs}$, $\cos\alpha_{ys}$) from the origin. This distance is equal to $\sin\theta$. For this reason a representation of this sort is called "$\sin\theta$ space." A feature of $\sin\theta$ space is that the antenna pattern shape is invariant to the direction of scan. As the beam is scanned, every point on the plot is translated in the same direction and by the same distance as in the beam maximum.

The region inside the unit circle where

$$\cos^2\alpha_x + \cos^2\alpha_y \leq 1$$

is defined as "real space," the hemisphere into which energy is radiated. The infinite region outside of the unit circle is referred to as "imaginary space." Although no power is radiated into imaginary space, the concept is useful for observing the motion of grating lobes as the array is scanned. In addition the pattern in imaginary space represents stored energy and contributes to the element impedance in the array.

The most common element lattices employ either a rectangular or a triangular grid. As shown in Fig. 9 the mn^{th} element is located at (md_x, nd_y). The triangular grid may be thought of as a rectangular grid where every other element has been omitted. In this case only every other value of mn contains an element. The element locations can be defined by requiring that (m + n) is even.

Calculations for the element steering phases are greatly simplified by the adoption of the direction cosine coordinate system. In this system

the linear phase tapers defined by the beam steering direction ($\cos\alpha_{xs}$, $\cos\alpha_{ys}$) may be summed at each element so that the phasing at the mn^{th} element is given by:

$$\psi_{mn} = m T_{xs} + n T_{ys} ,$$

where $T_{xs} = \frac{2\pi}{\lambda} d_x \cos\alpha_{xs}$ = element to element phase shift in the x direction, and $T_{ys} = \frac{2\pi}{\lambda} d_y \cos\alpha_{ys}$ = element to element phase shift in the y direction.

The array factor of a two-dimensional array may be calculated by summing the vector contribution of each element in the array at each point in space. For an array scanned to a direction given by the direction cosines, $\cos\alpha_{xs}$ and $\cos\alpha_{ys}$, the array factor of an M x N rectangular array of radiators may be written as:

$$E_a(\cos\alpha_{xs}, \cos\alpha_{ys}) = \sum_{m=0}^{M-1} \sum_{n=0}^{N-1} \left| A_{mn} \right| e^{j\, m(T_x - T_{xs}) + n(T_y - T_{ys})} .$$

where $T_x = \frac{2\pi}{\lambda} d_x \cos\alpha_x ,$

$T_y = \frac{2\pi}{\lambda} d_y \cos\alpha_y ,$

and A_{mn} = amplitude of the mn^{th} element.

An array may be visualized as having an infinite number of grating lobes only one of which (namely the main beam) is desired in real space. It is convenient to plot the position of the grating lobes when the beam is phased for broadside and observe the motion of these lobes as the beam is

scanned. Figure 11 shows the grating lobe locations for both rectangular and triangular spacings. For a rectangular array the grating lobes are located at

$$\cos\alpha_{xs} - \cos\alpha_x = \pm \frac{\lambda}{d_x} \cdot p$$

$$p, q = 0, 1, 2, \ldots$$

$$\cos\alpha_{ys} - \cos\alpha_y = \pm \frac{\lambda}{d_y} \cdot q$$

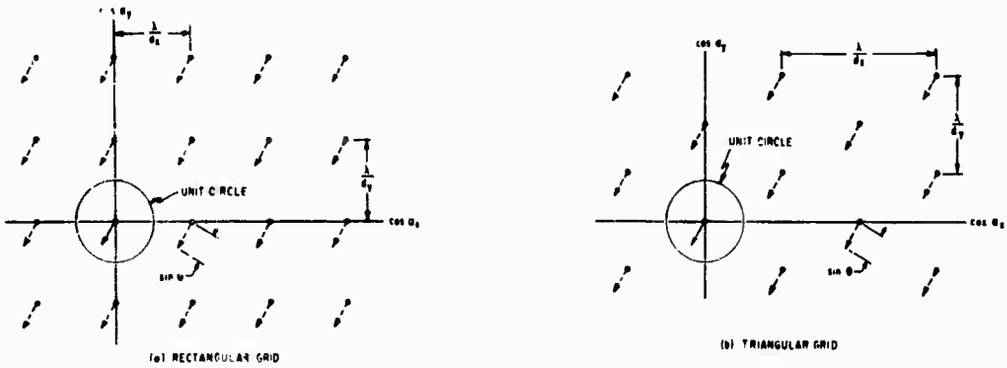

(a) RECTANGULAR GRID (b) TRIANGULAR GRID

Fig. 11 Grating Lobe Positions for Rectangular and Triangular Grids Showing the Motion of the Lobes as the Beam Is Scanned an Angle θ

The lobe at $p = q = 0$ is the main beam. A triangular grid is more efficient for suppressing grating lobes than a rectangular grid (Ref. 25) so that for a given aperture size fewer elements are required. If the triangular lattice contains elements at (md_x, nd_y) where $m + n$ is even, then the grating lobes are located at

$$\cos\alpha_{xs} - \cos\alpha_x = \pm \frac{\lambda}{2\, d_x} \cdot p$$

$$\cos\alpha_{ys} - \cos\alpha_y = \pm \frac{\lambda}{2\, d_y} \cdot q$$

where $p + q$ is even.

Since only one main lobe is normally desired in real space, an appropriate design will place all but one maximum in imaginary space for all angles of scan. With scanning, lobes that were originally in imaginary space may move into real space if the element spacing is greater than $\lambda/2$. As the array is scanned away from broadside, each grating lobe (in $\sin\theta$ space) will move a distance equal to the sine of the angle of scan and in a direction determined by the plane of scan. To insure that no grating lobes enter real space, the element spacing must be chosen so that for the maximum scan angle θ_m the movement of a grating lobe by $\sin\theta_m$ does not bring the grating lobe into real space. If a scan angle of 60° from broadside is required for every plane of scan, no grating lobes may exist within a circle of radius $1 + \sin\theta_m = 1.866$. The square grid that meets this requirement has:

$$\frac{\lambda}{d_x} = \frac{\lambda}{d_y} = 1.866 \quad \text{or} \quad d_x = d_y = 0.536\lambda \ .$$

Here, the area per element is:

$$d_x d_y = (0.536\lambda)^2 = 0.287\lambda^2 \ .$$

For an equilateral triangular array, the requirement is satisfied by:

$$\frac{\lambda}{d_y} = \frac{\lambda}{\sqrt{3}\, d_x} = 1.866 \text{ or } d_y = 0.536\lambda, \ d_x = 0.309\lambda \ .$$

Recalling that elements are located only at every other value of mn, the area per element is:

$$2\, d_x d_y = 2\ (0.536\lambda)\ (0.309\lambda) = 0.332\lambda^2 \ .$$

For the same amount of grating lobe suppression, the square geometry requires approximately 16% more elements.

Element Phasing Calculations

A computer is required to perform the steering computations for a phased array antenna. It can compensate for many of the known phase errors caused by the microwave components, the operating environment, and the physical placement of the elements. For example, if the insertion and differential phase variations (which may occur from phase shifter to phase shifter) are known, they may be taken into account in the computations. Compensation can also be made for known temperature variations across the array that induce phase errors. Finally, many feeds (e.g., optical and series feeds) do not provide equal phase excitation at the input to each phase shifter. The relative phase excitation caused by these feeds will be a known function of frequency. The computer must, in these cases, provide a correction based on the location of the element in the array and on the frequency of operation.

For a large array with thousands of elements, many calculations are required to determine the phasing of the elements. These calculations must be performed in a short period of time. The use of the orthogonal phase commands $m\,T_{xs}$, $n\,T_{ys}$ helps to minimize these calculations. Once the element to element phase increments T_{xs}, T_{ys} have been computed for a given beam pointing direction, the integral multiple of T_{xs} may be used to steer rows of elements, and the integral multiples of T_{ys} may be used to steer the columns (Fig. 9). If an adder is located at each element, the row and column values of $m\,T_{xs}$ and $n\,T_{ys}$ may be summed at the element. It is also possible to put two phase shifters in

series so that the summation can be done at microwave frequencies. This may be implemented with the use of a series feed, as shown in Fig. 12. Here the row steering commands apply to an entire row simultaneously. An amplifier between a row phase shifter and a series feed

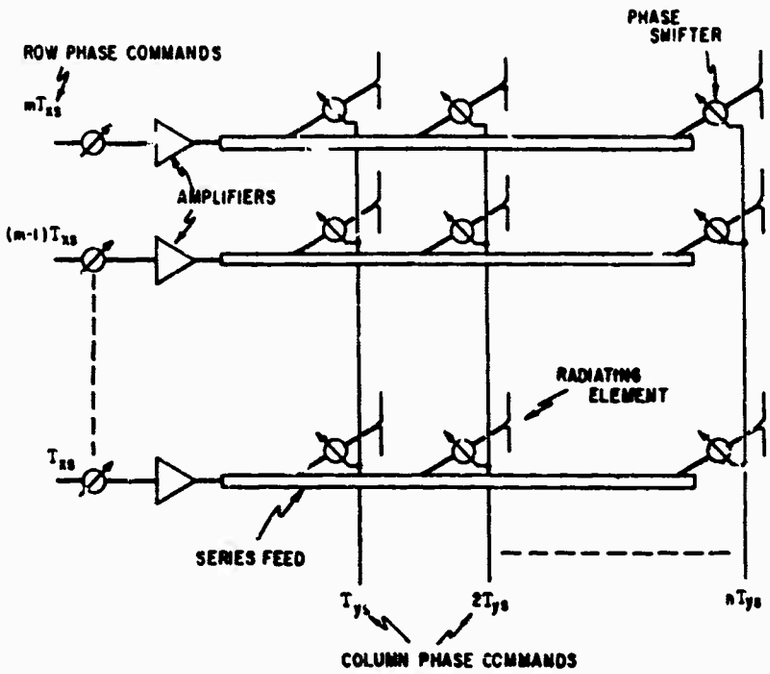

Fig. 12 Microwave Addition of Orthogonal Phasing Commands by Means of a Series Feed

is desirable so that the generated power does not have to take the loss of two phase shifters in series. In addition the row phase shifters must be capable of accurate phasing since their errors will add to the errors of the column phase shifters. Since relatively few row phase shifters are required, it is reasonable to make them considerably more accurate than the phase shifters in the array. Any corrections for a phase taper across the series feed may be applied for an entire column if all the feeds have the same phase characteristics.

Another technique for decreasing the required phase commands is through the use of subarrays. In this case, a second phase shifter and amplifier are placed behind each subarray (Section VII). The phases computed for the elements in one subarray may be used for similar elements in every subarray. In addition, the phases of the phase shifters behind each subarray must be computed. Once again, these additional phase shifters should be very accurate.

A large array requires many electronic drivers and very complex wiring to provide the drivers with control signals and energy. The problem is complicated by the relatively close spacing of elements in the array. Further, many phase shifters are of the digital type and require a driver and control signal for each bit. The problems are eased somewhat in the systems described above with two RF phase shifters in series since many elements may use the same steering commands and the same drivers. In other systems it may be necessary to provide each element in the array with a different phase command. This command may include a phase correction such as for a spherical phase front incident on the input aperture. An adder at each element (with perhaps some bias for the spherical correction) will provide rapid steering through the use of row and column steering commands. If high speed is not required, the computer may compute sequentially and store the phases for each of the elements. All the phase commands could then be delivered simultaneously.

IV. APERTURE MATCHING AND MUTUAL COUPLING (Refs. 8, 26, and 27)

Significance of Aperture Matching

By its very nature an antenna is a device that acts as a transformer to provide a good match between a source of power and free space. If the antenna is not matched to free space, power will be reflected back toward the generator, resulting in a loss in radiated power. In addition a mismatch produces standing waves on the feed line to the antenna. The voltage at the peaks of these standing waves is $(1 + |\Gamma|)$ times greater than the voltage of a matched line, where Γ is the voltage reflection coefficient. This corresponds to an increased power level that is $(1 + |\Gamma|)^2$ times as great as the actual incident power. Therefore, while the antenna is radiating less power, individual components must be designed to handle more peak power. With antennas that do not scan, the mismatch may often be tuned out by conventional techniques, preferably at a point as close to the source of the mismatch as possible.

In a scanning array the impedance of a radiating element varies as the array is scanned, and the matching problem is considerably more complicated. Compared to a conventional antenna where mismatch affects only the level of the power radiated and not the shape of the pattern, spurious lobes in the scanning array may appear as a consequence of the mismatch. Further, there are conditions where an antenna that is well matched at broadside may have some angle of scan at which most of the power is reflected.

The variation in element impedance and element pattern is a manifestation of the mutual coupling between radiating elements that are in close proximity to one another (less than a wavelength for scanning arrays). In the sections to follow, the nature of this mutual coupling will be discussed, along with its effects on element impedance and element pattern. Some simple methods will be described for computing the impedance in an array and for measuring the element pattern and impedance without actually building a large array. It will be seen that the impedance properties of the array are dependent on not only the form of the element and the radiating structure, but also on the feed structure, the type of phase shifting element, and the amplitude distribution across the array.

For a practical design, there are two empirical techniques which are of great value:

1. Waveguide simulators provide a means for determining the element impedance in an infinite array with the use of only a few elements. The effectiveness of a matching structure based on these measurements may also be determined in the simulator.
2. The element pattern obtained by exciting one element and terminating its neighbors is the best overall measure of array performance. If a large reflection occurs at some angle of scan, this will be exhibited by a null in the element pattern.

Both of these techniques will be discussed later in this section.

Effects of Mutual Coupling

When two antennas (or elements) are widely separated, the energy coupled between them is small and the influence of the receiving antenna

on the current excitation and pattern of the transmitting antenna is negligible. As the antennas are brought closer together, the coupling between them will increase In general, the magnitude of the coupling will be influenced by the distance between the elements, the pattern of the elements, and the structure in the vicinity of the elements. For example, the radiation pattern of a dipole has a null in the $\theta = \pm 90°$ direction and is omnidirectional in the $\theta = 0°$ plane. Therefore it can be expected that dipoles in line will be loosely coupled and parallel dipoles will be tightly coupled. When an element is placed in an array of many elements, the effects of coupling are sufficiently strong that the pattern and impedance of the element in the array are drastically altered.

For the purposes of this discussion the terms element pattern and element impedance refer to an element in its operating environment (i.e. in an array with its neighboring elements excited). In the array each excited element couples to every other element. The coupling from several elements to a typical central element, element 00, is shown in Fig. 13. The $C_{mn,pq}$ are mutual coupling coefficients relating the voltage (amplitude and phase) induced in the mn^{th} element to the voltage excitation

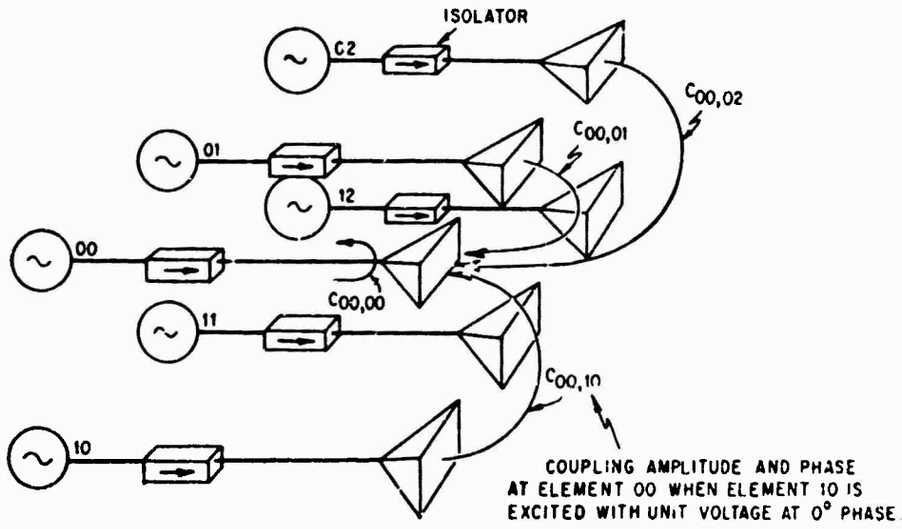

Fig. 13 Coupled Signals to a Central Element from Neighboring Elements

at the pq^{th} element. The coupled signals add vectorially to produce a wave traveling toward the generator of element 00, which appears to be a reflection from the radiator of element 00. As the phases of the neighboring elements are varied to scan the beam, the vector sum of the coupled signals changes and causes an apparent change in the impedance of element 00. For some scan angles the coupled voltages will tend to add in phase causing a large reflection and possibly the loss of the main beam. Large reflections often occur at scan angles just prior to the emergence of a grating lobe into real space, but in some instances such reflections may occur at smaller scan angles.

The description of the impedance variation given above made no reference to the feed network or the phase shifters and assumed that the only coupling between elements is via the radiating aperture. The coupling coefficients would be measured, and by superposition the phased voltage contributions from every element in the array (or at least those in the immediate vicinity) would be added vectorially to produce the voltage reflected back toward the generator. In a practical array the impedance variation does depend upon the feed system and the phase shifter. If these are taken into account, the impedance variation may be different from that which the above model might predict. Still, this description provides insight to the intrinsic impedance variation of the aperture when it is isolated from other effects as in the case where each element has an independent feed (e.g. its own generator and isolator). In this case it is a simple matter to measure the VSWR in any line and determine exactly the extent of the impedance and mismatch variation. For many feeding systems this is not possible, and a measurement of the reflected energy will provide erroneous information and a false sense of

security. Unless all of the reflections are collimated back at some central point (or independent feeds are used), some of the reflected energy will generally be re-reflected and contribute to large undesirable sidelobes. This will be discussed under nonisolating feeds.

For large arrays the impedance of an element located near the center of the array is often taken as typical of the impedance of every element in the array. As might be expected this element is most strongly influenced by elements in its immediate vicinity. When the array is scanned the influence of elements several wavelengths distant is also significant. For dipoles above a ground plane the magnitude of the coupling between elements decays rapidly with distance. For a reasonable indication of array performance, an element in the center of a 5 by 5 array may be taken as typical of an element in a large array. For dipoles with no ground plane (or the dual, slots in a ground plane) the coupling between elements does not decay so rapidly, and a 9 by 9 array appears reasonable. For an array of open ended waveguides, a 7 by 7 array should suffice. If accurate prediction of the array performance is required, many more elements will be needed than are indicated above (Refs. 27 and 28).

It is often convenient to assume that the array is infinite in extent, has a uniform amplitude distribution, and has a linear phase taper from element to element. In this manner every element in the array sees exactly the same environment, and the calculations for any element apply equally to all. These assumptions provide a significant simplification to the calculation of the element impedance variations presented in subsequent sections. In addition impedance measurements made in simulators correspond to the element impedance in an infinite array. In spite of the assumptions the infinite array model has predicted with good accuracy the

array impedance and the impedance variations. Even arrays of modest proportions (less than 100 elements) have been in reasonable agreement with the results predicted for an infinite array (Ref. 29).

Element Pattern

The radiation pattern of an array is the product of the element pattern and the array factor as previously defined,

$$E(\theta, \phi) = E_e(\theta, \phi)\, E_a(\theta, \phi) .$$

The array factor is determined by the geometric disposition of the elements and their phasing on the assumption that the elements are isotropic and that there is no mutual coupling. Its peak value is independent of the scan angle. The element pattern is the actual element radiation pattern taken in the array in the presence of all other elements and taking into account all coupling effects and mismatches. It follows from this definition that as the array is being scanned, the peak of the radiation pattern $E(\theta, \phi)_{max}$ will trace out the element pattern. The element pattern may be obtained experimentally by exciting one typical element and terminating each of the other elements in a matched load. The number of terminated elements used in practice is the same as the number used for providing a central element with a large array environment, as discussed above. If there are any positions of scanning where a main beam does not form or where a large loss in gain occurs, it will show up as a null in the element pattern.

From energy considerations the gain of a perfectly matched array will vary as the projected aperture area, as given in Eq. 24:

$$G(\theta) = \frac{4\pi A}{\lambda^2} \cos\theta .$$

Assuming that each of the N elements in the array share the gain equally, the gain of a single element is:

$$G_e(\theta) = \frac{4\pi A}{N\lambda^2} \cos\theta .$$

If the element is mismatched, having a reflection coefficient $\Gamma(\theta, \phi)$ that varies as a function of scan angle, then the element gain pattern is reduced to:

$$G_e(\theta) = \frac{4\pi A}{N\lambda^2} (\cos\theta) (1 - |\Gamma(\theta, \phi)|^2) .$$

The element pattern may be seen to contain information pertaining to the element impedance (Ref. 30). The difference between the power radiated in the element pattern and the power delivered to the antenna terminals must equal the reflected power. In terms of the radiation patterns of the scanning array, this means that since the scanned antenna patterns trace out the element pattern it follows that the average power lost from the scanned patterns is equal to the power lost from the element pattern owing to reflections. It is not enough to match one element in the presence of all its terminated neighbors. The element will deliver power to its neighbors: this loss in power corresponds to the average power lost when scanning. An ideal, although not necessarily realizable element pattern, would place all of the radiated power into the scan region giving a pattern like a cosine on a pedestal, thereby providing maximum antenna gain for the number of elements used.

Thinned Arrays

The number of radiating elements in an array may be reduced to a fraction of those needed to completely fill the aperture without suffering serious degradation in the shape of the main beam. However, the average sidelobes are degraded in proportion to the number of elements removed. The element density may be thinned so as to effectively taper the amplitude distribution; the spacing is such that no coherent addition can occur to form grating lobes. A thinned aperture, where elements have been removed randomly from a regular grid (Ref. 31) is shown in Fig. 14.

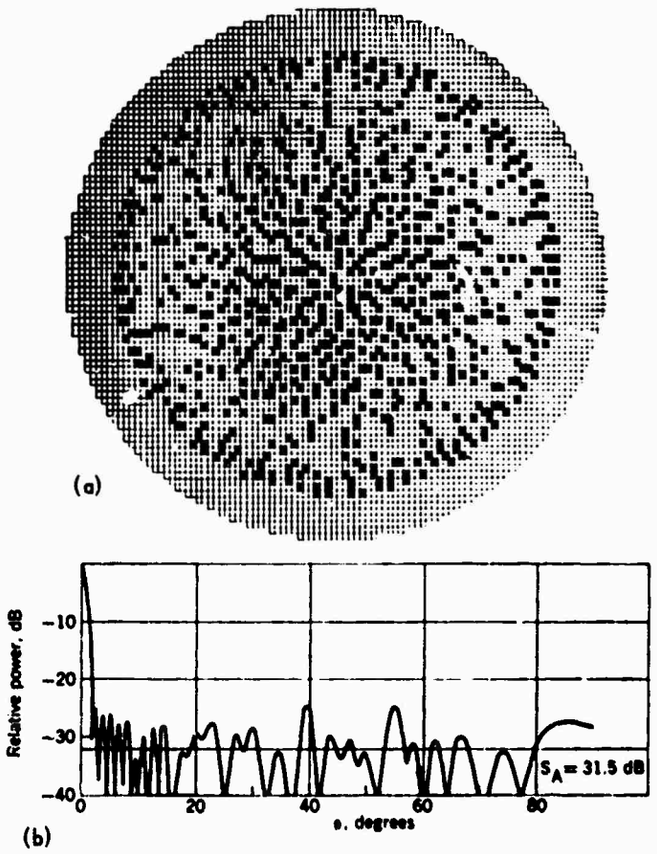

Fig. 14 (a) Thinned Array with 4000-Element Grid Containing 900 Elements. (b) Typical Pattern for Thinned Array (from Willey, Ref. 31). (S_A = Average Sidelobe Level)

The gain is that due to the actual number of elements $N G_e(\theta)$, but the beamwidth is that of the full aperture. For example, if the array has been thinned so that only 10% of the elements are used, then the gain of the array will drop by 10 db. However, since the main beam is virtually unchanged, about 90% of the power is delivered to the sidelobe region.

If the removed elements (in a regular thinned array) are replaced with matched loads, the element pattern is identical to that of one in the regular array with all elements excited. The element pattern is independent of the array excitation, and the same fractional amount of power will be lost (due to mismatch) whether the array is thinned, tapered, or uniformly illuminated. It should be noted that the concept of an element pattern which applies equally to every element is valid only when isolating feeds are used.

A thinned array may also be implemented with an irregular element spacing, although this is not common. In this case the element gain (and impedance) will vary from element to element depending upon the environment of a given element. To obtain the gain of the array, it is necessary to sum all the different element gains $G_{en}(\theta)$. Thus:

$$G(\theta) = \sum_n G_{en}(\theta) .$$

Impedance Variation of Free Space

Although this discussion is concerned with array antennas, it is of interest to examine the case of a large continuous aperture which may be considered to be the limiting case of an array of many very small elements (Ref. 32). If the aperture is matched to a wave at normal incidence, the mismatch may be calculated by determining the impedance variation of a plane wave as observed from the aperture. The impedance of the plane wave as viewed from the aperture is merely the ratio of the projection

onto the plane of the aperture of a fixed component of the electric intensity vector $\bar{E}$, to the orthogonal component of the magnetic intensity vector $\bar{H}$. At broadside the impedance is the ratio of $\bar{E}$ to $\bar{H}$.

$$R_o = \frac{\bar{E}}{\bar{H}} = 120\pi \text{ ohms} .$$

For scanning in the E plane ($\phi = 0$) the $\bar{E}$ vector is foreshortened by $\cos\theta$ and the impedance is

$$\eta_E = \frac{\bar{E}\cos\theta}{\bar{H}} = R_o \cos\theta .$$

For scanning in the H plane, the $\bar{H}$ vector is foreshortened and the $\bar{E}$ vector remains constant so that:

$$\eta_H = \frac{\bar{E}}{\bar{H}\cos\theta} = \frac{R_o}{\cos\theta} .$$

It may be seen that in the principal scan planes the resistance at a 60° scan angle differs from the broadside resistance by a factor of two and will produce a 2:1 VSWR in an aperture that had been matched at broadside. For scanning in any plane, the normalized impedance as viewed from the aperture is given by:

$$\eta(\theta, \phi) = \frac{R(\theta, \phi)}{R_o} = \frac{1 - \sin^2\theta \cos^2\phi}{\cos\theta} .$$

The impedance of a medium is seen to be dependent upon the observation angle, and the impedance variation of a scanning aperture is a natural consequence of this dependence. The continuous aperture described above appears to represent a lower limit to the impedance variation with scanning. This is indicated by Allen's results (Ref. 33) where the impedance variation with scanning was calculated for dipoles above a ground plane.

In spite of increased mutual coupling, or perhaps because of it, the more closely the dipoles were spaced, the smaller the impedance variation with scanning (Fig. 15). Although the impedance variation decreased, the absolute impedance of the dipoles also decreased making them more difficult to match at broadside. It is expected that to obtain an impedance variation smaller than that of free space some impedance compensation must be used. Compensation techniques will be discussed later in this section.

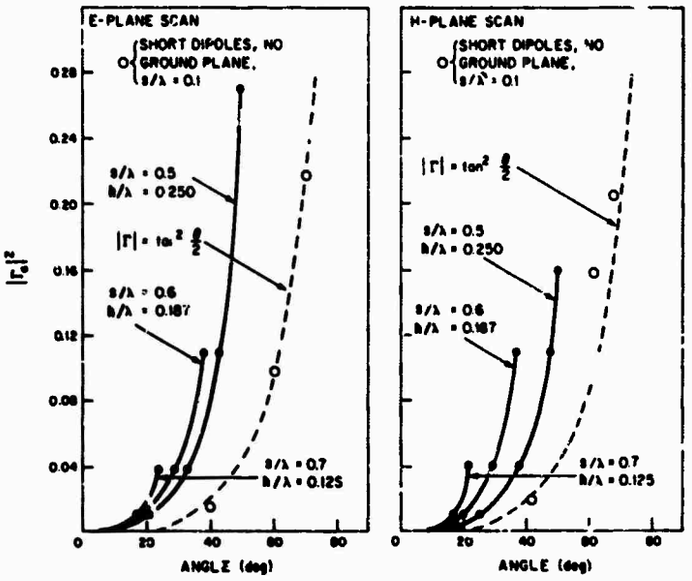

Fig. 15 Scanned Mismatch Variation for Different Element Spacings (h/λ Is Dipole Spacing above Ground Plane) (after Allen, Ref. 33)

Element Impedance

To simplify the computation of the element impedance in an array and the variation in impedance as the array is scanned, it is usually assumed that an isolating type of feed is used to distribute power to the individual elements. The simplest example of an isolating feed is a

separate generator and isolator behind each radiating element (Fig. 13). In this manner, the only coupling between elements occurs at the radiating aperture. To a lesser extent directional couplers and matched hybrids may also provide an isolating feed (Ref. 26). An equivalent circuit for each element in an array using isolating feeds is given in Fig. 16. An

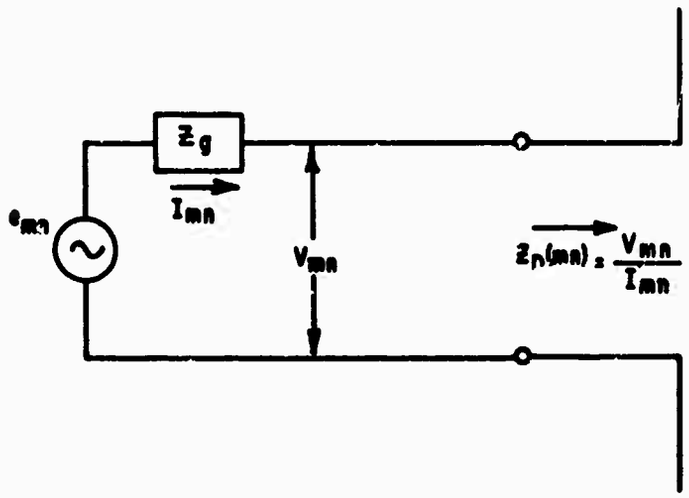

Fig. 16 Equivalent Circuit for an Independently Fed Dipole in an Array

example of a nonisolating feed is the space feed shown in Fig. 36. Here it is apparent that mutual coupling occurs at both the feed aperture and at the radiating aperture. This problem has been analyzed by Schwartzman (Ref. 34) who has obtained good results using a more complex equivalent circuit.

There are two general techniques available for computing the impedance variation of the elements in an array. Each has its own advantages and disadvantages. One technique uses the isolated element impedance and the mutual impedances between elements to compute the active element impedance. This technique is convenient for the analysis of thin dipoles where the mutual impedances between elements may be readily computed

(efs. 35 and 36). For other types of elements (e.g. open ended waveguides), the mutual impedances are not easily computed and the scattering matrix technique is more useful. The scattering method uses the coupling coefficients between elements, which may be readily measured by exciting one element and measuring the amplitude and phase of the voltage coupled to the other elements. Both of these techniques will be discussed, and an infinite array technique will be introduced.

Scattering Matrix Formulation

The simplest and most straightforward method for computing the variation in reflection coefficient (and impedance) is by means of the scattering matrix of mutual coupling coefficients. The mutual coupling coefficients may be easily measured for elements of all types by exciting one element and terminating each of the other elements in a matched load. The ratio of the induced voltage at element mn to the excitation voltage at element pq gives the amplitude and phase of the coupling coefficient $C_{mn, pq}$. Once these coefficients are determined it is a simple matter to compute the mismatch for any set of phasing conditions.

Consider the two-element array shown in Fig. 17 where each element is provided with an isolating feed. The incident wave in each ele-

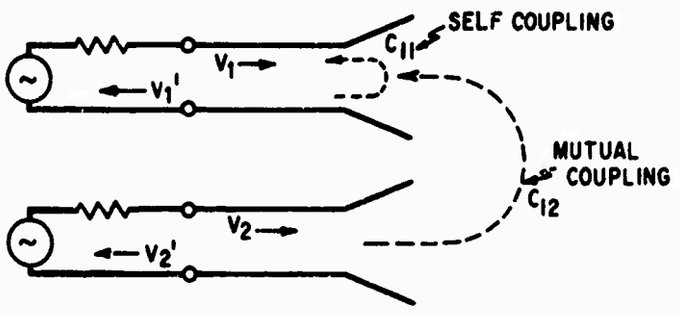

Fig. 17 Scattering Matrix Model for Two Element Array

ment is represented by V_1, V_2; the total reflected wave in each element is represented by V_1', V_2'. It should be apparent that the total reflected wave in any element is the vector sum of the couplings from all elements including its own reflection as a self coupling.

$$V_1' = C_{11}\ V_1 + C_{12}\ V_2$$

$$V_2' = C_{21}\ V_1 + C_{22}\ V_2 \ .$$

The reflection coefficient in each element is obtained by dividing the reflected voltage by the incident voltage in the channel.

$$\Gamma_1 = \frac{V_1'}{V_1} = C_{11}\ \frac{V_1}{V_1} + C_{12}\ \frac{V_2}{V_1} \ .$$

$$\Gamma_2 = \frac{V_2'}{V_2} = C_{21}\ \frac{V_1}{V_2} + C_{22}\ \frac{V_2}{V_2}$$

Note that all the quantities must contain both phase and amplitude, and that as the phases of V_1, V_2 are varied to scan the beam, the reflection coefficients (Γ_1, Γ_2) will vary. Although only two elements have been used in this example, the technique is completely general. For a large array the reflection coefficient of the nm^{th} element would be given by:

$$\Gamma_{mn} = \sum_{\text{all } pq} C_{mn,\,pq}\ \frac{V_{pq}}{V_{mn}} \ .$$

The general case is treated in more detail by Oliner and Malech (Ref. 8). No restrictions need be placed on either the amplitude or phase of the excitation at each element. There are also no restrictions placed on the spacing between the elements so long as the coupling coefficients are measured for the spacing and environment to be used. A considerable

simplification is obtained by assuming that each of the elements sees the same environment and has the same voltage excitation.

Then $\frac{|V_{pq}|}{|V_{mn}|}$ will always be unity, and the reflection coefficient at element mn is merely the sum of the mutual coupling coefficients with the excitation phase at each element taken into account.

$$\Gamma_{mn} = \sum_{\text{all } pq} C_{mn,pq}\, e^{j(m-p)T_{xs}}\, e^{j(n-q)T_{ys}},$$

where $e^{j(m-p)T_{xs}}$ and $e^{j(n-q)T_{ys}}$ give the relative phase excitations in the x and y directions of the pq^{th} element with respect to the mn^{th} element. The impedance variation relative to a matched impedance at broadside may be obtained immediately from

$$\frac{Z_{mn}(\theta,\phi)}{Z_{mn}(0,0)} = \frac{1+\Gamma_{mn}(\theta,\phi)}{1-\Gamma_{mn}(\theta,\phi)}$$

Mutual Impedance Method

The mutual impedance technique is formulated by relating the voltages to the currents at the antenna terminals. The parameter of interest is the impedance looking into the antenna terminals (i.e. $\frac{V_{mn}}{I_{mn}}$), and is referred to as $Z_D(mn)$, the driving impedance, or the active impedance. The equations relating the terminal voltages and currents are written as:

$$V_{mn} = \sum_{\text{all } pq} Z_{mn,pq}\, I_{pq}$$

With the assumption of an isolating feed, the equivalent circuit of Fig. 16 applies and the equations relating the terminal voltages to the generator voltages are:

$$V_{mn} = e_{mn} - Z_g I_{mn} .$$

The double subscript notation indicates the row and column placement of each of the elements in the array. $Z_{mn, pq}$ is the ratio of the voltage induced across the terminals in the mn^{th} element to the current in the pq^{th} element. Combining these two sets of equations:

$$e_{mn} - Z_g I_{mn} = \sum_{\text{all } pq} Z_{mn, pq} I_{pq} .$$

If the generator voltages and the mutual impedances are known, the currents may be determined. Once the current in an element is determined the driving impedance is given by $Z_D(mn) = \frac{e_{mn}}{I_{mn}} - Z_g$. To solve for the currents requires the inversion of a large matrix equal in size to the square of the number of elements to be included. In practice, a fraction of the elements in the array may be used, and a typical element in the center of the array may be selected as having the typical impedance variation. If it is assumed that the current excitation on each of the elements is identical except for a linear phase slope (i.e. regular, infinite array approximation), it is not necessary to solve for the currents and the calculations are simplified considerably. In this case:

$$V_{mn} = \sum_{\text{all } pq} Z_{mn, pq} I_{pq} ,$$

and

$$Z_D(mn) = \frac{V_{mn}}{I_{mn}} = \sum_{\text{all } pq} Z_{mn, pq} \frac{I_{pq}}{I_{mn}} .$$

Since the magnitudes of all the currents are the same,

$$Z_D(mn) = \sum_{\text{all } pq} Z_{mn,pq}\, e^{j(m-p)T_{xs}}\, e^{j(n-q)T_{ys}} .$$

This is seen to be the sum of the mutual impedances with the excitation phase at each element taken into account. The self impedance of the mn^{th} element is included in this sum. Once again not very many elements need be summed to obtain good results. Allen and Diamond (Refs. 26 and 27) treat the mutual impedance concept in greater detail and report good results with the equal current assumption. Figure 18 gives their results for the impedance of a central element in a 9 by 11 array of dipoles above a ground plane compared with the impedance of a dipole in an infinite array.

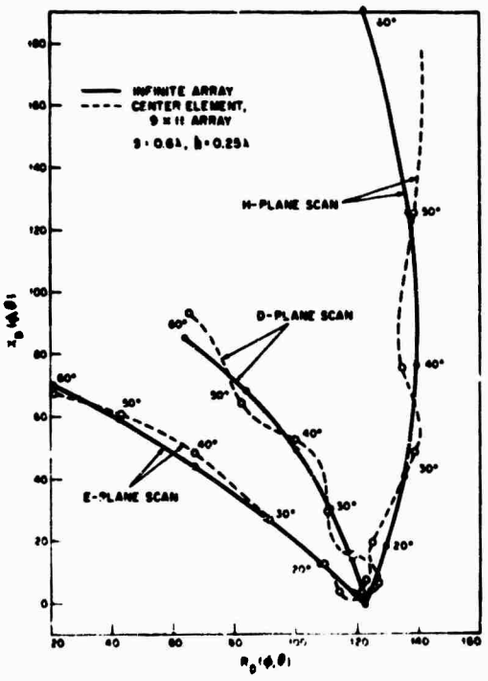

Fig. 18 Comparison of Impedance Variation of the Center Element in a 9 x 11 Equilateral Triangular Grid of $\lambda/2$ Dipoles above a Ground Plane with That of an Infinite Array (after Allen and Diamond, Ref. 27)

Grating Lobe Series

A very useful tool for the computation of the impedance variation with scanning is the grating lobe series (Refs. 37 and 38) which describes the impedance variation of an infinite array of regularly spaced elements. A detailed analysis is rather lengthy, and only a brief sketch will be given here. The technique uses the periodicity of the array lattice and the array phasing to expand the aperture excitation in a Fourier series. The aperture excitation is related to the radiated power and to the impedance which may also be written as a Fourier series. Each term in the series corresponds to a grating lobe position (in real or imaginary space). The value of the isolated element pattern (over real and imaginary space) at each of these grating lobe positions is summed to determine the impedance of an element in the array. As the array is scanned, the grating lobe pattern moves, samples new points in the isolated element pattern, and provides a new value of impedance.

Nonisolating Feeds

When nonisolating feeds are used, the mutual coupling effects become dependent on whether the phase shifting element is reciprocal or nonreciprocal. Figure 19 shows a space-fed array where it is assumed that the initial excitations at the input aperture are of equal amplitude and phase. If the phase shifters are nonreciprocal, the round trip phase of a signal reflected from the radiating aperture is independent of phase shifter setting. Therefore when reflections occur at the radiating aperture,

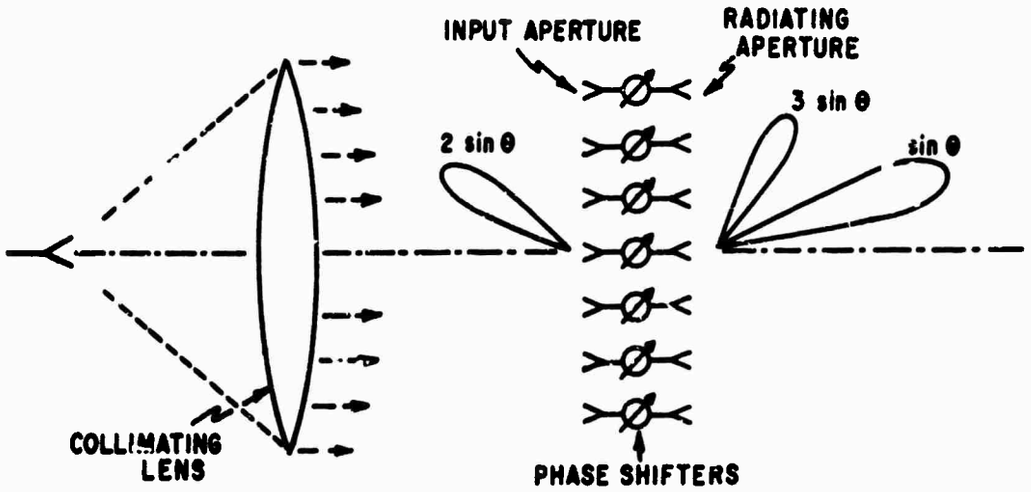

Fig. 19 Nonisolating Feed Showing Spurious Lobes when Reciprocal Phase Shifters Are Used

the reflected signal will be phased so that the input aperture appears as a mirror as seen from the feed side with the magnitude of the reflection being determined by the radiating aperture. Since the reflected beam does not scan, it should be possible to provide a good match at the input aperture. Matching the input aperture, in this case, is equivalent to providing the radiating aperture with independent feeds. Any secondary reflection from the input aperture will radiate in the original direction of scan.

If reciprocal phase shifters are used, the energy reflected from the radiating aperture will pick up equal additional phase shift on reflection from the radiating aperture, resulting in a beam at the input aperture which is phased to scan to twice the original scan angle (in $\sin\theta$ space). Some energy will undergo secondary reflection from the input aperture (which now has a mismatch corresponding to a scan of $2\sin\theta$) and will be phase shifted once again to produce a beam at the radiating aperture in the direction $3\sin\theta$. Additional reflections acquire twice the original

phase shift for each round trip resulting in radiated beams at positions of 5 sinθ, 7 sinθ, etc. The magnitude of these beams is approximately equal to the product of the voltage reflection coefficients, taking the number of bounces into account. For example, let $\Gamma_r(\sin\theta)$, $\Gamma_i(2\sin\theta)$ denote the reflection coefficients corresponding to scan angles of sinθ at the radiating aperture and 2 sinθ at the input aperture. If $\Gamma_r(\sin\theta) = 0.2$ and $\Gamma_i(2\sin\theta) = 0.5$, the magnitude of the radiated lobe directed at 3 sinθ would be $\Gamma_r(\sin\theta)\,\Gamma_i(2\sin\theta) = 0.1$, or 20 db down from the main lobe. Similar results can be expected from series feeds (Ref. 39) and from reactive parallel feeds (Ref. 26).

Mutual Coupling and Surface Waves

The mutual coupling between two small isolated dipoles (Ref. 40) should decrease as $\frac{1}{r}$ in the H plane and $\frac{1}{r^2}$ in the E plane (E and H planes are interchanged for slots). Coupling measurements (Ref. 41) have shown that in the array environment the rate of decay is slightly greater than predicted above, indicating that some of the energy is delivered to other elements in the array and may be dissipated and reradiated from these elements. The same measurements have shown that the phase difference of the energy coupled to elements is directly proportional to their distance from the excited elements, indicative of a surface wave traveling along the array, leaking energy to each of the elements. For best performance the velocity of the surface wave should be very close to that of free space. If the array contains waveguides or horns loaded with dielectric, the velocity will decrease slightly. Further, if the dielectric protrudes from the radiators or if a dielectric sheet is used in front of the array, the velocity of the surface wave may decrease dramatically.

This surface wave is important since it can cause a large reflection (and an accompanying loss of the beam) for some angles of scan. This can best be seen by examining the condition of phasing for which the couplings from many elements will add in phase to cause a large reflection in a typical element.

Consider an array in which the velocity of the surface wave is that of free space. The difference in the phase of the voltages coupled from an adjacent pair of elements to element 00 (Fig. 20) is related to the scan angle by:

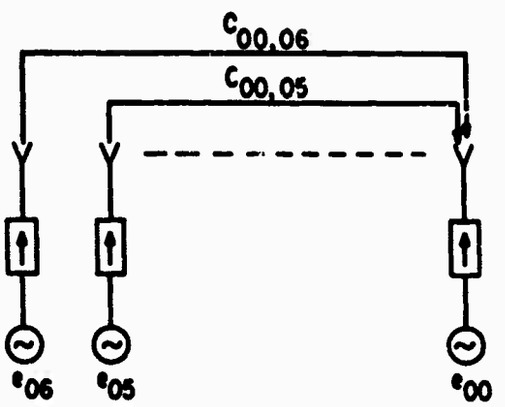

Fig. 20 Two Adjacent Elements Coupling to Another Element in the Same Row

$$\Delta\psi = \frac{2\pi s}{\lambda} + \frac{2\pi s}{\lambda}\sin\theta_s$$

$$= \frac{2\pi s}{\lambda}(1 + \sin\theta_s).$$

The couplings will be in phase when $\Delta\psi = 2\pi$, or when

$$\frac{s}{\lambda} = \frac{1}{1 + \sin\theta_s}.$$

This is seen to be exactly the same condition as previously determined for the emergence of a grating lobe into real space. Therefore, it may be expected that when a grating lobe is about to emerge into real space, the coupled voltages tend to add in phase and cause a large mismatch. If the dielectric protrudes from the aperture or if a dielectric sheet covers the aperture (this is one technique for scan compensation discussed below), a large reflection may occur well before the grating lobe reaches real space (Ref. 42). Assuming a surface wave velocity of v_s, the couplings will add in phase when

$$\frac{s}{\lambda} = \frac{1}{\frac{c}{v_s} + \sin\theta_c} \quad .$$

For the purposes of mutual coupling, a slow wave across the aperture may be envisioned as being equivalent to spacing the elements farther apart in free space.

A phenomenon that produces similar effects can come about without dielectric in front of the aperture; e.g., by using a periodic structure of baffles. Under certain conditions an array of open-ended waveguides will perform as though a slow wave were propagating across the aperture. This effect has been analyzed and studied experimentally (Refs. 43 and 44), and it has been shown that as the array is scanned, higher order modes are excited in the waveguides. Even though these modes are cut off, they contribute to the active impedance. At certain angles, almost all of the energy is reflected, causing a null in the element pattern. To guard against these reflections it is best to design the radiators so that higher

order modes are well in the cutoff region. Figure 21 shows the results obtained by Diamond using a waveguide array. When only the dominant TE_{10} mode was taken into account the null could not be explained. When the TE_{20} mode (which was only slightly cut off) was taken into account, the null showed up clearly. Since a null in the element pattern indicates constructive addition of the mutually coupled signals, it appears that the array of open-ended waveguides causes the couplings between elements to have a phase variation corresponding to a velocity slower than that of free space.

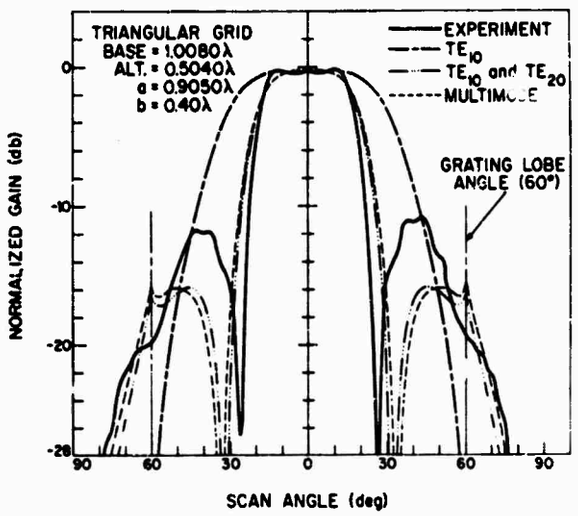

Fig. 21 Comparison of Theoretical and Experimental H-Plane Element Pattern; Triangular Array of Wave Guides with 2:1 Ratio of Width to Height (from Diamond, Ref. 44)

Regardless of the cause of the null, it will show up in the element pattern. If only a few elements surround the central element, the null will normally be shallow and broad. If many elements are used, the null will be deep and sharp. The null will also show up if the mutual coupling coefficients are measured and used to calculate the reflection coefficie

Array Simulators

A good deal of effort has gone into matching a radiator in the presence of an array of radiators. The use of waveguide simulators as developed by Wheeler Laboratories has made is possible to determine the matching structure experimentally without the need of building an array. A waveguide, operating in a TE_{10} mode, may be considered to contain two inclined plane waves propagating down the guide. The angle each of the plane waves makes with the longitudinal direction (Fig. 22) is determined by the H dimension of the waveguide and simulates the angle of scan of an infinite array

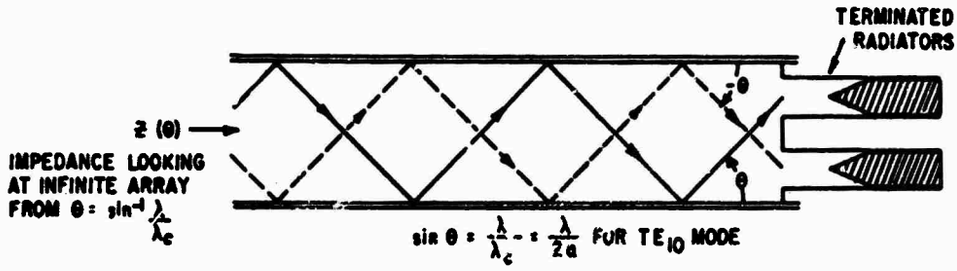

Fig. 22 Array Simulator Terminated with Two Dummy Elements

$$\sin\theta = \frac{\lambda}{\lambda_c} \tag{31}$$

where θ = scan angle, λ = free space wavelength, and λ_c = cutoff wavelength of the guide. Additional scan angles may be simulated by exciting other modes. The waveguide dimensions are chosen so that a radiating element (or elements) placed in the waveguide sees mirror images in the walls of the waveguide that appear to be at the same spacing as the array to be simulated. Both rectangular and triangular arrays may be simu-

lated as shown in Fig. 23. The impedance measurements are made by looking into a waveguide simulator that is terminated with dummy elements. This is equivalent to looking at an infinite array from free space at a scan angle given by Eq. 31. A matching structure designed from the simulator impedance data may be placed into the simulator to measure its effectiveness. Several simulator designs, results, and a complete discussion of the topic have been presented by Hannan and Balfour (Ref. 45). The technique is limited in that only discrete scan angles can be simulated. Several scan angles in both planes of scan will give a general idea of the array impedance, but may miss a large reflection of the type described in this section under "Mutual Coupling and Surface Waves." Nevertheless, the array simulator is the best method available for empirically determining the array impedance without building an array.

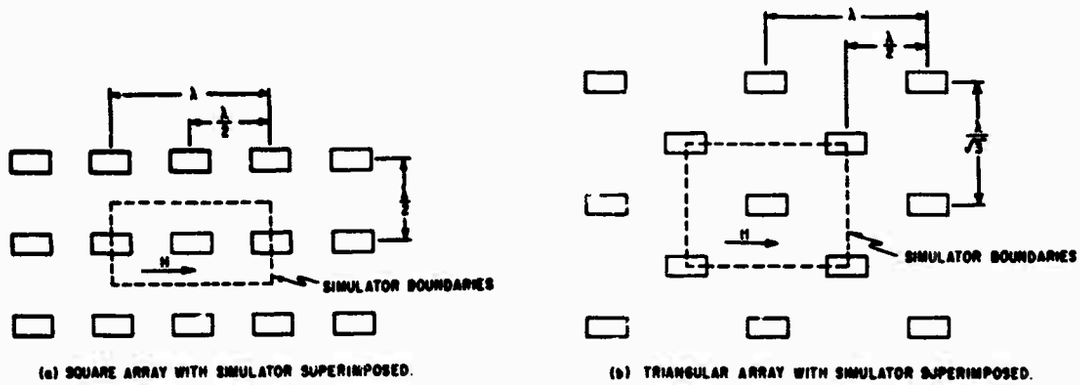

(a) SQUARE ARRAY WITH SIMULATOR SUPERIMPOSED. (b) TRIANGULAR ARRAY WITH SIMULATOR SUPERIMPOSED.

Fig. 23 Rectangular and Triangular Array Geometries with Simulator Boundaries Superimposed

Under certain conditions, the matched element impedance may be determined analytically by envisioning a simulator (Ref. 46). For example, if the waveguide simulator is terminated by a single dummy element, the matched impedance of the element is exactly the impedance of the waveguide. Since waveguide impedances are well known, the matched impedance at the simulator scan angle is also known.

Compensation for Scanned Impedance Variation

The impedance of an element in an array has been discussed and has been shown to vary as the array is scanned. An array which is matched at broadside can be expected to have at least a 2:1 VSWR at a 60° angle of scan. To compensate for the impedance variation, it is necessary to have a compensation network that is also dependent on scanning. Two methods have been suggested by Wheeler Laboratories to provide such scan dependent compensation.

The first method uses a thin sheet of high dielectric constant material (e.g. alumina) spaced a fraction of a wavelength from the array as shown in Fig. 24. The properties of a thin dielectric sheet (less than a quarter wave in the medium) are such that to an incident plane wave it appears as a susceptance that varies with both the plane of scan and the angle of scan. With respect to the broadside susceptance, the approximate variation with scan angle is given by:

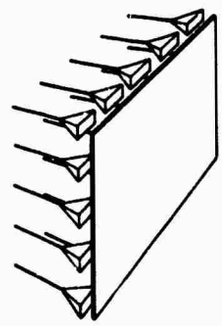

Fig. 24 Planar Array with Thin Dielectric Sheet Spaced a Fraction of a Wavelength from the Radiators

$$\text{H plane:} \quad \frac{B(\theta)}{B(0)} = \frac{1}{\cos\theta} ,$$

$$\text{E plane:} \quad \frac{B(\theta)}{B(0)} = \cos\theta - \frac{\sin^2\theta}{\epsilon_r \cos\theta} ,$$

where ϵ_r = relative permittivity. Magill and Wheeler (Ref. 47) describe

the technique in greater detail and present the results of a particular design using simulators. An alumina matching sheet is attractive because it simultaneously provides a natural radome. It should be cautioned that a dielectric sheet in front of the aperture may produce a slow surface wave and a possible null in the element pattern. However, a thin dielectric matching sheet has been used for a 400-element array (Ref. 29), and some compensation was achieved without any noticeable slow wave phenomenon.

A second method for providing impedance compensation is to use interconnecting networks between the radiating elements. As shown in Fig. 25, some of the phase shifted energy may be coupled into adjacent channels to effect at least partial cancellation of the variation in coupling via the radiating elements. This technique is described in detail by Hannan et al. (Ref. 48). By measuring the coupling coefficients between elements in a 1000 element square grid array and computing the impedance variation for a central element, workers at BTL (Ref. 6) have shown reasonable compensation with a simple interconnecting network which consists of coupling holes between adjacent waveguide channels as in Fig. 25.

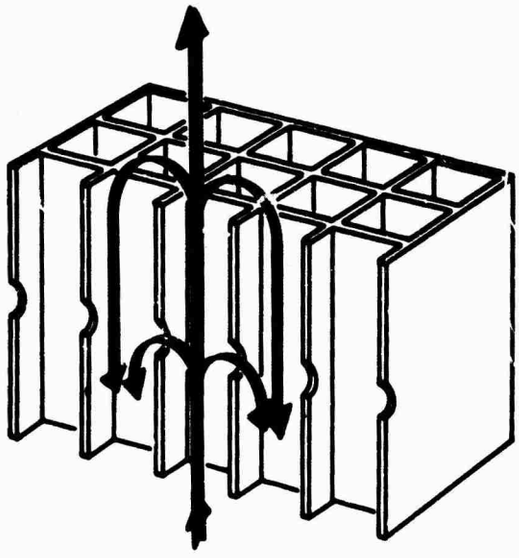

Fig. 25 Coupling between Adjacent Elements to Provide Compensation for Impedance Variation with Scanning (from Amitay et al., Ref. 6)

BLANK PAGE

V. QUANTIZATION ERRORS IN PHASED ARRAYS

The effect on the gain and the radiation pattern of random errors in the antenna excitation function are discussed in Ref. 5. Of concern here are errors peculiar to phased arrays, which are due to the quantization of amplitude and phase, and the lobes that occur when these errors are repeated periodically.

Phase Quantization

Phase Errors

Many different types of phase shifters are suitable for steering phased arrays. Most of these phase shifters are digitally controlled and can be set with an accuracy that is a function of the number of bits. For simplicity of phase shift computation and operation, and for minimal cost, a small number of bits is desired. This number controls the detailed performance of the array, affecting the gain, sidelobes, and beam pointing accuracy.

With a phase shifter having P bits, the phase can be set to the desired value with a residual error:

$$\text{Peak phase error} = \alpha = \pm\frac{\pi}{2^P} \tag{32}$$

$$\text{RMS phase error} = \alpha_{RMS} = \frac{\pi}{\sqrt{3}\,2^P} \tag{33}$$

Loss in Gain

Following the treatment of Miller (Ref. 49) the radiation pattern maximum $E'(\theta)_{max}$ of an array of N elements, with equal amplitude excitation of all elements and with a phase quantization error α_n at the n^{th} element, is

$$E'(\theta)_{max} \propto \sum_{n=0}^{n=N-1} \cos\alpha_n + j\sum_{n=0}^{n=N-1} \sin\alpha_n \ .$$

The phase errors are usually distributed symmetrically about the aperture so that $\sum_{n=0}^{n=N-1} \sin\alpha_n = 0$. Since α_n is small, $\cos\alpha_n \approx 1 - \frac{\alpha_n^2}{2}$ and the peak of the beam becomes:

$$E'(\theta)_{max} \propto \sum_{n=0}^{n=N-1} (1 - \frac{\alpha_n^2}{2}) \ .$$

Normalizing with respect to the peak of the error free pattern $E(\theta)_{max}$, gives in terms of the RMS phase error:

$$\frac{E'(\theta)}{E(\theta)} \approx 1 - \frac{\alpha_{RMS}^2}{2} \ . \qquad (34)$$

The loss in gain caused by phase errors is:

$$\Delta G = 1 - \left(\frac{E'(\theta)}{E(\theta)}\right)^2 \ ,$$

which combines with Eqs. 33 and 34 to

$$\Delta G \approx \alpha_{RMS}^2 = \frac{1}{3}\frac{\pi^2}{2P} \ . \qquad (35)$$

With many array elements this result is statistically independent of the amplitude distribution. An enumeration of Eq. 35 gives

Number of phase shifter bits, P		2	3	4
Loss in Gain ΔG,	db	1.0	0.34	0.06

From the point of view of gain, therefore, 3 or 4 bits would appear ample.

RMS Sidelobes

Phase quantization decreases the gain of the main beam as shown above. The energy that has been lost is distributed to the sidelobes. Within the region of space scanned by the array, the element gain is the same, on the average, for the main beam and the sidelobes. The sidelobe energy must, therefore, be compared with the average gain G_{AV} that the whole antenna has above that of the radiating element, to provide a gain that is averaged over the region of scan. For practical systems Miller allows an additional loss in gain of 2 db to account for illumination taper and scanning degradation. With N elements the average gain then becomes:

$$G_{AV} = 0.63N\,(1 - \alpha_{RMS}^2)\,.$$

With Eq. 35 this gives a relative RMS sidelobe level

$$\text{Sidelobes}_{RMS} = \frac{\Delta G}{G_{AV}} \approx \frac{\alpha_{RMS}^2}{0.63N} \approx \frac{5}{2^{2P_N}}\,. \qquad (36)$$

Figure 26 shows the RMS sidelobe level as a function of the number of bits and total number of radiating elements. Three or 4 bits should be adequate for most practical phased arrays.

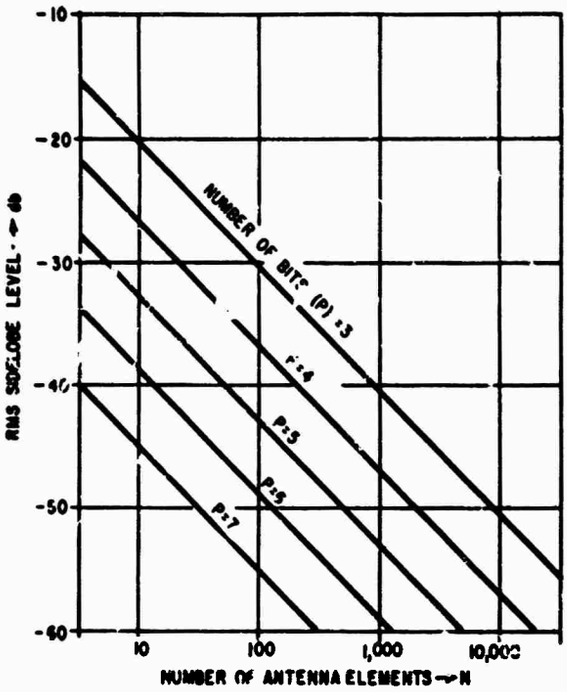

Fig. 26 RMS Sidelobes Due to Phase Quantization (from Miller, Ref. 49)

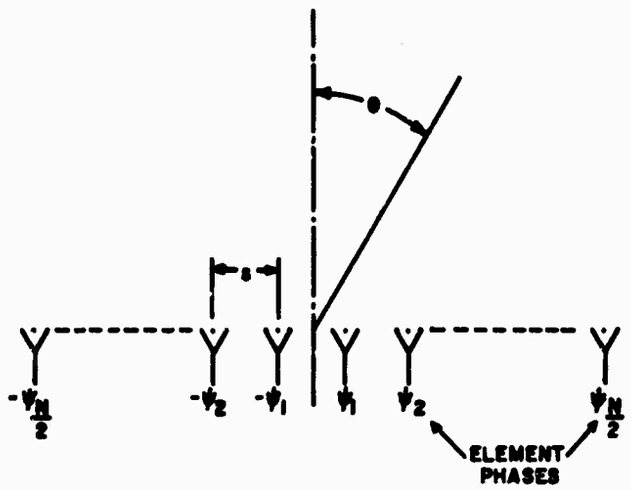

Fig. 27 Antisymmetrically Phased Array

Beam Pointing Accuracy

The accurate determination of the direction of targets is made with the monopulse difference pattern. The accuracy of the null position of the difference pattern is, therefore, of interest. With quantized phase shifters the position of this null can be moved with a granularity that is a function of the bit size.

Following the analysis of Frank and Ruze (Ref. 50), Fig. 27 shows an aperture with an even number of elements N, separated by distances s. All elements are excited with equal amplitude and antisymmetric phase, to give a difference pattern

$$D(\theta) = 2j \left\{ \sin\left(\frac{\pi s}{\lambda} \sin\theta - \psi_1\right) + \sin\left(\frac{3\pi s}{\lambda} \sin\theta - \psi_2\right) \cdots \right.$$
$$\left. \cdots + \sin\left(\frac{(N-1)\pi s}{\lambda} \sin\theta - \psi_{\frac{N}{2}}\right) \right\} .$$

For a null of the difference pattern at θ_0:

$$\sum_{n=1}^{n=\frac{N}{2}} \sin\left\{\frac{(2n-1)\pi s}{\lambda} \sin\theta_0 - \psi_{nj}\right\} = 0 .$$

If the phases are nearly those required to produce a null at θ_0, then the sine can be replaced by its argument and the equation simplifies to:

$$\sin\theta_0 = \frac{4}{\pi \frac{s}{\lambda} N^2} \sum_{n=1}^{n=\frac{N}{2}} \psi_n . \qquad (37)$$

If a phase increment equal to the smallest bit size $\frac{2\pi}{2^P}$ is applied antisymmetrically to a pair of radiators, then the null will shift by $\delta\theta$ radians, such that:

$$\delta\theta \cos\theta_o = \frac{4}{\pi \frac{s}{\lambda} N^2} \cdot \frac{\omega}{2^P} . \tag{38}$$

It should be noted that the movement of the null is independent of the position of the radiators and that the phase on any symmetric pair of radiators may be changed with equal effectiveness. Equation 38 can be expressed in terms of beamwidth from Eq. 14, with aperture = Ns:

$$\frac{\delta\theta}{\theta_{B(\text{scanned})}} = \frac{9}{N2^P} . \tag{39}$$

Small steering increments are possible. For example, with an array with 100 elements and 3-bit phase shifters, the beam may be steered in increments of about 1% of a beamwidth. If only one element has the phase changed rather than a symmetric pair, then the beam is moved by half the amount indicated by Eq. 39.

The sum $\sum_{n=1}^{n=\frac{N}{2}} \psi_n$ in Eq. 37 represents the total phase increments to all elements. This may be used in performing the beam steering computations by distributing the total phase increments to all the elements in a linear manner. The monopulse null will then have an absolute accuracy of one half of the value given by Eq. 39.

With tapered amplitude distributions the phase bits become proportionately weighted.

The exact pointing direction of the sum pattern peak may be derived by similar means. Surprisingly, it does not move synchronously with the difference pattern. Its motion is dependent on both the weighting and the position of the elements.

Periodic Errors

Periodic Amplitude and Phase Modulation

Both amplitude and phase quantization lead to discontinuities which may be periodic and give rise to quantization lobes which are similar to grating lobes.

Amplitude or phase errors that vary cosinusoidally may be analyzed simply, after Brown (Ref. 31). Figure 28a shows an original amplitude distribution F(x) disturbed by a cosinusoidal ripple $q \cos \frac{2\pi x}{s}$, giving a new distribution F'(x) such that:

$$F'(x) = F(x) + q\,F(x) \cos \frac{2\pi x}{s}$$

$$= F(x) + \frac{q}{2} \left\{ F(x)\, e^{j \frac{2\pi x}{s}} + F(x)\, e^{-j \frac{2\pi x}{s}} \right\} .$$

If the original radiation pattern, due to F(x), was E(θ), then the modified pattern becomes:

$$E'(\theta) = E(\theta) + \frac{q}{2} E \left(\sin\theta + \frac{1}{s/\lambda} \right) + \frac{q}{2} E \left(\sin\theta - \frac{1}{s/\lambda} \right) .$$

That is, amplitude quantization lobes occur at $\sin\theta = \pm \frac{1}{s/\lambda}$ and have an amplitude $\frac{q}{2}$.

Similarly, small phase ripples $\beta \cos \frac{2\pi x}{s}$, as shown in Fig. 28b, modify the aperture distribution to

$$F'(x) = F(x)\, e^{j\beta \cos \frac{2\pi x}{s}} \approx F(x) \left\{ 1 + j\beta \cos \frac{2\pi x}{s} \right\}$$

$$\approx F(x) + j \frac{\beta}{2} \left\{ F(x)\, e^{j \frac{2\pi x}{s}} + F(x)\, e^{-j \frac{2\pi x}{s}} \right\} ,$$

giving the radiation pattern

$$E'(\theta) = E(\theta) + \frac{\beta}{2} E\left(\sin\theta + \frac{1}{s/\lambda}\right) + \frac{\beta}{2} E\left(\sin\theta - \frac{1}{s/\lambda}\right) .$$

That is, quantization lobes occur at $\sin\theta_1 = \pm\frac{1}{s/\lambda}$ and have an amplitude $\frac{\beta}{2}$.

When the beam is scanned to θ_0, the quantization lobes occur at an angle θ_1 where $\sin\theta_1 = \sin\theta_0 - \frac{1}{s/\lambda}$. The gain of the aperture varies as $\cos\theta$ and the relative amplitude of the quantization lobe is modified by the factor $\sqrt{\frac{\cos\theta_1}{\cos\theta_0}}$.

Figure 28c and (d) show square amplitude and phase variations. The calculation of the quantization lobes for these and other repetitive errors consists of calculating the value of the radiation pattern generated by the repetitive portion of the aperture in the direction of the quantization lobe θ_1, and normalizing it with respect to the value at the scan angle θ_0. This calculation is shown here for the case of the square phase modulation of Fig. 28d. Referring to the figure, with n radiators in the sub-element sperture $\frac{s}{2}$, each with a pattern $\sqrt{\cos\theta}$,

Sub-element pattern: $S_e(\theta) = \sqrt{\cos\theta}\,\frac{\sin\left[\frac{\pi s}{2\lambda}(\sin\theta - \sin\theta_0)\right]}{n\sin\left[\frac{\pi s}{2n\lambda}(\sin\theta - \sin\theta_0)\right]}$.

Element pattern: $E_e(\theta) = S_e(\theta)\cos\left[\frac{\pi s}{2\lambda}(\sin\theta - \sin\theta_0) + \beta\right]$.

Quantization lobe angle = θ_1, where $\frac{\pi s}{\lambda}(\sin\theta_1 - \sin\theta_0) = -\pi$.

Phase quantization lobe = $\frac{E_e(\theta_1)}{E_e(\theta_0)} = \sqrt{\frac{\cos\theta_1}{\cos\theta_0}}\,\frac{1}{n\sin\frac{\pi}{2n}}\tan\beta$.

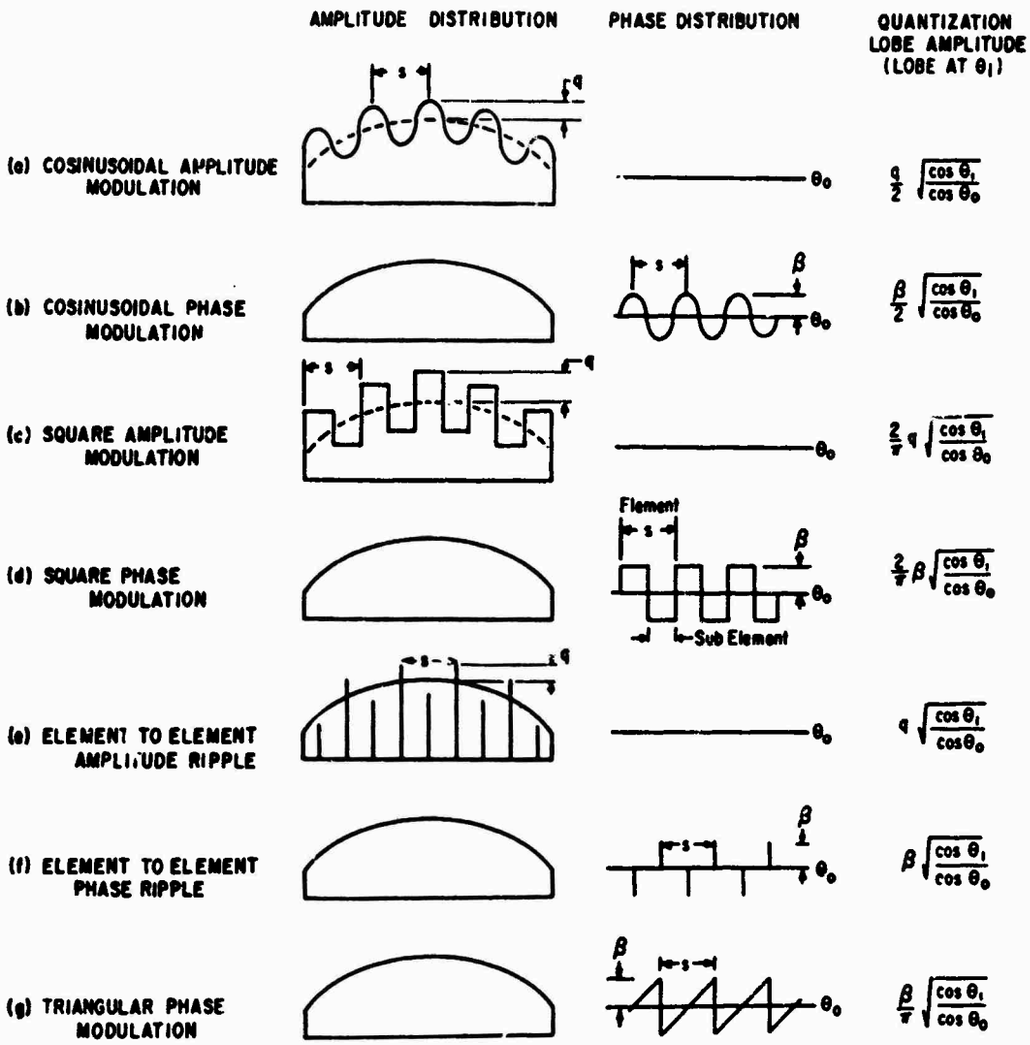

Fig. 28 Effects of Periodic Amplitude and Phase Modulation

The phase quantization lobe quickly converges to a limiting value as n increases so that:

$$\text{Phase quantization lobe } (n \geq 3) \approx \frac{2}{\pi}\,\beta\sqrt{\frac{\cos\theta_1}{\cos\theta_0}} \quad .$$

When n = 1 there is only one radiator in the sub-element, and its pattern is $\sqrt{\cos\theta}$. The phase varies from element to element by 2β, and the phase quantization lobe is increased from the above expression (by 4 db) to:

$$\text{Phase quantization lobe } (n = 1) \approx \beta\sqrt{\frac{\cos\theta_1}{\cos\theta_0}} \quad .$$

This result and the corresponding one for element-to-element amplitude ripples are shown in Figs. 28(e) and (f). Under (g) are shown triangular phase errors and the resulting quantization lobe.

Peak Phase Quantization Lobes

Peak quantization sidelobe values will be derived by considering the actual aperture phase distribution. Figure 29, after Miller, shows

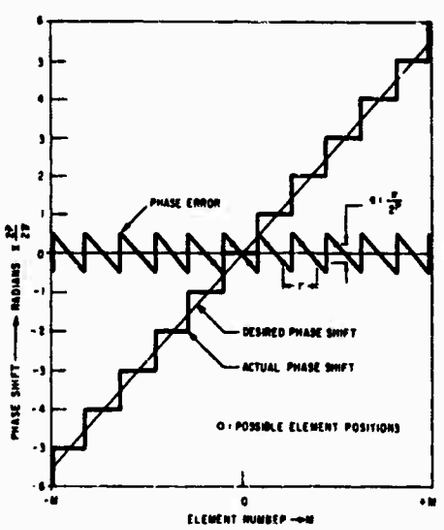

Fig. 29 Aperture Phase Errors Due to Phase Quantization (from Miller, Ref. 49)

this distribution for some scan angle θ_0 and the resulting errors due to phase quantization. Although a continuous curve has been drawn, only points corresponding to integral values of M are meaningful.

The greatest phase quantization lobes seem to occur with a phase slope such that the elements are spaced, as indicated in the figure, by a distance exactly half the period r or an exact odd multiple thereof. Since the distance between elements is about $\lambda/2$, the value of r is about one wavelength, and the array has to be scanned from broadside before the quantization lobe emerges. It will appear at an angle θ_1, given (Eq. 10) by

$$\sin\theta_1 = \sin\theta_0 - \frac{1}{r/\lambda}$$

$$\approx \sin\theta_0 - 1 \quad . \tag{40}$$

The phase error under these conditions has element-to-element phase ripples with a peak-to-peak value $\alpha = \frac{\pi}{2^P}$. From Fig. 28f this is seen to give:

$$\text{Peak phase quantization lobe} \approx \frac{\pi}{2} \cdot \frac{1}{2^P} \sqrt{\frac{\cos\theta_1}{\cos\theta_0}} \quad . \tag{41}$$

These values are shown in Fig. 30.

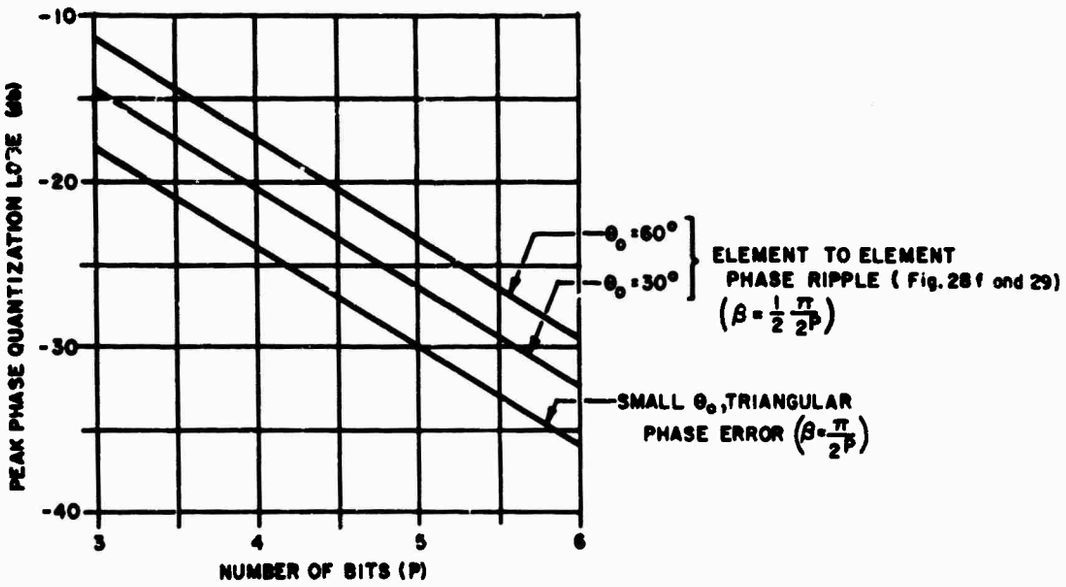

Fig. 30 Peak Sidelobes Due to Phase Quantization

The triangular repetitive phase error shown in Fig. 29 appears at the aperture if the beam points close to broadside and there are many radiators within the distance r. The same shape of phase error is obtained, although spanning several sawtooth cycles, if the element spacing corresponds to a distance slightly greater than r, or multiples thereof. Figure 28g gives, for this triangular phase error of $\pm \frac{\pi}{2^P}$,

$$\text{Peak phase quantization lobe} \simeq \frac{1}{2^P} \qquad (42)$$

This value is shown in Fig. 30 for small scan angles, when $\sqrt{\frac{\cos\theta_1}{\cos\theta_0}} \simeq 1$. In this case the position (θ_1) of the quantization lobe is given by $\sin\theta_1 = \sin\theta_0 - \frac{1}{r/\lambda}$ where, from Fig. 29, $\frac{2\pi r}{\lambda} \sin\theta_0 = 2\alpha = \frac{2\pi}{2^P}$. This simplifies to

$$\sin\theta_1 \simeq (1 - 2^P)\,\theta_0 \quad .$$

An examination of Fig. 30 shows that peak phase quantization lobes are significant and attempts should be made to reduce them.

Reduction of Peak Phase Quantization Lobes

Miller points out that the peak quantization lobes can be reduced by decorrelating the phase quantization errors. This may be done by adding a constant phase shift in the path to each radiator, with a value that differs from radiator to radiator by amounts that are unrelated to the bit size. The variable phase shifter is then programmed to account for this additional insertion phase. Better than random distribution of sidelobe energy can be obtained. With a spherical or parabolic law of insertion phase variation, as obtained with optical feed systems (Section VII), the reduction in peak quantization lobes are equivalent to adding one bit to the phase shifters in a 100-element array, two bits in a 1000-element array, and three bits in a 5000-element array.

Amplitude Quantization

When the aperture of a phased array is divided into [illegible]al subarrays, then across each subarray the amplitude distribution is constant. Aperture taper for the antenna is approximated by changing amplitude from subarray to subarray, and quantization lobes arise from these discontinuities. The value of these lobes may be estimated from the various results shown in Fig. 28 or actually computed by summing all contributions at the known quantization (grating) lobe angles. The distribution becomes smoother as the number of subarrays is increased or as they interlaced, as shown in Fig. 41.

BLANK PAGE

VI. BANDWIDTH OF PHASED ARRAYS

Scanned arrays which operate over a wide signal bandwidth require that the aperture excitation of the individual radiators is advanced or delayed in time, as shown in Fig. 3b, to form the desired inclined equiphase front. This time delay has to be achieved with absolute precision and requires many components. With phased arrays (Fig. 3a), the desired scanned phase front is obtained by adjusting the delay up to a maximum value of one period of oscillation, that is, modulo 2π in phase. This limits the signal bandwidth since a change in frequency changes the beam pointing direction. In contrast to the signal bandwidth of interest here and which will be calculated in the following, the "tuneable" bandwidth of a phased array is wide if the phase at each element is readjusted with frequency.

Parallel Fed Phased Arrays

When all radiating elements of a phased array are fed in parallel by equal line lengths, then their excitation will be frequency independent, and bandwidth limitations will result only from the characteristics of the phase controlled aperture.

At a frequency f_1, wavelength λ_1, the beam is steered to a direction θ_0 with a phase setting (Fig. 3a) $\psi = \frac{2\pi x}{\lambda_1} = \frac{2\pi x}{c} \sin\theta_0$ on the element located a distance x from the array center. At a frequency f_2 this same phase setting steers the beam to a new direction, $\theta_0 + \delta\theta$, so that

$$\frac{2\pi x}{c} f_1 \sin\theta_0 = \frac{2\pi x}{c} f_2 \sin(\theta_0 + \delta\theta) . \qquad (43)$$

With a small change in frequency, the change in direction $\delta\theta$ is small, and

$$\sin(\theta_o + \delta\theta) \approx \sin\theta_o + \delta\theta \cos\theta_o ,$$

which gives, with Eq. 43:

$$\delta\theta \approx \frac{f_1 - f_2}{f_2} \tan\theta_o \quad \text{radians.} \tag{44}$$

As the frequency is increased, the beam scans towards broadside by an angle that is independent of the aperture size or beamwidth.

In terms of percentage bandwidth, Eq. 44 gives, by measuring $\delta\theta$ relative to the band center,

$$\delta\theta \approx \pm \frac{\text{Bandwidth (\%)}}{200} \tan\theta_o \quad \text{radians}$$

$$\approx \pm 0.29 \text{ Bandwidth (\%)} \tan\theta_o \quad \text{degrees.} \tag{45}$$

The amount $\delta\theta$ that the beam scans with a change in frequency increases as the tangent of the scan angle. At broadside, the beam remains stationary as the frequency is changed, but at a scan angle of 60°, $\delta\theta$ (degrees) $\approx \pm \frac{1}{2}$ Bandwidth (%). The permissible amount that the beam may scan with frequency is related to the beamwidth since pattern and gain deteriorations are a function of the fractional beamwidth scanned. The angle that the beam actually scans, on the other hand, is related to the percentage bandwidth. A bandwidth factor may, therefore, be defined in terms of the broadside beamwidth:

$$\text{Bandwidth Factor} = K = \frac{\text{Bandwidth (\%)}}{\text{Beamwidth (degrees)}} . \tag{46}$$

From Eq. 45, $\delta\theta$ normalized to its local beamwidth becomes:

$$\frac{\delta\theta}{\theta_{B(\text{scanned})}} \approx 0.29\, K \sin\theta_o \ . \tag{47}$$

A reasonable criterion is to limit the bandwidth so that the beam never scans by more than $\pm \frac{1}{4}$ of a local beamwidth with frequency, i.e.,

$$\underline{\text{criterion}}: \left|\frac{\delta\theta}{\theta_{B(\text{scanned})}}\right| \leq \frac{1}{4} \tag{48}$$

This criterion gives, as limiting value,

$$K = \frac{0.87}{\sin\theta_c} \ . \tag{49}$$

With a scan of 60° this gives K = 1 and in terms of broadside beamwidth the limit is:

Bandwidth (%) = Beamwidth (degrees).

As long as $\theta_c \approx \sin\theta_o$, Eq. 49 (with Eq. 46) may be stated with equal accuracy as:

$$\text{Bandwidth (\%)} \approx \frac{50}{\text{Number of Beamwidths scanned}} \ ,$$

where the beamwidth is the broadside beamwidth.

When a monopulse system is used, the <u>difference pattern null</u> is scanned with a change in frequency by the amount $\delta\theta$ given by Eq. 44. The amplitude of the difference pattern at an angle $\delta\theta$ from its null, relative to the peak of the sum pattern, can be shown to be:

$$D(\delta\theta) \approx 2\, \frac{\delta\theta}{\theta_{B(\text{scanned})}} \tag{50}$$

With Eqs. 47 and 49 this gives:

$$D(\delta\theta) \approx 0.4K \sin\theta_o \ , \tag{51}$$

and with the bandwidth criterion of Eq. 48,

$$D(\delta\theta) \approx 0.35 \ . \tag{52}$$

The bandwidth criterion of Eq. 48 thus implies that at the maximum scan angle the beam moves with frequency up to $\pm \frac{1}{4}$ of its local beamwidth and the difference pattern "null" increases up to -9 db relative to the peak of the sum pattern.

The bandwidth factor K may be expressed in terms of the equivalent pulse length. If the whole band were used, a pulse could have been formed of duration $T = \frac{1}{\text{Bandwidth}}$ (between 4 db points), or length L given by:

$$L = cT = \frac{c}{\text{Bandwidth}} = \frac{c\ 100}{f\ \text{Bandwidth (\%)}} = \frac{100\lambda}{\text{Bandwidth (\%)}} \ ,$$

and from Eqs. 46 and 5,

$$L \approx \frac{2}{K} a \ , \tag{53}$$

where 'a' is the aperture size. When K = 1 (60° scan), the corresponding statement to Bandwidth (%) = Beamwidth (degrees) is (min) Pulse Length = Twice Aperture Size.

Subarrays with Time Delay

The radiating elements of a phased array may be grouped into subarrays where time delay elements are added. This is shown in Fig. 31.

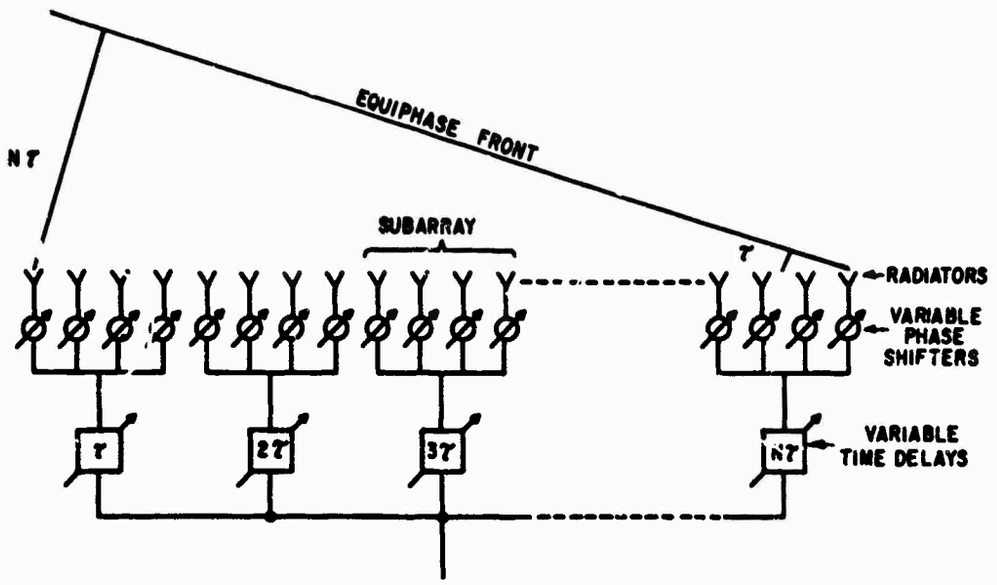

Fig. 31 Phased Array Using Subarrays with Time Delay

The antenna may be regarded as an array of subarrays. The subarray pattern forms the element factor; it is steered by phase shifters in the desired direction but it will scan with frequency as indicated by Eq. 44. The array factor is scanned by adjusting the frequency independent time delay elements. All subarrays are steered in the same manner. The total radiation pattern is the product of array factor and element factor. A change in frequency gives rise to grating lobes rather than shifts of the beam position. This can be seen from Fig. 32. One subarray pattern is shown at the design frequency f_o and is seen to have a null a the position of the grating lobe. As the frequency is changed by δf, the pattern is scanned. It is shown dotted in a position where it has been scanned by a little more than half its beamwidth. This is clearly too much, for the product of array and element factors gives two beams of equal amplitude.

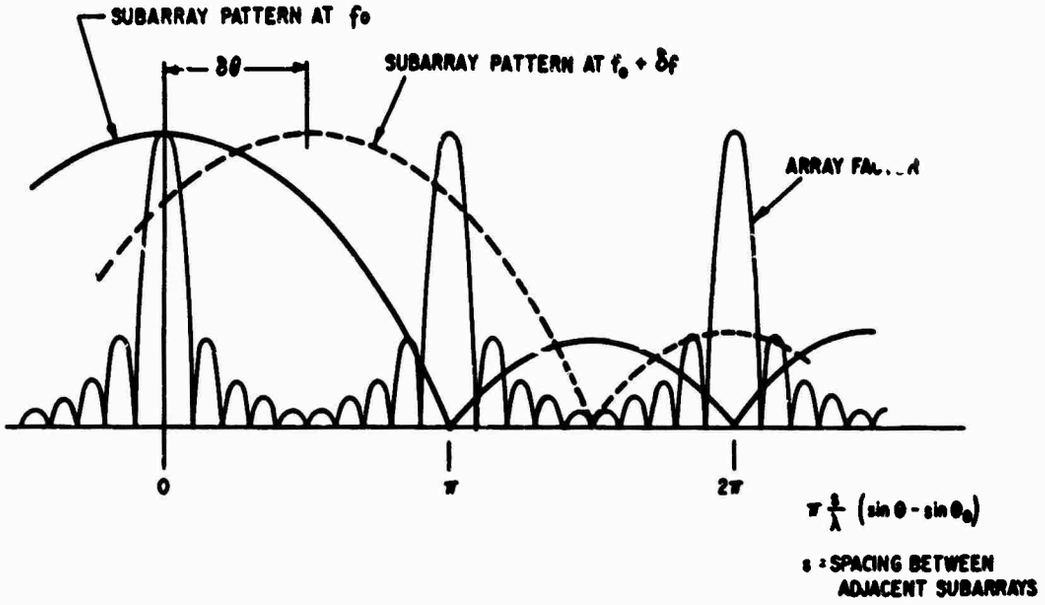

Fig. 32 Generation of Grating Lobes by Change of Frequency

The loss in gain and the magnitude of the grating lobe are a function of the fractional subarray beamwidth that has been scanned as a result of the change in frequency. The values may be derived from array theory in a manner similar to that used in Section V to calculate square phase quantization lobes. The results may be expressed in terms of the bandwidth factor K (referred to the subarray broadside beamwidth). At the edges of the band, ignoring the element factor,

$$\text{Relative Grating Lobe Amplitude} \approx \frac{1}{\frac{4}{K \sin\theta_0} - 1} \tag{54}$$

$$\text{Loss in Gain } \Delta G \approx 1 - \left[\frac{\sin\left(\frac{\pi}{4} K \sin\theta_c\right)}{\frac{\pi}{4} K \sin\theta_c}\right]^2 . \tag{55}$$

Figure 33 shows these values as a function of K for a scan of 60°.

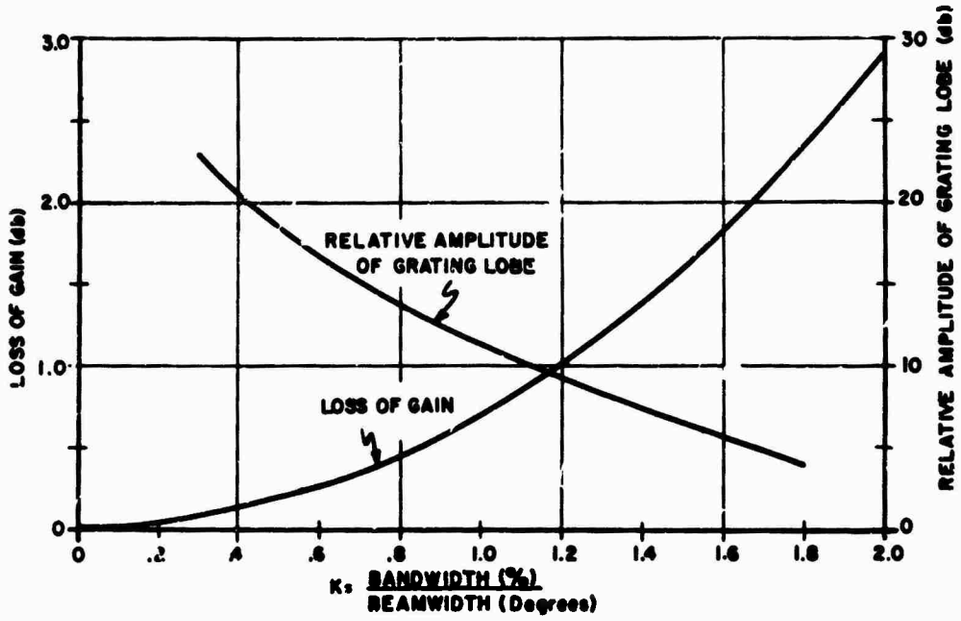

Fig. 33 Loss of Gain and Grating Lobe Amplitude as a Function of Bandwidth (Phased Subarrays with Time Delay, Scanned 60°). The Actual Value of the Grating Lobe at θ_1 will be increased by $\sqrt{\frac{\cos\theta_1}{\cos\theta_0}}$ from the Value Shown

K = 1 was the value previously used for scanning 60° and appears acceptable here, where the relevant beamwidth is the broadside beamwidth of the subarray. Thus if the aperture is split into N subarrays in one plane, with time delay networks at each subarray level, then the bandwidth is increased by a factor of N. This same bandwidth criterion leads to a reduction in gain of about 0.7 db and a grating lobe of about -11 db at the edges of the band with 60° scan. Interlacing of subarrays can reduce the occurrence of these grating lobes (Fig. 41).

The monopulse null position is unaffected by the behavior of the subarrays as long as they all respond in the same way. The null position is determined only by the time delay networks or phase shifters at the subarray level and corresponds to the array factor null, which is unaffected when multiplied by the element pattern.

Time Delay Networks

Figure 34a shows a time delay network that is digitally controlled by switches. The total delay path length that has to be provided nondispersively amounts to '$a \sin\theta_{max}$,' where θ_{max} is the maximum scan angle for the aperture 'a'. The smallest bit size is about $\lambda/2$ or λ, with the precise setting adjusted by an additional variable phase shifter. A 1° beam scanned 60°, for example, requires a time delay of 6 or 7 bits, the largest being 32 wavelengths, as well as an additional phase shifter. The tolerances are tight, amounting in this case to a few degrees out of about 20,000, and are difficult to meet. Problems may be due to leakage past the switch, to a difference in insertion loss between the alternate paths, to small mismatches at the various junctions, to variations in temperature or to the dispersive characteristics of some of the reactive components. Painstaking design is necessary. The switches may be diodes or circulators. Leakage past the switches may be reduced by adding another switch in series in each line. The difference in insertion loss between the two paths may be equalized by padding the shorter arm. The various problems are comprehensively assessed and analyzed by Temme and Betts (Ref. 26).

On transmitting, the tolerances are less severe since the requirements are usually for power on target rather than for accurate angle determination.

Figure 34b shows another configuration that has the advantage of simplicity. Each of the switchable circulators connects either directly across (counterclock wise) or via the short-circuited length. Isolation in excess of 30 db is required, and the higher insertion loss of the longer path cannot easily be compensated.

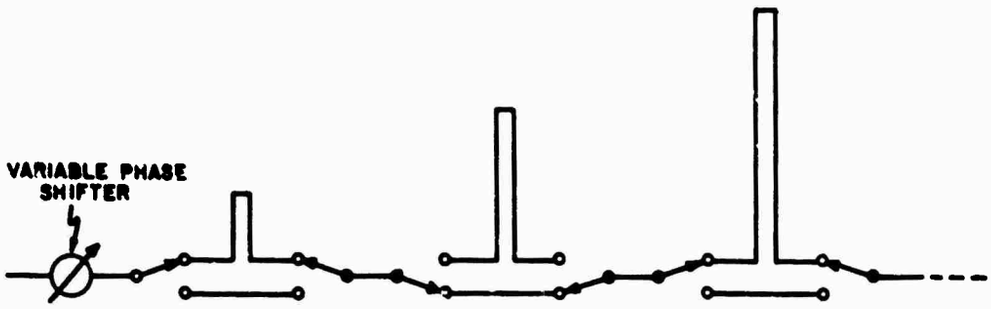

(a) TIME DELAY BY CHOOSING UPPER OR LOWER PATHS

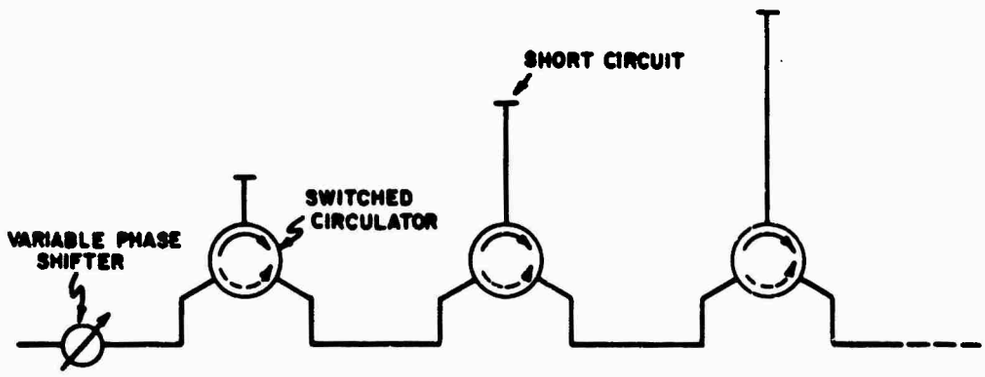

(b) TIME DELAY USING SWITCHED CIRCULATORS

Fig. 34 Time Delay Configurations

A further method of providing delay is possible by translating the problem from the microwave domain and delaying at IF.

It is clear that the insertion loss of time delay circuits is too high for most practical systems. They would, therefore, precede a final power amplifier on transmitting and follow a preamplifier on receiving.

Only the edge elements or edge subarrays of the antenna require the full range of time delay. The center does not need any time delay, only a biasing line-length. The amount of delay required increases as the edge of the aperture is approached. This is shown in Fig. 35.

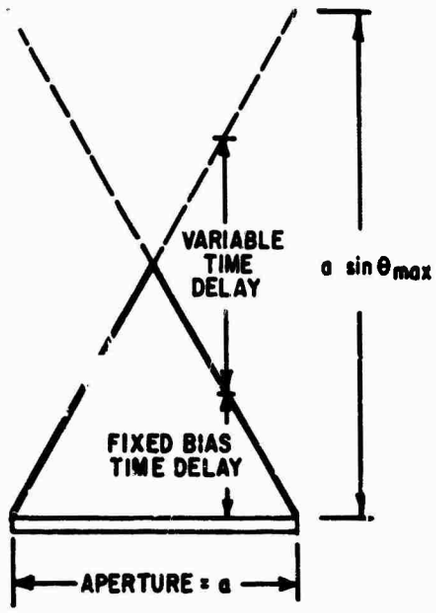

Fig. 35 'Variable' and 'Fixed Bias' Time Delay for an Aperture

End-Fed Series Arrays

An end-fed series array is shown in Fig. 37a. The radiating elements are in series and progressively further and further removed from the feed point. When the frequency is changed the phase at the

radiating elements changes proportionately to the length of feed line so that the phase at the aperture tilts in a linear manner and the beam is scanned. This effect is useful for frequency scanning techniques but in the case of phased arrays it is undesirable and reduces the bandwidth. It has been shown previously that with phased arrays the pointing direction of a scanned beam also changes with frequency (e.g. Eq. 44) since phase rather than time delay is adjusted. These two changes in beam pointing direction may add or subtract, depending on the direction the beam has been scanned. The worst case will be considered here.

With a change in frequency a nondispersive transmission line having free space propagation characteristics and a length 'a' equal to the size of the aperture that it feeds, will produce a linear phase variation across the aperture with a maximum value at the edges of

$$\Delta\psi = \pm \frac{2\pi a}{\lambda} \frac{\text{Bandwidth (\%)}}{200} \text{ radians} . \qquad (56)$$

The beam is thereby scanned through an angle:

$$\delta\theta = \frac{\Delta\psi}{\frac{2\pi}{\lambda} a \cos\theta_0} = \pm \frac{\text{Bandwidth (\%)}}{200 \cos\theta_0} \text{ radians},$$

where θ_0 is the scan angle.

Normalizing this expression with respect to the scanned beamwidth (Eqs. 14 and 46) gives, for scanning due to the feed system,

$$\frac{\delta\theta}{\theta_B(\text{scanned})} = \pm 0.29 \text{ K} . \qquad (57)$$

The total fractional beamwidth scanned with frequency includes the amount scanned due to the aperture being adjusted in phase rather than by time

delay. Scanning in one direction will tend to make the two effects cancel but they will add when scanning in the other direction, giving, from Eqs. 47 and 57:

$$\frac{\delta\theta_{(\text{Total})}}{\theta_{B(\text{scanned})}} \approx + 0.29K\,(1 + \sin\theta_0)\,. \tag{58}$$

Using the previous criterion $\frac{\delta\theta_{(\text{Total})}}{\theta_{B(\text{scanned})}} = + \frac{1}{4}$, which led to the monopulse difference pattern deterioration of Eq. 52, gives the bandwidth factor:

$$K = \frac{\text{Bandwidth (\%)}}{\text{Beamwidth (degrees)}} \approx \frac{0.87}{1 + \sin\theta_0}\,. \tag{59}$$

With 60° of scan this gives $K \approx 0.5$ which is one half of the value obtained with a parallel fed array.

When the transmission line is waveguide, it can be shown that the change of phase as a function of frequency is increased by the factor $\frac{\lambda_g}{\lambda_a}$. This modifies the last equation, giving

$$K \approx \frac{0.87}{\frac{\lambda_g}{\lambda_a} + \sin\theta_0}\,. \tag{60}$$

Bailin (Ref. 52) has calculated the effects of bandwidth on an end-fed waveguide array with $\lambda_g = 1.4\lambda_a$ for a broadside beam ($\theta_0 = 0$). He suggests a minimum pulse length of $L = 3a$, which corresponds (Eq. 53) to $K = 2/3$. This agrees with the result of Eq. 60.

Center-Fed Series Arrays

With center-fed series arrays the phase deviation as a function of frequency is only half that of the end-fed array, since the length of the feed line is halved. The phase distribution is symmetric and gable shaped, leading to beam distortions, but it does not scan the beam.

With a nondispersive transmission line with free space characteristics, the peak phase variation as a function of frequency is:

$$\Delta\psi = \pm \frac{2\pi}{\lambda} \frac{a}{2} \frac{\text{Bandwidth (\%)}}{200} \text{ radians,}$$

which gives, with Eqs. 5 and 46,

$$\Delta\psi = \pm \frac{\pi}{4} K \quad \text{radians .} \tag{61}$$

With a waveguide feed, the value of $\Delta\psi$ is increased to

$$\Delta\psi = \pm \frac{\pi}{4} K \frac{\lambda_g}{\lambda_a} \quad \text{radians .} \tag{62}$$

This gable distribution is permissible for values perhaps as high as $\Delta\psi = \pm \frac{\pi}{2}$, and the feed system of a center-fed series array is not usually the limiting factor in the determination of bandwidth.

BLANK PAGE

VII. FEED NETWORKS FOR PHASED ARRAYS

Optical Feed Systems

Phased array apertures may be used in the form of lenses or reflectors, as shown in Fig. 36, where an optical feed system provides the proper aperture illumination. The lens has input and output radiators coupled by phase shifters. Both surfaces of the lens require matching. The primary feed can be optimized to give an efficient aperture illumination with little spillover (1 to 2 db), for both sum and difference patterns. If desired the transmitter feed can be separated

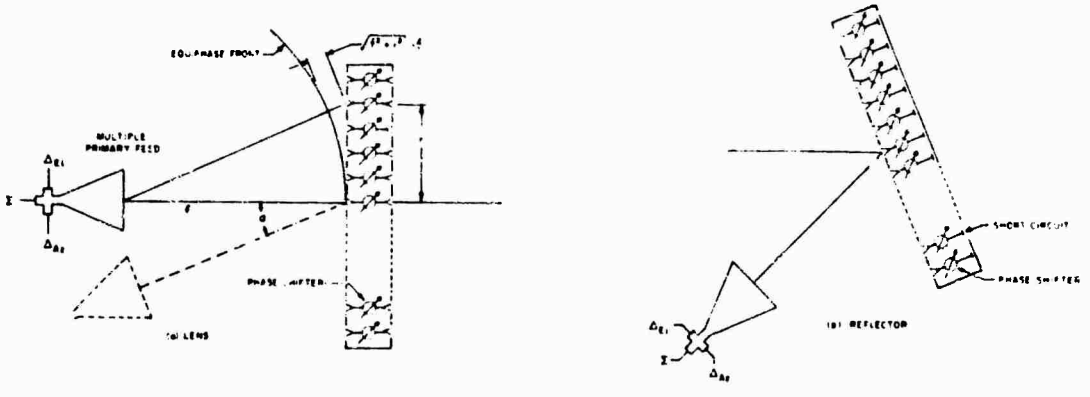

Fig. 36 Optical Feed Systems

from the receiver by an angle α, as shown. The antenna is then rephased between transmitting and receiving so that in both cases the beam points in the same direction. The phasing of the antenna has to include a correction for the spherical phase front. This can be seen to amount to

$$\frac{2\pi}{\lambda}\left(\sqrt{f^2 + r^2} - f\right) \quad - \frac{\pi}{\lambda}\,\frac{r^2}{f}\left\{1 - \frac{1}{4}\left(\frac{r}{f}\right)^2 + \cdots\right\} \quad .$$

With a sufficiently large focal length, the spherical phase front may be approximated by that of two crossed cylinders, permitting the correction to be applied simply with row and column steering commands. Correction of the spherical phase error with the phase shifter reduces peak phase quantization lobes (Section V). Space problems may be encountered in assembling an actual system, especially at higher frequencies, since all control circuits have to be brought out at the side of the aperture.

Multiple beams may be generated by adding further primary feeds. All the beams will be scanned simultaneously by equal amounts in $\sin\theta$.

The phased array reflector shown in Fig. 36b has general characteristics similar to those of the lens. However, the same radiating element collects and re-radiates after reflection. Ample space for phase shifter control circuits exists behind the reflector. To avoid aperture blocking, the primary feed may be offset as shown. As before, transmit and receive feeds may be separated and the phases separately computed for the two functions. Multiple beams are again possible with additional feeds.

The phase shifter must be reciprocal so that there is a net controllable phase shift after passing through the device in both directions. This rules out nonreciprocal phase shifters.

Constrained Feeds

Series Feeds

Figure 37 shows several types of series feeds. In all cases the path length to each radiating element has to be computed as a function of

frequency and taken into account when setting the phase shifters. Figure 37a is an end-fed array. It is frequency sensitive and leads to more severe bandwidth restrictions than most other feeds. Figure 37b is center fed and has essentially the same bandwidth as a parallel feed network (Section VI). The series feed lends itself to simple assembly techniques. Sum and difference pattern outputs are available, but they have contradictory requirements for optimum amplitude distribution that cannot both be satisfied. As a result, either good sum or good difference patterns can be obtained, but no reasonable compromise seems possible that gives good sum and difference patterns simultaneously.

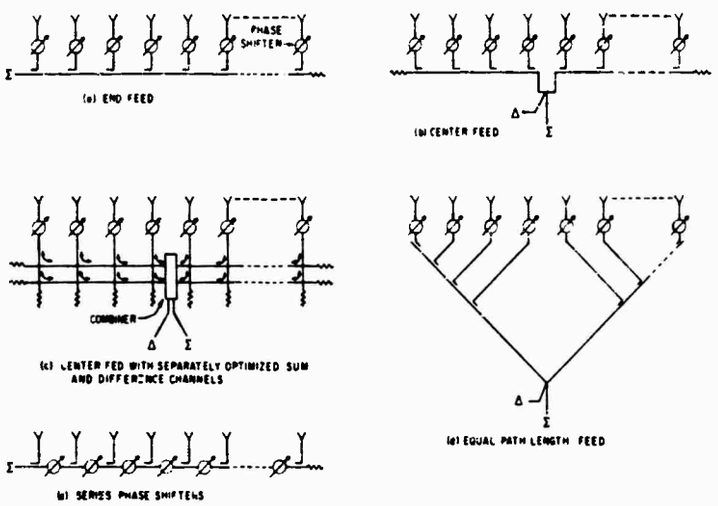

Fig. 37 Series Feed Networks

At the cost of some additional complexity the difficulty can be overcome by the method shown under Fig. 37c. Two separate center-fed feed lines are used and combined in a network to give sum and difference pattern outputs (Ref. 53). Independent control of the two amplitude distributions is possible. For efficient operation the two feed lines require

distributions that are orthogonal within each branch of the array, that is, in each branch the two feed lines give rise to patterns where the peak value of one coincides with a null from the other and the aperture distributions are respectively even and odd.

A very wide band series feed with equal path lengths is shown in Fig. 37d. If the bandwidth is already restricted by the phase shifters at the aperture, very little advantage is obtained at the cost of a considerable increase in size and weight. The network of Fig. 37e permits simple programming since each phase shifter requires the same setting. The insertion loss increases for successive radiators and the tolerances required for setting the phases are high.

Parallel Feeds

Figure 38 shows a number of different parallel feed systems. They would usually combine a number of radiators into subarrays and the subarrays would then be combined to form sum and difference patterns.

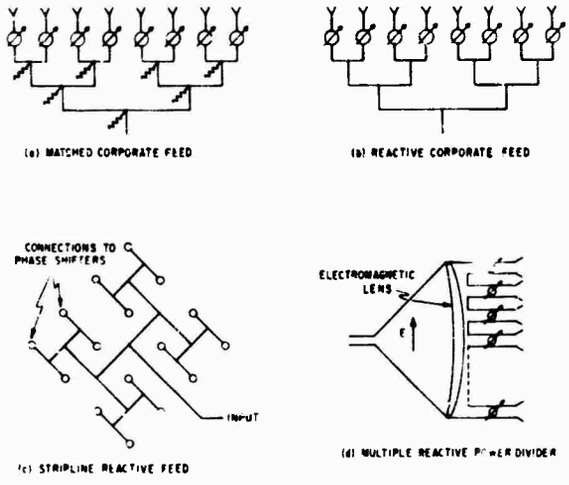

Fig. 38 Parallel Feed Networks

Figure 38a shows a matched corporate feed which is assembled from matched hybrids. The out-of-phase components of mismatch reflections from the aperture and of other unbalanced reflections are absorbed in the terminations. The in-phase and balanced components are returned to the input, and no power reflected from the aperture is re-radiated. To break up periodicity and reduce peak quantization lobes (Section V), small additional phase shifts may be introduced in the individual lines and compensated by corresponding readjustments of the phase shifters.

With nonreciprocal phase shifters the two-way path length is a constant, independent of the phase shifter setting. Under these conditions the performance of a reactive corporate feed is similar to that of the matched corporate feed. However, if additional phase shifts are added to the individual arms or if reciprocal phase shifters are used, then the out-of-phase components of the reflections due to the aperture mismatch will be re-radiated (Section IV). Figure 38b shows a schematic layout for a reactive power divider which may use waveguide. A stripline power divider is shown under Fig. 38c. A constrained-optical power divider using an electromagnetic lens is shown under Fig. 38d. The lens may be omitted and the correction applied at the phase shifters. With nonreciprocal phase shifting, a fraction of the power reflected from the aperture will then be re-radiated rather than returned to the input. The amplitude distribution across the horn is given by the waveguide mode. It is constant with an E-plane horn as shown.

Subarrays

The phased array aperture may be divided into subarrays that are combined to form suitable sum and difference patterns. Figure 39a shows a method of doing this by combining opposite subarrays into their sums and differences. All sum channels are then added with proper weighting to obtain the desired amplitude distribution. The difference channels are treated similarly with independent amplitude weighting. This method may be extended to also include combination in the other plane.

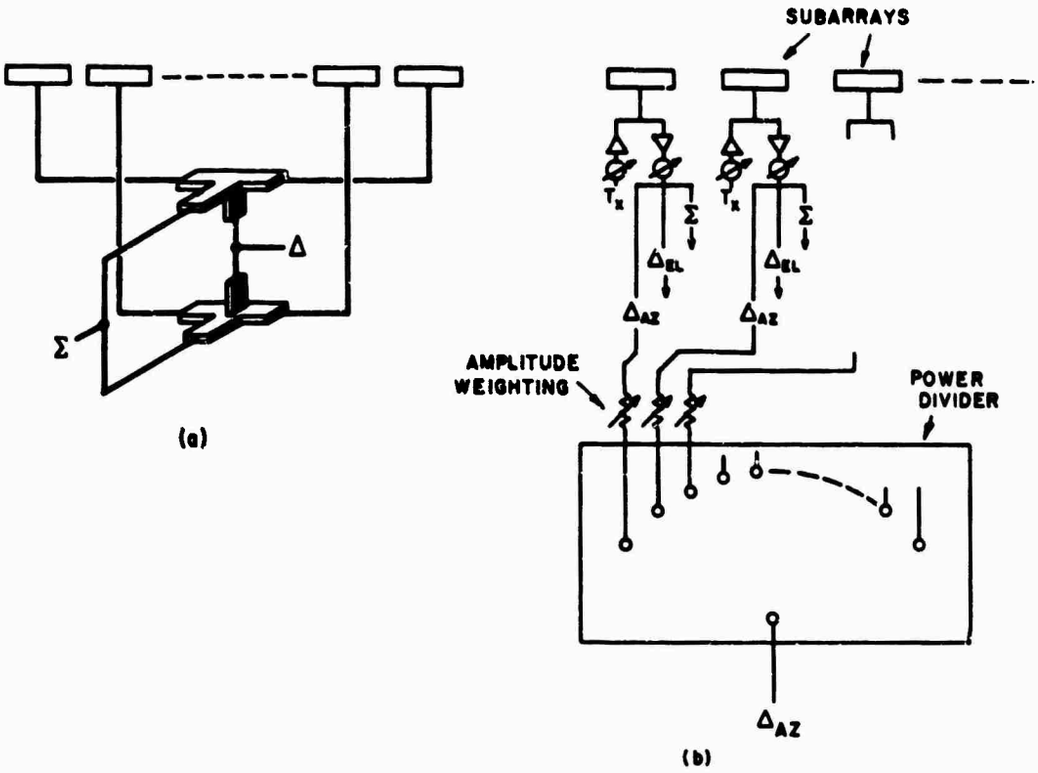

Fig. 39 Combination of Subarrays to Form Sum and Difference Channels. (a) Combining Opposite Subarrays, (b) Combining Subarrays after Amplification

Amplification on receiving or on both receiving and transmitting may be convenient at the subarray level. On receiving the noise figure is established by the preamplifier so that further processing may include lossy circuits. The receive channel may be split three ways as indicated in Fig. 39b, into the sum and the elevation and azimuth difference channels. These are then weighted and summed with corresponding outputs from the other subarrays. On transmitting, all separate power amplifiers may be energized equally to give maximum power on the target. The additional phase shifters shown at the subarray level simplify the beam steering computation, permitting all subarrays to receive identical steering commands (Section III). They may be replaced by time delay circuits, giving a wide instantaneous bandwidth.

A simple method of providing T-R switching is obtained by combining two halves of a subarray with a four-port hybrid. The transmitter input into one port energizes both halves of the aperture, say, in phase. The receiver, connected to the isolated port, then requires that the phase shifters of half the aperture give an additional phase shift of π during the receive period. This is easily programmed.

Multiple beams may be formed by combining the subarrays in as many different ways as separate beams are required. This is indicated in Fig. 40. The limitation is that the beams have to lie in a cone whose included angle is appreciably smaller than the subarray beamwidth in order to avoid excessive grating lobes. A cluster of receiver beams requires a wider transmitting beam. This may be obtained efficiently from the same antenna with a gabled phase distribution.

The aperture amplitude taper is applied in steps depending on the number of subarrays and their size and shape. The steps cause quantization

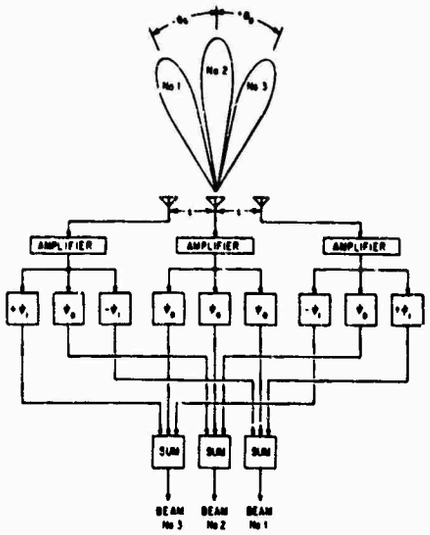

Fig. 40 Simultaneous Postamplifier Beam Formation Using Array Antenna, ψ_0 = Constant Phase

$$|\psi_1 - \psi_0| = |\Delta\psi| = |2\pi \frac{s}{\lambda} \sin\theta_0|$$

lobes (Section V) and should be minimized. Figure 41 shows qualitatively how the amplitude steps can be reduced with interlaced and shaped subarrays.

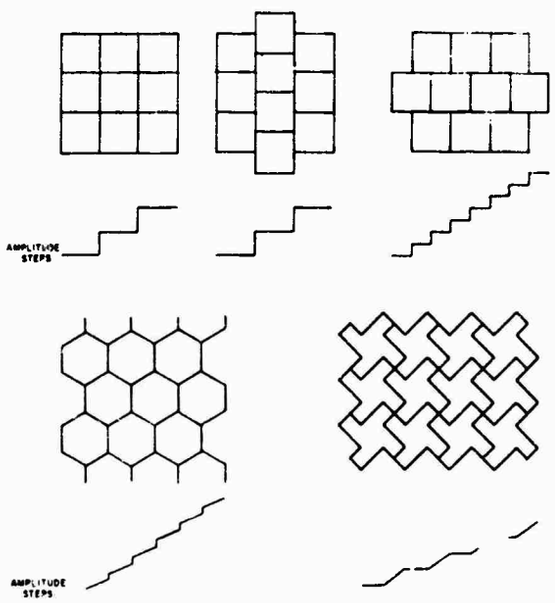

Fig. 41 Interlaced and Shaped Subarrays and Resulting Steps in the Amplitude Distribution

VIII. PHASED ARRAY SYSTEMS

Various phased array systems have been developed and at least partially evaluated. A representative number is described below.

Blass Reflectarray (Ref. 54)

An S-Band reflectarray of the type shown in Fig. 36b has been developed for the Naval Ship Systems Command by the Blass Electronics Corporation and has been evaluated by the U. S. Naval Research Laboratory. The reflectarray is in the shape of an octagonal flat surface, about 8 feet in diameter and tilted back by about 18° from the normal. It contains 1892 ridged waveguide radiators spaced in the H-plane by 0.53λ and interlaced in the E-plane to form triangles with sides of 0.6λ. The phase shifter contains three diodes in stripline, giving the equivalent of 2-bit control. Figure 42 shows the simple construction of a module consisting of eight radiators with phase shifters and drivers. The spherical phase error is corrected in the programming.

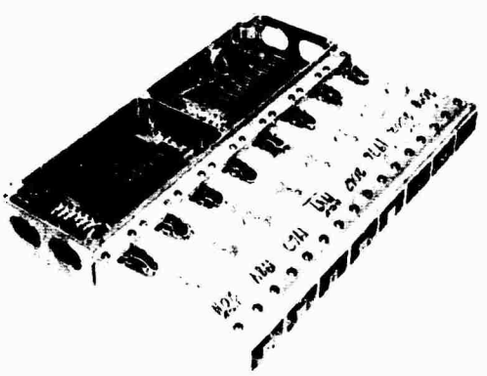

Fig. 42 Blass Reflectarray: Module with Eight Radiators, Phase Shifters, and Drivers (Courtesy Naval Research Laboratory)

The measured gain with the beam at antenna broadside is 34 db. All losses including spillover, phase shifter, input and output mismatch, amplitude taper, and phase quantization amount to about 4 db. The broadside beamwidth is 2.5°, and the operational bandwidth is 6%, provided the phase shifters are readjusted with frequency. Figure 43 shows scanned azimuth radiation patterns.

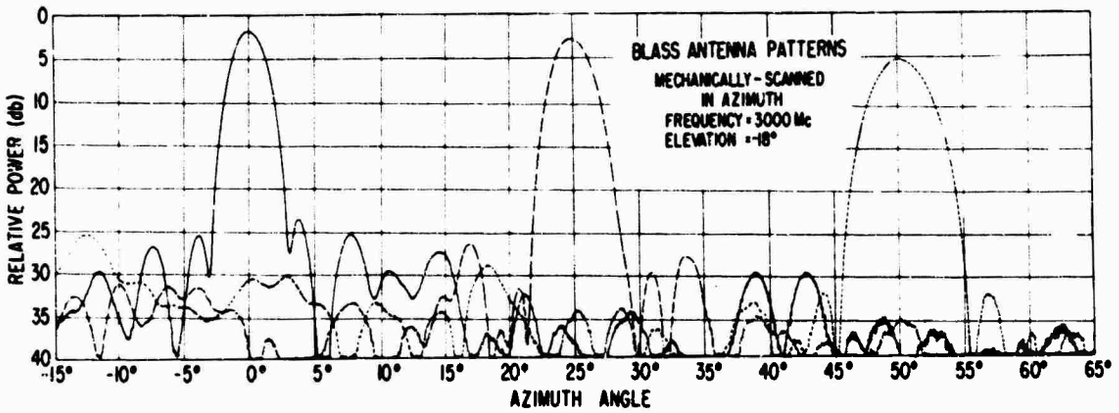

Fig. 43 Blass Reflectarray: Scanned Radiation Patterns (Courtesy Naval Research Laboratory)

Raytheon Reflectarray

The Raytheon Company has developed an experimental X-Band phased array (Ref. 55) with 1300 elements, assembled in an offset reflectarray of the type shown in Fig. 36b. The active device is a circularly polarized analogue phase shifter. Although the phase shifter is actually nonreciprocal, its effective behavior in the array, where it is terminated with a short circuit, is as if it were reciprocal.

This is because the reflection at the short circuit not only reverses the direction of energy flow but also the sense of circularity, so that on both passes through the phase shifter, the same amount of phase shift is added. The experimental antenna is shown in Fig. 44.

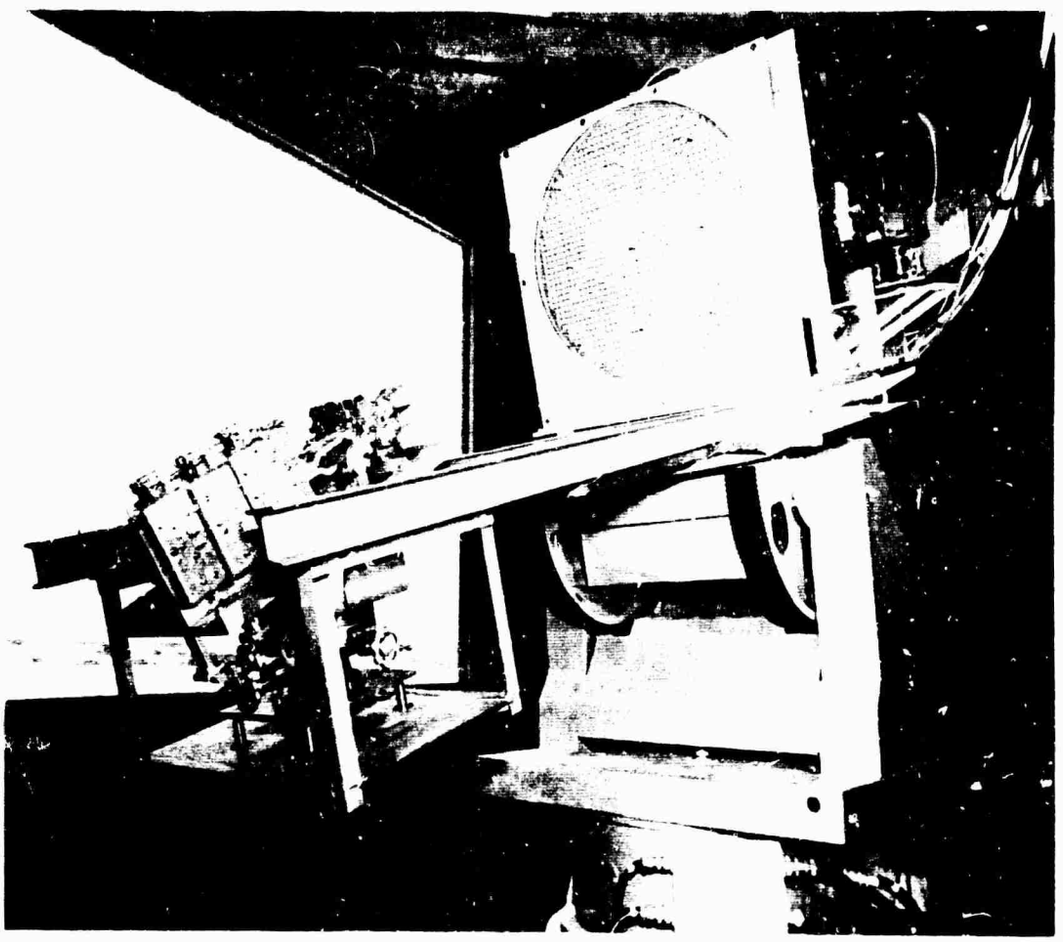

Fig. 44 Raytheon Reflectarray: Experimental Model with 1300 Elements (from Mohr and Lewis, Ref. 55)

When the reflectarray is used in a radar system, the sequence of events starts with the transmitter illuminating the array with, say, right-hand circular polarization (RHCP). Energy passes through the phase shifter twice and is radiated with left-hand circular polarization

(LHCP) after a phase shift that corrects for the spherical phase front and adds a linear phase tilt to point the beam. The reflection from a single bounce target has RHCP, which is received by the array. It is the same polarization that was originally generated by the transmitter, and the phase shifters are properly set to collimate the received signal at the focus. After reflection by the array, the signal has LHCP and the receiver polarization is orthogonal to that of the transmitter. A dually polarized feed is, therefore, required with sum and difference outputs in the receive channel.

A mode giving a measure of rain suppression is possible by receiving the double bounce target return (rain echoes predominantly correspond to single bounce returns while aircraft have significant energy returned by double bounce). In this case, in contrast to the previous one, the target signal received by the antenna has LHCP requiring that the phase shifters are switched, after transmitting, to the opposite state to collimate the signal. Finally, the signal is received in the same feed used on transmitting, with matching circular polarization.

The radiating elements of the antenna are spaced by about 0.6λ, at mid-band, in a square grid. This permits grating lobe free scanning up to about 40°. The VSWR for near broadside beams is about 1.4 over a 10% band.

Radiation patterns and gain measurements were taken with a circularly polarized four-square-horn-feed giving a 10 db tapered illumination. At 10 GHz the measured gain showed an overall antenna efficiency of about 45%. At the edges of the band the gain decreased as a result of depolarization of the relatively narrow band circular polarizer that was used. Figure 45 shows gain variations as a function of scanning. The losses include polarization and mismatch losses.

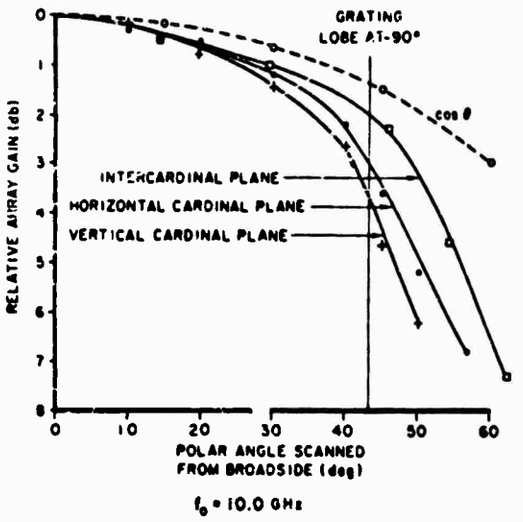

Fig. 45 Raytheon Reflectarray: Variation of Gain as a Function of Scan Angle (from Mohr and Lewis, Ref. 55)

The absolute beam pointing error of the monopulse null was measured for scanning up to 45° and found to give an RMS error of approximately 1/40 of a beamwidth.

Polarization circularity was found to hold up well to at least 30°, the ellipticity ratio being less than 1.5 db. In the rain-rejection mode this would correspond to a theoretical rejection of 15 db.

HAPDAR (HArd Point Demonstration Array Radar)

HAPDAR (Ref. 56) was sponsored by the Advanced Research Project Agency and developed by the Sperry Gyroscope Company. It performs search-acquisition-track functions on a time sharing basis. The antenna system uses an electronically steered lens with a thinned

aperture and 3-bit diode phase shifters. Figure 46 shows the building with the antenna aperture tilted back by 30°.

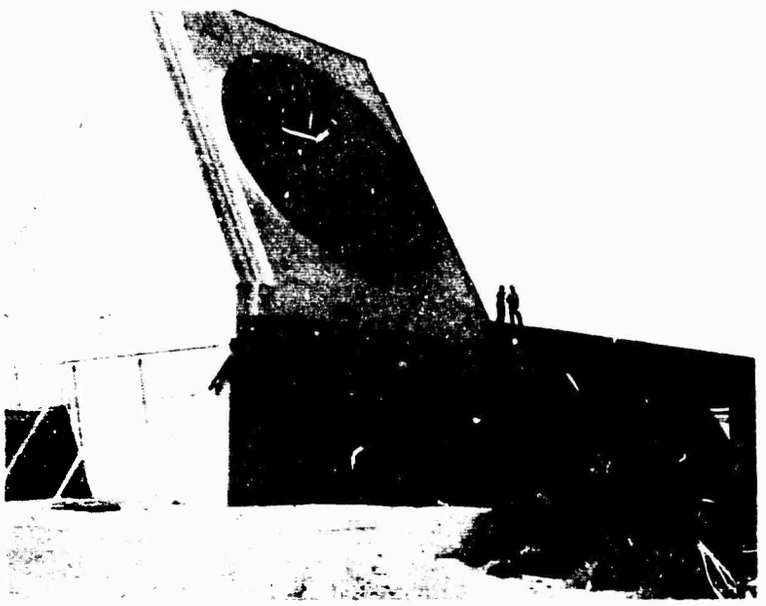

Fig. 46 HAPDAR Building Showing Phased Array (Courtesy Sperry Gyroscope Company)

The principle of the antenna is shown in Fig. 47. On the feed side the lens has a full complement of elements. Either a single element connects directly to a phase shifter or two elements are combined in phase (with a fixed bias if necessary) and then connected to a phase shifter. Each phase shifter in turn connects to an active element at the radiating aperture. In this way substantially all the transmitter energy incident on the feed side of the lens is utilized and distributed to a more economic aperture which has a reduced number of phase shifters. Terminated dummy elements at the aperture maintain the proper impedance environment without introducing a loss (Section VI, Thinned Arrays). The shape of the main beam is substantially that due to the complete aperture; the gain is determined by the number of active elements.

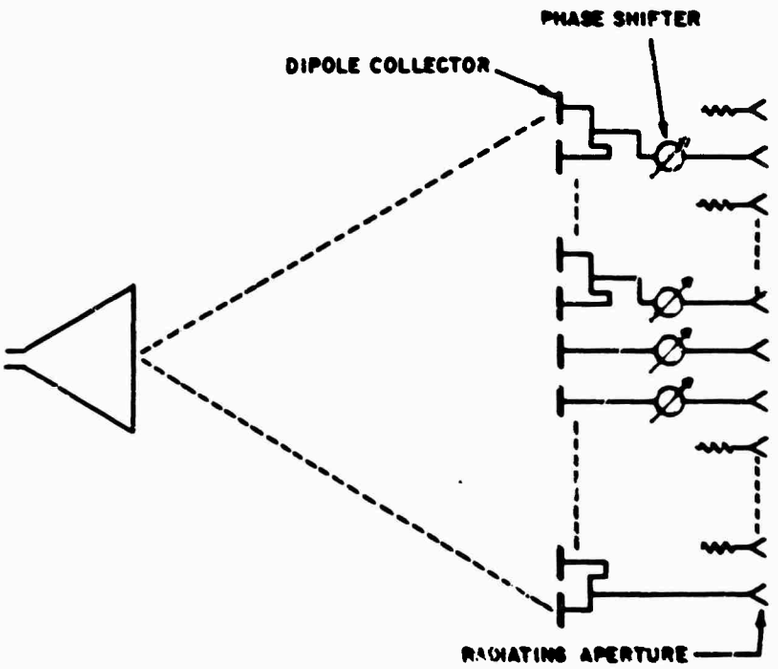

Fig. 47 HAPDAR: Thinned Lens

The feed side of the lens is shown in Fig. 48. The element is a printed dipole above a ground plane, connected to a stripline and the phase shifter, either directly or after combining with another dipole. The unit

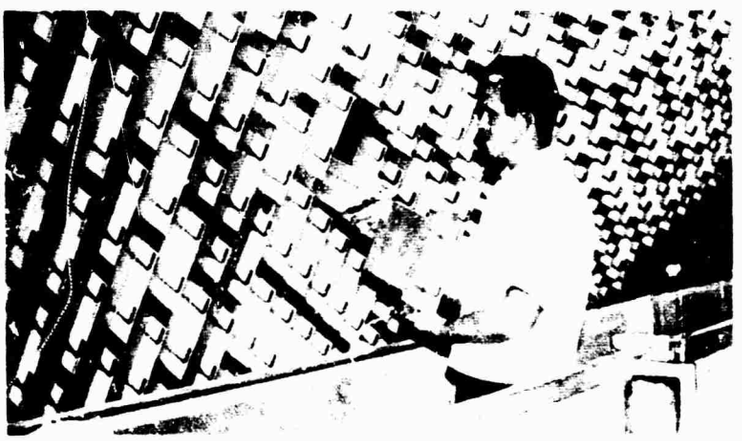

Fig. 48 HAPDAR: Lens Surface Facing Primary Feed, Showing Dipole Elements (Courtesy Sperry Gyroscope Company)

shown withdrawn contains a pair of dipoles, the phase shifter and a transducer which, when plugged in, will energize the wave guide horn radiator at the aperture surface.

The phase shifter contains three bits and has an average insertion loss of 1.2 db. It is programmed to correct the spherical phase front in addition to the normal beam steering commands.

There are 3750 element positions in the lens. About one quarter of these have dipoles directly connected to phase shifters and radiators. The remainder, with the exception of some terminated collectors, are combined in pairs as described. This results in an aperture with 2165 active radiators and 1585 terminated radiators. The elements are spaced to form equilateral triangles, with sides of 0.67λ to provide a scan capability of 45°.

The aperture illumination from the feed horn is modified by the thinning of the aperture and results in a 34 db Taylor amplitude taper ($\bar{n} = 4$). The location of the active radiators was determined by a pseudo-random process. The match at the radiating aperture gives a VSWR of about 2:1, approximately unchanged with scanning. Matching at the feed side is appreciably better.

Beam steering is achieved in steps of 1/32 of a beamwidth and interpolated to 1/500 of a beamwidth. Automatic testing of the phase shifters is available with computer printout of the location of faulty diodes.

The measured antenna gain was 35.9 db. This was calculated to be 3.6 db down from the array directivity.

APL Subarray Antenna System

A C-band phased-array antenna system using subarrays has been developed by The Johns Hopkins University, Applied Physics Laboratory (Ref. 57) under the sponsorship of the Naval Ordnance Systems Command and the Advanced Research Projects Agency. The subarray has 48 parallel fed radiating elements, each controlled by a 4-bit latching ferrite phase shifter of relatively small dimensions.

Figure 49 shows schematically how the subarray is assembled. It consists of an H-plane 4:1 power divider connecting four adjacent E-plane

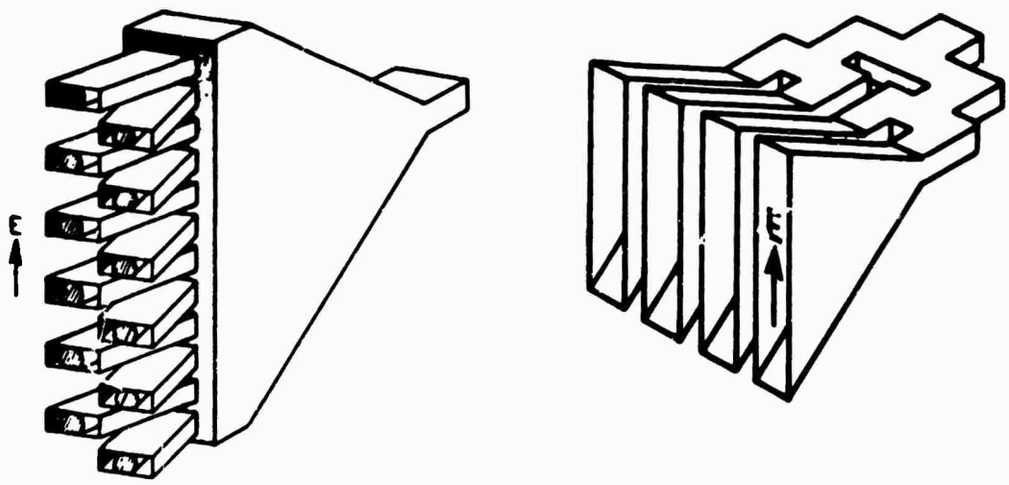

Fig. 49 Schematic of APL Subarray Assembly

sectoral horns in parallel. Each E-plane horn contains a matched dielectric lens (not shown) and feeds 12 waveguides with equal amplitude and phase. The waveguides contain the phase shifters with a matching section at each end. They are arranged as shown, aligned at the mouth of the horn, and interlaced at the radiating aperture with triangular spacing of about 0.6λ. No aperture discontinuities occur between adjacent

subarrays, and adequate space is available for the shielded control wires leading to the drivers behind the subarray. The aperture is matched in several steps, the last being a thin radome of $\epsilon_r = 9$ material which provides a measure of match compensation with scanning (Section IV). Figure 50 shows the complete subarray which weighs about 25 pounds.

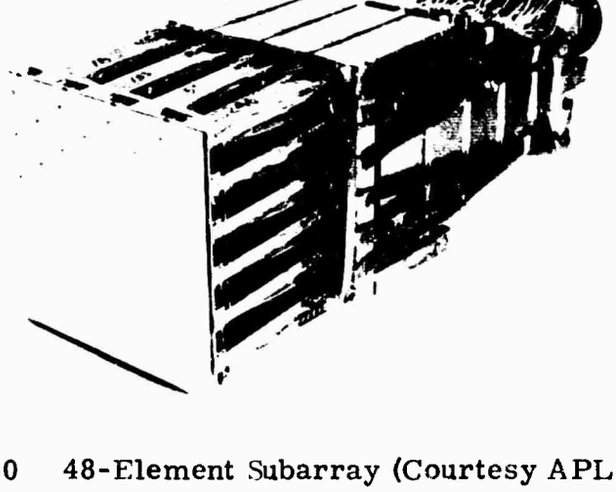

Fig. 50 48-Element Subarray (Courtesy APL/JHU)

Eight subarrays were built and tested (Ref. 29) in various configurations and combined with various amplitude tapers. An efficiency greater than 70% was obtained at broadside when excited with constant amplitude distribution. This included all losses such as those due to the power dividing network, phase shifters, and residual mismatch. With scanning, the gain varied approximately as $\cos\theta_o$, as expected. Over a 10% band the VSWR at broadside was < 1.5, with 60° scanning in the H-plane it was < 2.6 and with 60° scanning in the E-plane it was < 2.1. Absolute beam-pointing accuracy to within $\frac{1}{50}$ beamwidth was measured

for scan angles up to 60°. Figure 51 shows the broadside radiation pattern of eight subarrays combined with constant amplitude in the H-plane. The theoretical $\frac{\sin x}{x}$ envelope is shown for comparison. The close agreement between theoretical and measured patterns demonstrates the precision with which the aperture excitation of phased arrays can be controlled.

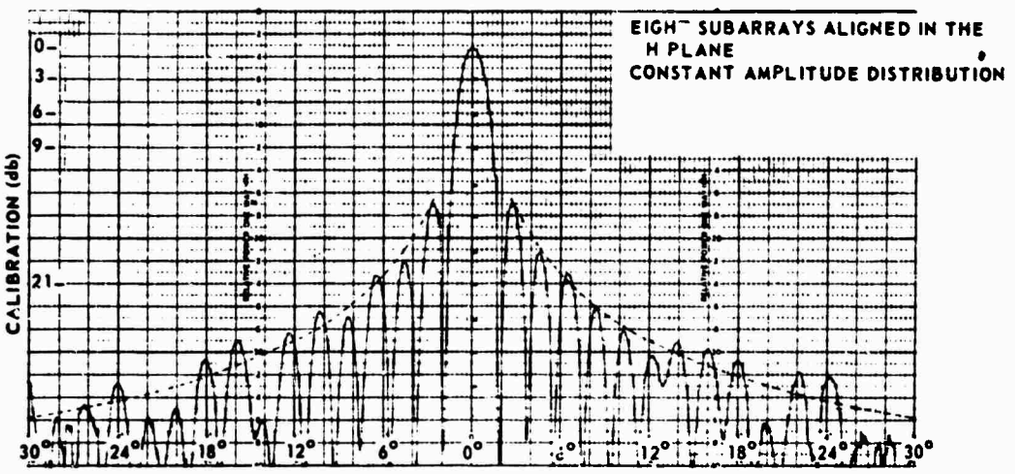

Fig. 51 APL Antenna Broadside Pattern Compared with Theoretical $\frac{\sin x}{x}$ Envelope (from Frank, Ref. 29)

RCA REST Antenna

A C-band phased array antenna system with limited scan has been developed by RCA for an instrumentation radar (Ref. 58) under a study of "Radar Electronic Scan Technique" (REST) sponsored by the Air Force Electronics System Division. The system offers complete polarization diversity and utilizes the simplifications that are possible when scanning is limited to a cone with an included angle of 10°.

A schematic view of the system is shown in Fig. 52. The antenna aperture is divided into subarrays. The size of a subarray is sufficiently small so that its beam encompasses the total scan volume. The subarray beam can then remain stationary in space. Each subarray contains 64 dipoles, arranged in two orthogonally polarized sets of 32. Each set is fed by a 1:32 power divider in a type of stripline, with equal path lengths to all

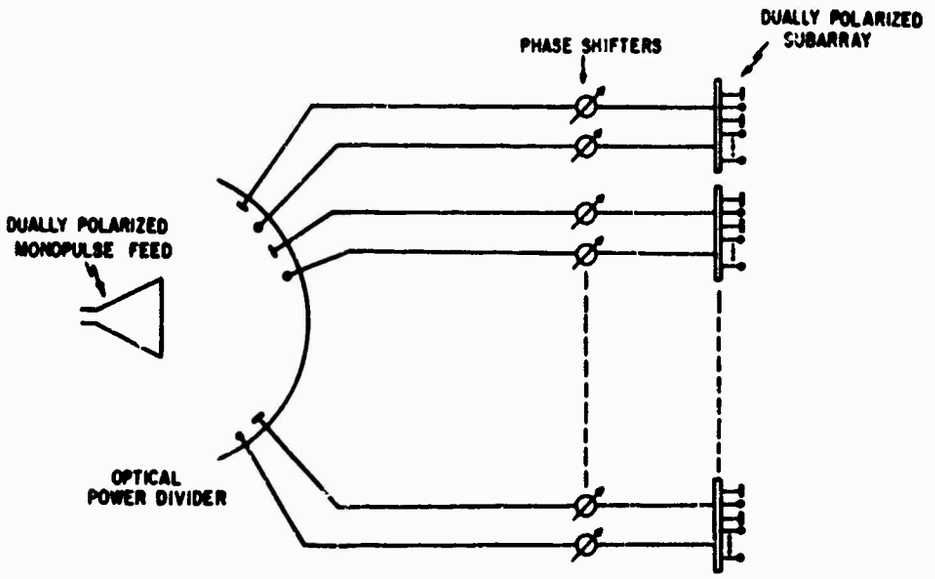

Fig. 52 Schematic of RCA REST Antenna

dipoles. The two power dividers (for the two orthogonal sets) are constructed in two parallel layers. With the limited scanning requirement, the dipoles in each set may be separated by a distance approaching a wavelength. The two orthogonal sets of dipoles are arranged in a square interlaced grid. The subarray with its 64 dipoles and the feed network is shown in Fig. 53.

The subarrays are spaced aperiodically over the aperture to avoid the formation of grating lobes. The beam is scanned with digital latching phase shifters, one at each of the two ports of the subarray, as shown in Fig. 52. The subarrays are combined (separately for each polarization)

by an optical power divider. This power divider consists of a dually polarized monopulse feed horn at the center of a spherical shell, formed by two sets of orthogonally polarized dipoles that connect to the phase shifters and subarrays. The dipoles are illuminated with equal phase by

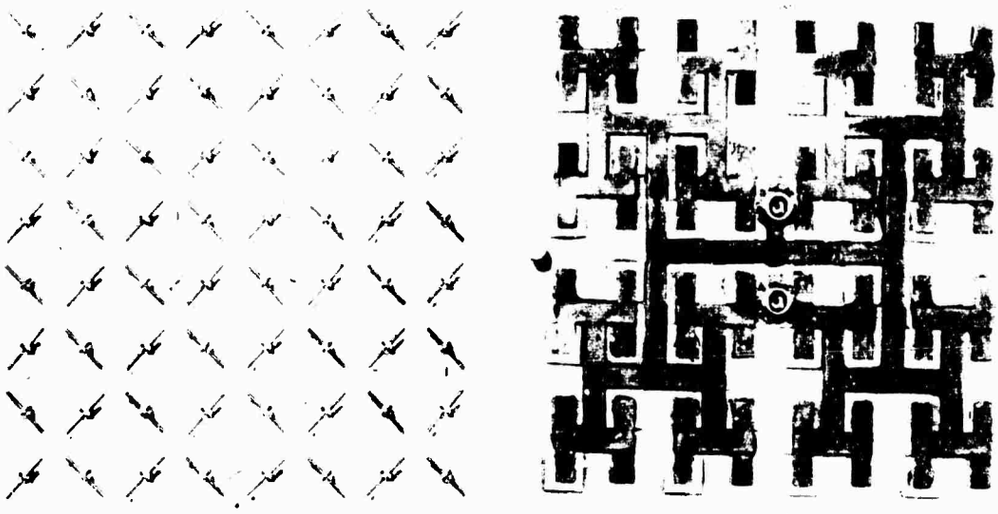

Fig. 53 RCA REST Antenna: Dually Polarized Subarray and Feed Network (Courtesy RCA)

the feed horn with an edge taper of 10 db. On transmitting, the array will generate a beam with the same polarization that has been used to illuminate the spherical shell. On receiving, complete polarization diversity is possible.

Figure 54 shows an experimental model with a 10-foot-diameter antenna containing 112 subarrays.

Sampled MOSAR

MOSAR (MOdulation Scanned ARray) is an IF beam-scanning system developed by the General Electric Company, which can provide a

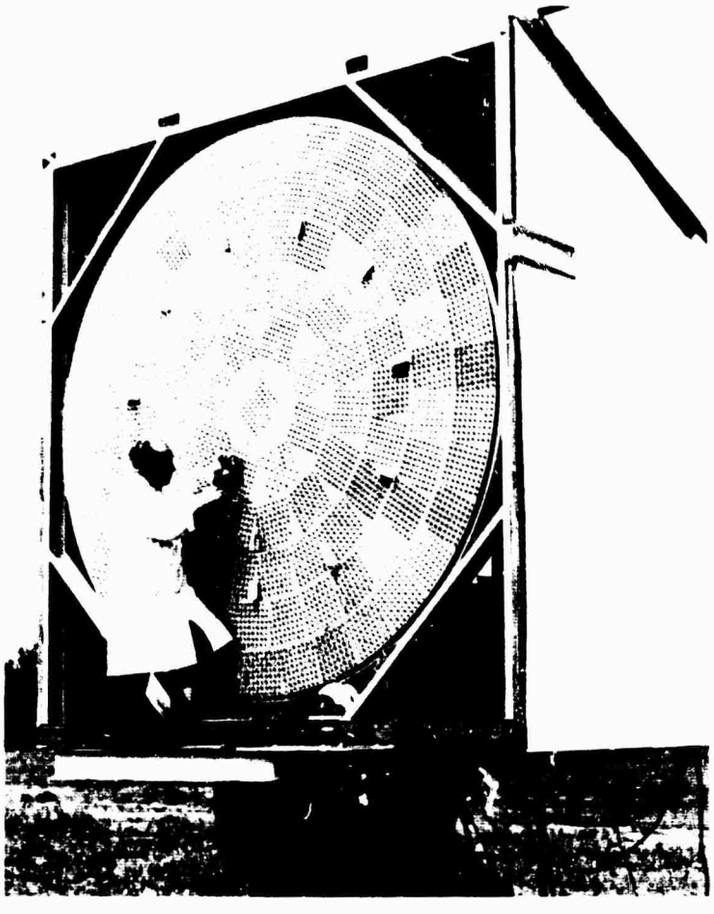

Fig. 54 Experimental RCA REST Antenna (from Evanzia, Ref. 58)

number of independently steered beams with variable beamwidth. The system and other IF beam steering concepts have been described by Johnson (Ref. 59).

The general principle of operation is indicated in Fig. 55 where a transmitting array generates phase-locked frequencies which differ by f_s from element to element. The phase of each element rotates through 2π radians relative to its neighbor in a period $1/f_s$. The radiated beam is, therefore, scanned in that period through 180°. The same result is

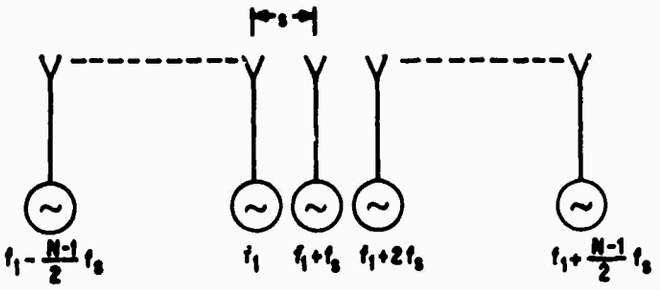

Fig. 55 Scanning with Multiple Frequencies

obtained in a receiving system if the local oscillator frequency to each successive element is changed by an incremental amount f_s, since the resulting IF carries the sum of the phases of both the received signal and the local oscillator.

Figure 56 is a schematic of the sampled MOSAR receiving system. The desired phase-locked local oscillator signals are obtained in the form

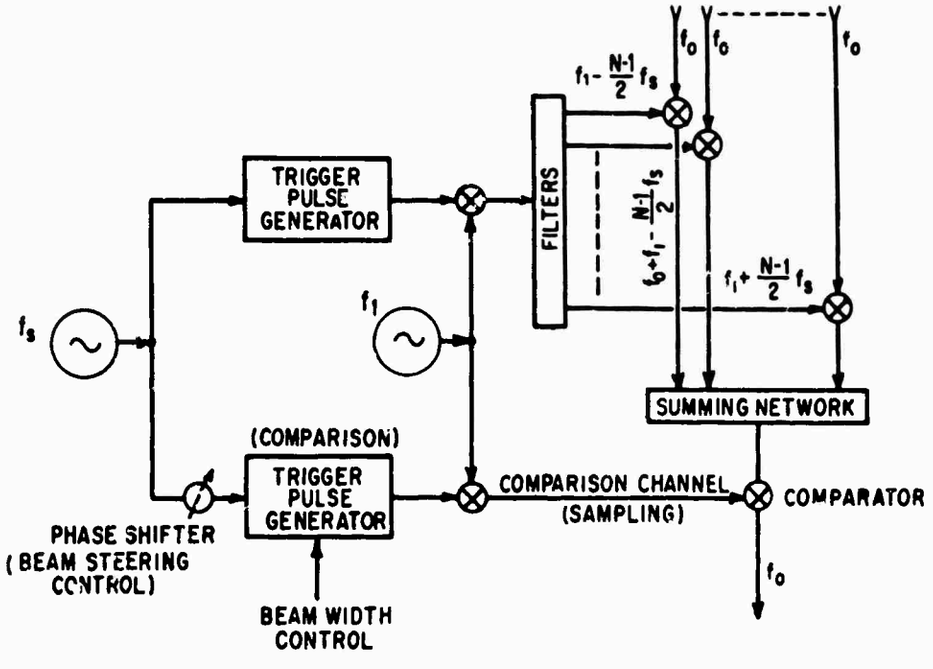

Fig. 56 Sampled MOSAR (from Johnson, Ref. 59)

of sidebands: A signal source of frequency f_s triggers a pulse generator, giving pulses with a PRF of f_s, which are used to modulate an RF signal of frequency f_1. This results in a signal containing the frequency f_1 and sidebands separated by f_s. The sidebands are extracted by filters and mixed with the received signal f_0 at the appropriate element of the N element array. Up-mixing is used, giving an IF of $f_1 + f_0 \pm nf_s$.

After mixing, the N outputs are summed in a network and form a received beam that scans through 180° in the period $1/f_s$. If a signal is received from a given direction, then, as the radiation pattern sweeps past that direction, a pulse is formed at the summed output port. The pulse shape is the radiation pattern, and the time of occurrence of the pulse is a measure of the angle of arrival. It is measured by comparing it with the occurrence of a reference pulse from the comparison pulse generator, which is adjusted for time coincidence by a phase shifter in the excitation line. The phase shifter setting gives the direction of arrival of the signal.

Several comparison pulse generators may be used in parallel, each with its own phase shifter, to deal independently with signals arriving from several directions. Each comparison channel samples the scanning beam at the proper times.

With linear mixing beam shape control is available by adjusting the amplitudes of the sidebands. This can be done in several ways, but particularly it may be done electronically by adjusting the width of the pulse from the pulse generator. Since, in the comparison stage, the received signal is multiplied by the pulse from the comparison pulse generator, the pulse width of this second generator may be adjusted, so that with several such generators each beam can be treated separately.

To prevent overlapping frequencies in the summing network, the frequency spacing f_s must be greater than the bandwidth of the received signal. For an N element array the summing network bandwidth, i.e. the processing bandwidth, is more than N times greater than the bandwidth of the received signal and can be quite large for a particular system.

BLANK PAGE

IX. MULTIPLE BEAM FORMING AND BEAM SWITCHING

Multiple Beam Forming Networks

Multiple beam forming systems consist of networks that generate or, more usually, receive simultaneous beams from an aperture, with each beam having the gain and beamwidth of the whole antenna. One or more beams are selected by switches. On receiving, the total number of beams that may be processed simultaneously is limited primarily by the number of receivers that can be made available. On transmitting, multiple beams would be possible but the total generated power must be shared by them. In general, beam forming systems are of greater complexity than phased arrays.

A multiple beam-forming network after Blass is shown in Fig. 3d. Beams are formed in one plane only. For efficient operation the individual radiation patterns have to follow Allen's criteria of orthogonality (Ref. 12) where the direction of the peak of one beam corresponds to nulls of the other beams. This corresponds to a beam crossover at about 4 db. High efficiency can be obtained with large arrays, but careful design procedures (Ref. 13) are necessary to avoid the formation of spurious beams.

Figure 57 shows two other beam-forming networks. Again, beams are formed in one plane only. The first is rather similar to the Blass array but is designed with equal path lengths to the radiating elements, giving wide bandwidth with beams that are stationary as the frequency is changed. The second network described by Butler (Ref. 60) and Shelton

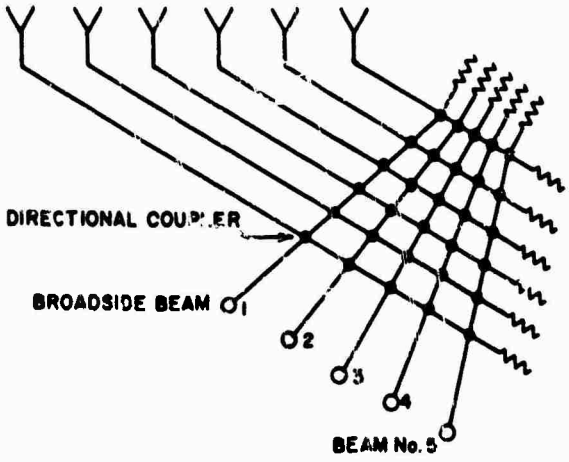

(a) EQUAL PATH LENGTH BEAM-FORMING MATRIX

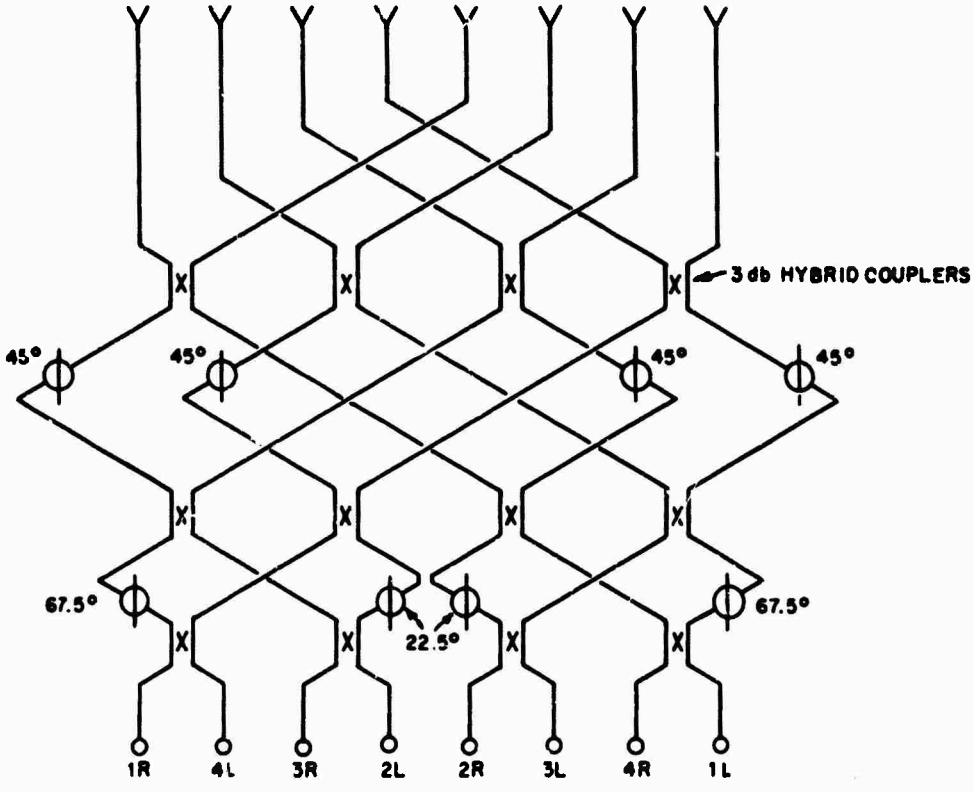

(b) EIGHT ELEMENT, EIGHT BEAM MATRIX. (from Butler [60])

Fig. 57 Beam Forming Networks

and Kelleher (Ref. 61) contains hybrid couplers and fixed phase shifters. In this example an eight-element array forms eight orthogonal beams which lie to the right and left of the broadside direction. The terminals have been labelled to identify the beams.

Many further network combinations are possible, leading to other beam forming systems. A comprehensive survey has been made by Butler (Ref. 62) including IF beam forming techniques.

Shelton and Kelleher describe a multiple beam forming system using a Luneberg lens (Ref. 63). This lens is spherical and has a dielectric constant that varies as a function of the radius. It has the property that an incident plane wave is brought to a focus on its far surface so that adjacent feeds on its surface correspond to overlapping beams. In this application as suggested by J. B. Garrison, the Luneberg lens has feeds arranged over all its surface and is used as a phase correction generator to feed a spherical array.

Switching Matrices

The beam forming networks combine the energy from the aperture in M different ways to give M different beams. A switching matrix then selects one or more of these beams which are stationary in space. It takes M - 1 single-pole double-throw switches arranged in a tree of m levels to condense M terminals into one outlet, where $2^m = M$.

Monopulse beam forming is possible by taking the sum and difference of adjacent beams to interpolate between beam positions. With a system where the beams are formed in one plane only, beams may be labelled consecutively as A B A B... One switching matrix selects one

of the A beams and another matrix one of the B beams. Monopulse amplitude comparison is then carried out between the outputs of the two matrices. An extension of this technique permits full monopulse in both azimuth and elevation. A further extension permits the generation of one or several beam clusters of arbitrary size and shape.

For monopulse operation the electrical path length through the whole switching matrix must be maintained with tight tolerances. The switches must give good isolation since this is the only means of attenuating the other beams. Switching networks tend to be lossy, and amplification at the antenna terminal is desirable. On receiving, the signals from the various beams may be changed to IF where the beam selection is carried out.

Multiple Beam Systems

AHSR-1

The AHSR-1 is a Federal Aviation Agency S-band height finding radar using the Blass beam-forming principle of Fig. 3d. The proposed antenna has three faces, each covering 120° in azimuth. One face has been built by the Maxson Corporation (Ref. 64) as the prototype (Fig. 58). It has two linear arrays, each with 528 radiators combined to give a total of 111 beams covering elevations from 0.5° to 40°, with a beamwidth that varies from 0.16° to 1.4°. It uses 10 miles of waveguide and 40,000 directional couplers.

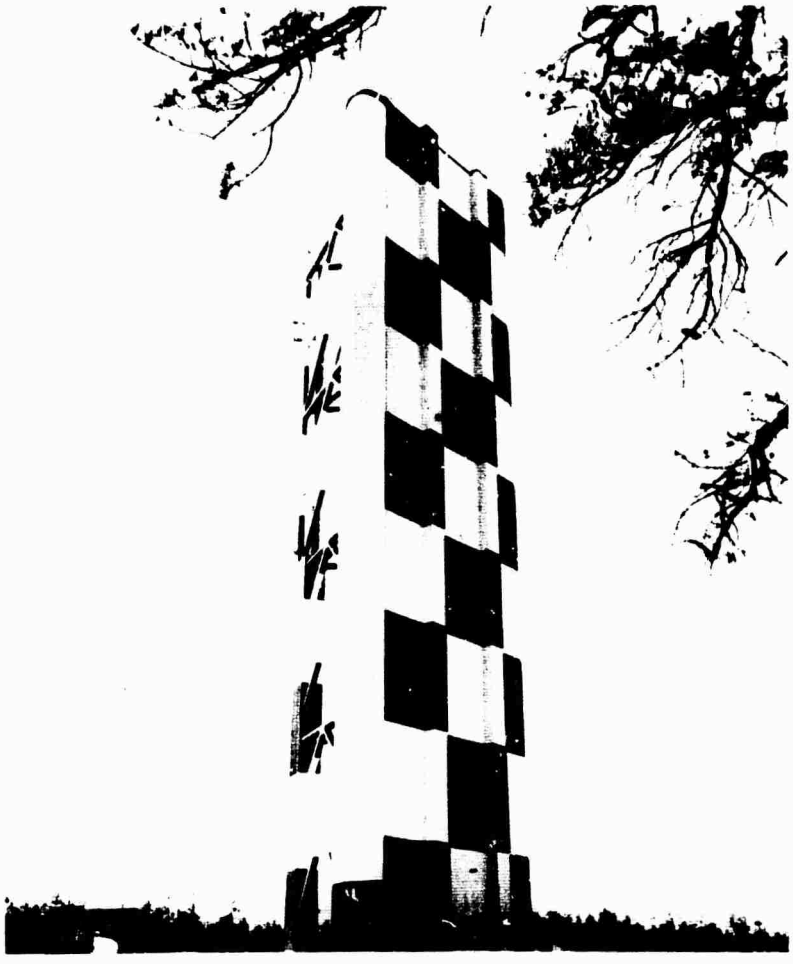

Fig. 58 ASR-1 FAA Height-Surveillance Radar (Courtesy Maxson Electronics Corporation)

Hughes Aircraft Multiple Beam Systems

The Hughes Aircraft Corporation developed a 3-D multiple beam system using a constrained lens (Ref. 65). The system has true time delay, giving a wide instantaneous bandwidth. Polarization diversity is possible. The system is complex but does give simultaneous beams in both planes.

Figures 59 and 60 show a schematic view and an experimental model respectively. The surface S_2 is spherical and has a radius R. If it had been a reflector it would have had an approximate focal surface

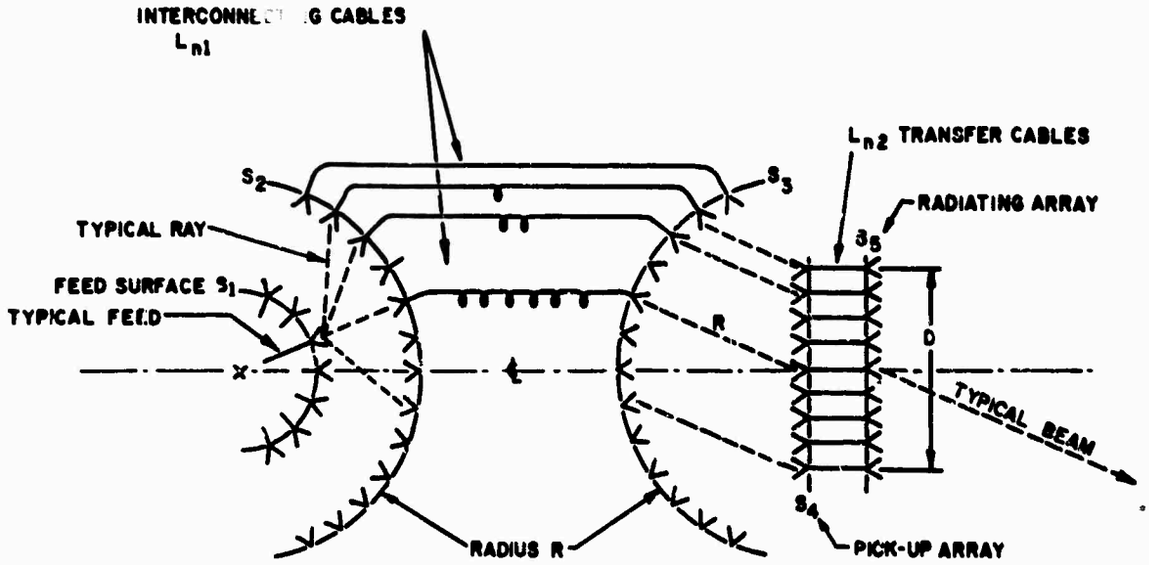

Fig. 59 Hughes Aircraft Multiple Beam Experimental System (from McFarlane and Ajioka, Ref. 64)

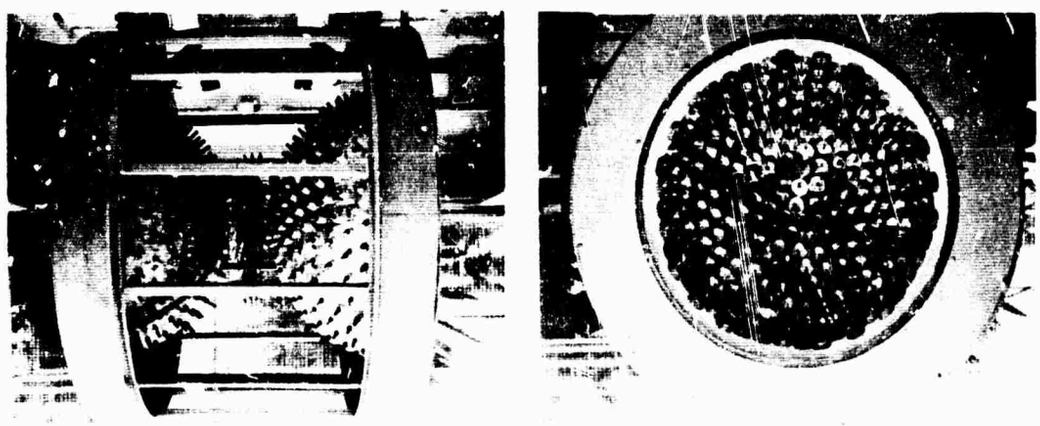

Fig. 60 Hughes Aircraft Multiple Beam Forming Systems (from McFarlane and Ajioka, Ref. 64)

that was concentric, with a radius slightly greater than R/2. The surface S_1 is this focal surface and contains the feeds, each corresponding to a beam whose direction is given by the line joining the feed with the center of the sphere. The feeds are directive and illuminate only part of the surface S_2. This decreases the phase errors that arise from S_2 being spherical rather than parabolic. The surface S_2 is not a reflector, and the illumination on it is transferred in amplitude and phase to a similar surface S_3 by means of pick-up horns on S_2 and transfer cables and radiating horns on S_3. The surface S_3 generates beams in exact correspondence to the direction determined by the position of the feed on surface S_1.

The beam is directed through the center of the sphere S_2. It is possible to add at that place the optional pick-up and radiating planar arrays S_4 and S_5 that are smaller than the spherical surface but still intercept substantially all of the radiated power. Electronic phase shifters could be interposed between surfaces S_4 and S_5. This would permit a scheme of scanning where the transmitter is always coupled to the same feed and does not have to go through a switch network. On receiving, the phase shifters would be quiescent to permit the formation of simultaneous beams.

Phase errors resulting from the surfaces being spherical can be exactly compensated for at any particular scan angle and substantially compensated for in all scan positions by adding a correction in the form of line length to the cables Ln_4 and Ln_5.

To illustrate the quantities involved, for a 1° beam scanned in all directions by ± 45° the final aperture diameter D is 70λ, the diameter of the lens surfaces 2R is 140λ and the maximum phase error is λ/16. There are about 35,000 elements on each of the two lens surfaces.

Polarization diversity is available with dually polarized lens elements. The radiated polarization is then determined by the polarization of the feed.

X. INTEGRATED ANTENNA ARRAYS

Solid-state devices are being developed for integration into array antennas to phase and form beams and for amplifi ation. Microstrip transmission circuits have be.n developed that contain the various active microwave circuit elements such as switches and circulators as well as amplifiers, mixers, and multipliers (Ref. 66). With these devices systems become possible where many relatively low power transmit amplifiers are used, distributed over the aperture, each amplifier connected to a radiating element. The power amplifiers may be transistors or phase-locked transit-time oscillators, the latter having the potential of high peak power at the higher microwave frequencies. On receiving, the noise figure may be established by low noise transistor preamplifiers. The phase shifters and feed networks may then contain lossy elements.

The expected advantages of integrated antennas include high reliability and low cost, simple low voltage power supplies for the RF amplifiers and a system that is simple and light in weight and yet capable of operating with relatively high RF power.

Figure 61 shows an early L-band phased array module developed by Texas Instruments. On transmitting, the signal passes through a 4-bit phase shift network which consists of diodes that switch line-lengths. The signal is then amplified (24 db) to 5 watts and radiated. On receiving, the signal passes through a low noise preamplifier, followed by the phase shifter. T-R switching is achieved with additional diodes.

An X-band integrated antenna system (MERA) using frequency multiplication is presently being developed (Ref. 67).

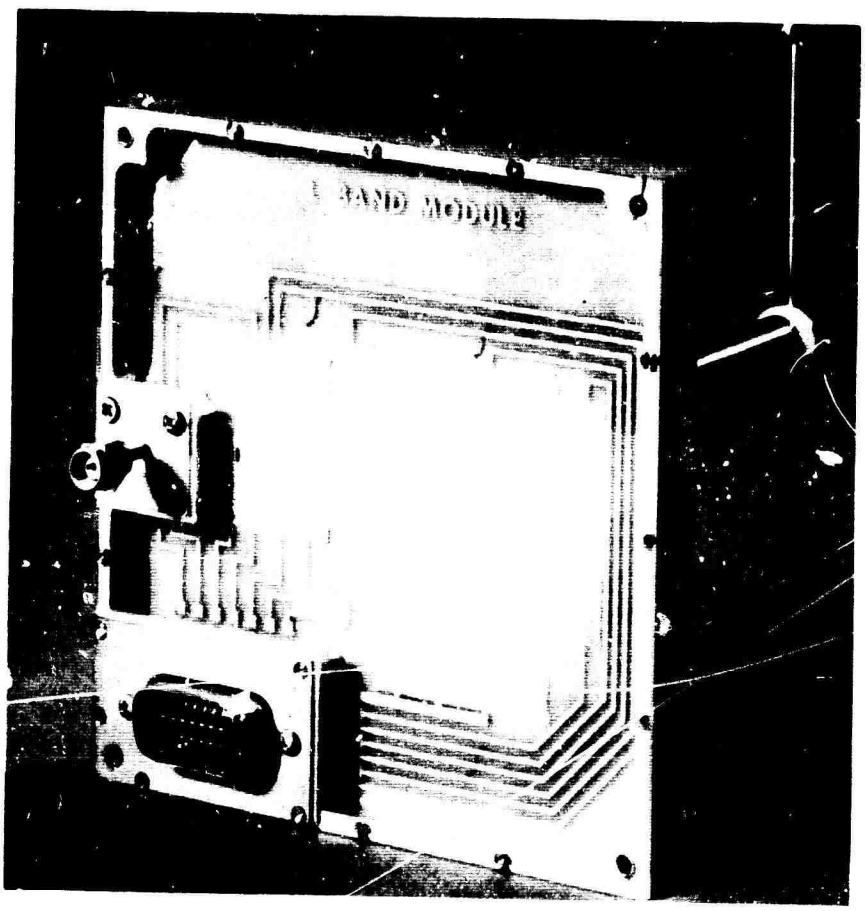

Fig. 61 L-Band Module Containing Phase Shifters, Power Amplifiers, Low Noise Amplifiers and T-R Switches (Courtesy Texas Instruments, Inc.)

REFERENCES

1. Brown, S. G., British Patent 14,449 (1899), see also Ref. 2.

2. Foster, R. M., "Directive Diagrams of Antenna Arrays," Bell System Tech. J., Vol. 5, pp. 292-307, April 1926.

3. Ogg, F. C., "Steerable Array Radars," IRE Trans. Vol. MIL-5, pp. 80-94, April 1961.

4. Allen, J. L., "The Theory of Array Antennas," MIT Lincoln Lab. Tech. Rept. 323, July 1963.

5. Hansen, R. C., "Microwave Scanning Antennas," Vol. I, II, and III, Academic Press, 1964.

6. Amitay, N., R. C. Pecina, and C. P. Wu, "Radiation Properties of Large Planar Arrays," Bell Telephone System Monograph 5047, February 1965.

7. Schroeder, K. G., "Near Optimum Beam Patterns for Phase Monopulse Arrays," Microwaves, pp. 18-27, March 1963.

8. Hansen, R. C., loc. cit, 2, Vol. II, Chapters 2-4 by A. A. Oliner and R. G. Malech.

9. Parad, L. I. and R. W. Kreutel, "Mutual Effects between Circularly Polarized Elements," Abstr. 1962 Symp. on U.S.A.F. Antenna Research and Develop., Antenna Arrays Section, University of Illinois, Urbana.

10. Skolnik, M. I., Introduction to Radar Systems, Section 12.7, McGraw Hill, 1962.

11. Queriod, H., J. Frank, and T. C. Cheston, "Wide Band Phase Shifters," IEEE Trans., Vol. AP-15, No. 2, p. 300, March 1964.

12. Allen, J. L., "A Theoretical Limitation on the Formation of Lossless Multiple Beams in Linear Arrays," IRE Trans., Vol. AP-9, pp. 350-352, July 1961.

13. Blass, J., "The Multidirectional Antenna: A New Approach to Stacked Beams," 1960 IRE Internat'l Conv. Record, Vol. 8, Pt. 1, pp. 48-50.

14. Schelkunoff, S. A., "A Mathematical Theory of Linear Arrays," Bell System Tech. J., Vol. 22, pp. 80-107, January 1943.

15. Ramsay, J. F., J. P. Thompson, and W. D. White, "Polarization Tracking of Antennas," 1962 IRE Internat'l Conv., Session 8, Antennas I.

16. Woodward, P. M., "A Method of Calculating the Field over a Planar Aperture Required to Produce a Given Polar Diagram," J. IEE, Vol. 93, Pt. IIIA, pp. 1554-1558, 1946.

17. Ramsay, J. F., "Lambda Functions Describe Antenna Diffraction Pattern," Microwaves, pp. 70-107, June 1967.

18. Ksienski, A., "Equivalence between Continuous and Discrete Radiating Arrays," Can. J. Phys., Vol. 39, pp. 335-349, 1961.

19. Bickmore, R. W., "Note on Effective Aperture of Electrically Scanned Arrays," IRE Trans., Vol. AP-6, No. 2, pp. 194-196, April 1958.

20. Cheng, D. K. and M. T. Ma, "A New Mathematical Approach for Linear Array Analysis," IRE Trans., Vol. AP-8, pp. 255-259, May 1960.

21. Jury, E. J., Theory and Application of the Z-Transform Method, Wiley, 1964.

22. Christiansen, P. L., "On the Closed Form of the Array Factor for Linear Arrays," IEEE Trans., Vol. AP-11, p. 198, March 1963.

23. Cheng, D. K., "Z-Transform Theory for Linear Array Analysis," IEEE Trans., Vol. AP-11, p. 593, September 1963.

24. Von Aulock, W. H., "Properties of Phased Arrays," IRE Trans., Vol. AP-9, pp. 1715-1727, October 1960.

25. Sharp, E. D., "Triangular Arrangement of Planar-Array Elements That Reduces Number Needed," IRE Trans., Vol. AP-9, No. 2, pp. 126-129, March 1961.

26. Allen, J. L., et al., "Phased Array Studies," MIT Lincoln Lab. Tech. Rept. 381, pp. 299-318, March 1965.

27. Allen, J. L. and B. L. Diamond, "Mutual Coupling in Array Antennas," MIT Lincoln Lab. Tech. Rept. 424, October 1966.

28. Allen, J. L., loc. cit. 15, Pt. III, Chapter 3 by B. L. Diamond.

29. Frank, J., "Phased Array Antenna Development," APL/JHU TG-882, March 1967.

30. Hannan, P. W., "Element-Gain Paradox for a Phased-Array Antenna," IEEE Trans., Vol. AP-12, pp. 423-433, July 1964.

31. Willey, R. E., "Space Tapering of Linear and Planar Arrays," IRE Trans., Vol. AP-10, pp. 369-377, July 1962.

32. Wheeler, H. A., "Simple Relations Derived from a Phased-Array Antenna Made of an Infinite Current Sheet," IEEE Trans., Vol. AP-13, pp. 506-514, July 1965.

33. Allen J. L., "On Array Element Impedance Variation with Spacing," IEEE Trans., Vol. AP-12, No. 3, p. 371, May 1964.

34. Schwartzman, L. and L. Topper, "Characteristics of Phased Array Lenses," Digest 1967 Internat'l Symp. on Antennas and Prop., Ann Arbor, Michigan.

35. Kraus, J. D., Antennas, McGraw-Hill, 1950.

36. Carter, P. S., Jr., "Mutual Impedance Effects in Large Beam Scanning Arrays," IRE Trans., Vol. AP-8, pp. 276-285, May 1960.

37. Wheeler, H. A., "The Grating-Lobe Series for the Impedance Variation in a Planar Phased-Array Antenna," IEEE Trans., Vol. AP-13, pp. 825-827, September 1965.

38. Stark, L., "Radiation Impedance of Dipole in Infinite Planar Phased Array," Radio Science, Vol. 1, No. 3, pp. 361-377, March 1966.

39. Kurtz, L. A. and R. S. Elliott, "Systematic Errors Caused by the Scanning of Antenna Arrays: Phase Shifters in the Branch Lines," IRE Trans., Vol. AP-4, pp. 619-627, October 1956.

40. Hannan, P. W., "The Ultimate Decay of Mutual Coupling in a Planar Array Antenna," IEEE Trans., Vol. AP-14, No. 2, pp. 246-248, March 1966.

41. Debski, T. T. and P. W. Hannan, "Complex Mutual Coupling Measured in a Large Phased Array Antenna," Microwave J., pp. 93-96, June 1965.

42. Lechtrek, L. W., "Cumulative Coupling in Antenna Arrays," Digest 1965 IEEE Internat'l Symp. on Antennas and Prop., pp. 144-147, Washington, D. C.

43. Farrell, G. F., Jr. and D. H. Kuhn, "Mutual Coupling Effects of Triangular Grid Arrays by Modal Analysis," IEEE Trans., Vol. AP-14, pp. 652-654, September 1966.

44. Diamond, B. L., "Resonance Phenomena in Waveguide Arrays," Digest 1967 IEEE Internat'l Symp. on Antennas and Prop., Ann Arbor, Michigan.

45. Hannan, P. W. and M. A. Balfour, "Simulation of a Phased-Array Antenna in a Waveguide," IEEE Trans., Vol. AP-13, No. 3, pp. 342-353, May 1965.

46. Balfour, M. A., "Active Impedance of a Phased-Array Antenna Element Simulated by a Single Element in Waveguide," IEEE Trans., Vol. AP-15, No. 2, pp. 313-314, March 1967.

47. Magill, E. G. and H. A. Wheeler, "Wide-Angle Impedance Matching of a Planar Array Antenna by a Dielectric Sheet," IEEE Trans., Vol. AP-14, No. 1, pp. 49-53, July 1966.

48. Hannan, P. W., D. S. Lerner, and G. H. Knittel, "Impedance Matching a Phased-Array Antenna over Wide Scan Angles by Connecting Circuits," IEEE Trans., Vol. AP-13, No. 1, pp. 28-34, January 1965.

49. Miller, C. J., "Minimizing the Effects of Phase Quantization Errors in an Electronically Scanned Array," Proc. 1964 Symp. on Electronically Scanned Array Techniques and Applications, RACD-TDR-64-225, Vol. 1, pp. 17-38, RADC, Griffiss Air Force Base, N. Y.

50. Frank, J. and J. Ruze, "Steering Increments for Anti-symmetrically Phased Arrays," IEEE Trans., Vol. AP-15, No. 6, November 1967.

51. Brown, J., Unpublished Communication, 1951.

52. Bailin, L. L., "Fundamental Limitations of Long Arrays," Hughes Aircraft Company, Tech. Memo 330, October 27, 1953.

53. Lopez, A. R., "Monopulse Networks for Series Feeding an Array Antenna," Digest 1967 IEEE Internat'l Symp. on Antennas and Prop., Ann Arbor, Michigan.

54. Meads, S. K. (NRL), Private Communication, 1967.

55. Mohr, M. C. and L. R. Lewis, "A Reflective Phased Array Antenna Using Circularly Polarized Phase Shifters," Digest 1966 IEEE Internat'l Symp. on Antennas and Prop., pp. 447-453, December 1966.

56. Kaprilas, P. J. and D. M. Jahn, "Hardpoint Demonstration Array Radar," Supplement to 1966 IEEE Trans. on Aerospace and Electronic Systems, Vol. AES-2, No. 6, pp. 286-289.

57. Cheston, T. C. and H. M. Grady, "A Phased Array Using Subarray Techniques," Digest 1965 IEEE Internat'l Symp. on Antennas and Prop., pp. 98-101, Washington, D. C.

58. Evanzia, W. J., "Quick-Change Technique Converts Monopulse Radar into Phased Array," Electronics, pp. 145-150, May 29, 1967.

59. Johnson, M. A., "Mixer Steering Concepts for Array Antennas," General Electric Co. Rept., R66EM439, September 1966.

60. Butler, J. L., "Multiple Beam Antennas," Sanders Associates, Nashua, N. H., Internal Memo RF 3849, January 8, 1960.

61. Shelton, J. P. and K. S. Kelleher, "Multiple Beams from Linear Arrays," IEEE Trans., Vol. AP-9, pp. 154-161, March 1961.

62. Hansen, R. C., loc. cit. 5, Vol. III, Ch. 3 by J. L. Butler.

63. Shelton, J. P., Jr. and K. S. Kelleher, "Recent Electronic Scanning Developments," Proc. 1960 Conv. on Military Electronics, pp. 30-34.

64. Kahn, W. K. and E. J. Shubel, "Passive Series Fed Multibeam Antennas," Digest 1965 IEEE Internat'l Symp. on Antennas and Prop., pp. 82-89, Washington, D. C.

65. McFarlane, J. L. and J. S. Ajioka, "Multiple-Beam Constrained Lens," Microwaves, pp. 81-89, August 1963.

66. Digest, Internat'l Symp., PGMTT, Boston, May 1967, Sessions V and VI.

67. Klass, P. J., "New Phased-Array Radar Uses Microwave Microcircuitry," Aviation Week and Space Technology, pp. 92-100, January 16, 1967.

UNCLASSIFIED
Security Classification

DOCUMENT CONTROL DATA - R & D

Security classification of title, body of abstract and indexing annotation must be entered when the overall report is classified)

1. ORIGINATING ACTIVITY (Corporate author)	2a. REPORT SECURITY CLASSIFICATION
The Johns Hopkins University Applied Physics Lab. 8621 Georgia Avenue Silver Spring, Maryland	Unclassified 2b. GROUP

3. REPORT TITLE

Array Antennas

4. DESCRIPTIVE NOTES (Type of report and inclusive dates)

5. AUTHOR(S) (First name, middle initial, last name)

T. C. Cheston and J. Frank

6. REPORT DATE	7a. TOTAL NO. OF PAGES	7b. NO. OF REFS
March 1968	175	67

8a. CONTRACT OR GRANT NO	9a. ORIGINATOR'S REPORT NUMBER(S)
NOw 62-0604-c b. PROJECT NO	TG-956
c.	9b. OTHER REPORT NO(S) (Any other numbers that may be assigned this report)
d.	

10. DISTRIBUTION STATEMENT

This document has been approved for public release and sale; its distribution is unlimited.

11. SUPPLEMENTARY NOTES	12. SPONSORING MILITARY ACTIVITY
	Naval Ordnance Systems Command Advanced Research Project Agency

13. ABSTRACT

Array antennas in their various forms are discussed and analyzed with special reference to electronic scanning. The effects of mutual coupling of the radiating elements are considered and methods of matching are given. Quantization errors, particularly those found in phased arrays, are calculated and bandwidth limitations are derived. Specific array antenna systems are described.

DD FORM 1 NOV 65 1473

UNCLASSIFIED
Security Classification

14.

KEY WORDS

Array antennas

Antenna arrays

Phased arrays

Electronic scanning

Mutual coupling in antenna arrays